UiT
THE ARCTIC
UNIVERSITY
OF NORWAY

Faculty of Health Science, Department of Medical Biology,
Molecular Cancer Research Group

Identification of protein interaction candidates for the GOLD domain of FYCO1

Betty Martine Normann Furulund
Master thesis in Biomedicine May 2016

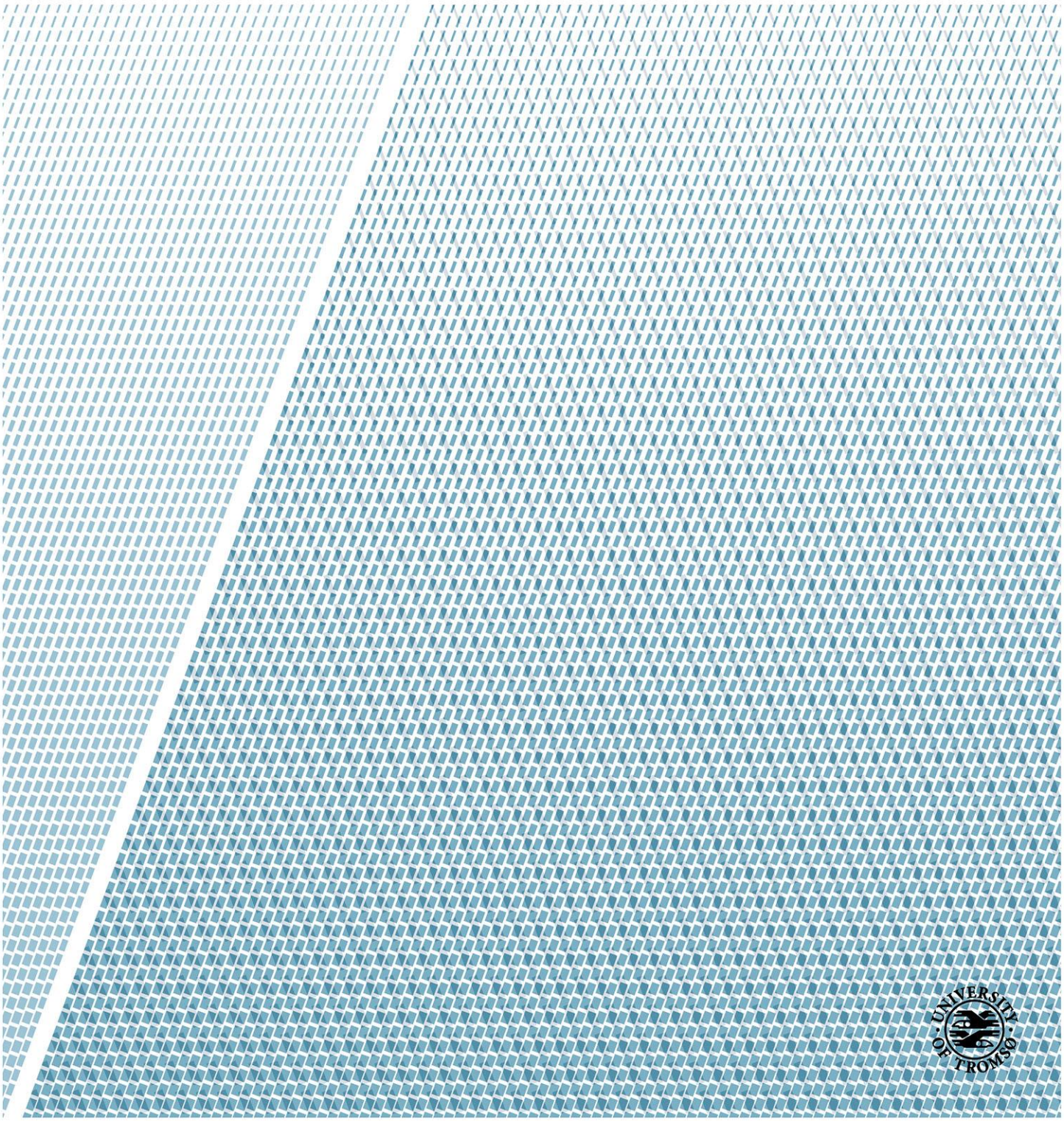

Year: 2016

Title: Identification of protein interaction candidates for the GOLD domain of FYCO1

www.munin.no

Acknowledgments

The work presented in this thesis was performed at University of Tromsø, Norway, from August 2015 to May 2016 at the Faculty of Health Sciences, Department of Medical Biology in the Molecular Cancer Research Group of Terje Johansen.

First, I would like to thank my main supervisor, Professor Terje Johansen, for the opportunity to be a part of this excellent research group, for his intelligence and support throughout the work and always being available for questions. I would also like to thank my co-supervisor, Associate professor Trond Lamark for all the guidance, support, enthusiasm and advice shown during the writing process.

Then, I will give a big thanks to my co-supervisor, Dr. Hallvard Olsvik, for great supervision, support, advice and being patient for all my numerous questions and sharing your knowledge throughout the project.

Thanks for all the fantastic people in the molecular cancer research group for the help in the lab, both in the mornings and in the late evenings, always answer my questions and sharing their knowledge. I would especially like to thank Gry Evjen, Hanne Brenne for all the help with the lab work, Aud Øvervatn for helping me with the cell experiments, Jack-Ansgar Bruun for all the excellent guidance and help with the mass spectrometry, Kenneth Bowitz Larsen for helping me with the confocal microscopy and Yakubu Abudu for his positivity and for allowing me to borrow plasmids.

Furthermore, I want to thank my fellow master students and friends Michael, Ibrahim, Bryan, for brightening up the time spent in the office, Christine, Merete, Sunniva, for all the support and encouragements in Tromsø.

Finally, I would like to thank all family, specially my parents Morten and Inger and my brother,Matin for all their love and support. A special thanks goes to Runar for all the support, encourage and for always cheering me and always believing in me and drag me out in the beautiful nature.

Tromsø, May 2016

Betty Martine Normann Furulund

Summary

Autophagy is an evolutionary conserved degradative pathway, where damaged or surplus cytosolic components are sequestered into double membrane vesicles, autophagosomes, which become degraded through the lysosomal system. The autophagy is a dynamic process, which is depended of transport of autophagosomes along microtubule, to become degraded by lysosomes. One of the proteins involved in this transport process is FYVE and Coiled-coil [CC] domain containing protein 1 (FYCO1). FYCO1 is involved in transporting autophagosomes and late endosomes along microtubules, in the plus-end direction, by interacting with kinesin. FYCO1 interacts with membranes through phosphatidylinositol-3 phosphate via its FYVE domain. It is regulated by RAB7 interaction, via its coiled-coil region, and involved in autophagy through its interaction with LC3, via its LIR-region. No interaction partners or roles for the N-terminal RUN domain or the C-terminal GOLD domain have been revealed. Interestingly, patients with autosomal-recessive congenital cataracts have been identified with a mutation, L1376P, in the GOLD domain of FYCO1. This mutation has been suggested to link FYCO1 and human lens development and transparency together. The major aim for this study was to identify putative interaction candidates for the GOLD domain and examine the effect L1376P mutation had on the GOLD domain. From our mass spectrometry study, the GOLD domain may seem to be involved in protein-protein interactions. 182 proteins co-precipitated together with the insolated GOLD domain, but it is unknown if these interact with the GOLD domain directly or indirectly. Of these proteins, TUBA4A, DNAJA1, TXNDC5, NIPSNAP1, NIPSNAP2 (GBAS), ARF4, VPS4A, RUVBL2 and MON1B were selected for further examination. The GOLD domain showed different distribution when co-expressed with TUBA4A and VPS4A. TUBA4A was showed to be located at the centrosome in association with the GOLD domain. TUBA4A redistribute the GOLD domain to centrosomes. In addition, VPS4A was observed to localize as aggregates, and it was shown in this study that the GOLD domain may be redistributed to these VPS4A structures. It is still unclear if these interactions with the GOLD domain are indirect or direct. In addition, we studied the L1376P mutation of the GOLD domain. This mutation dramatically changes the subcellular distribution of an over-expressed GFP-GOLD domain construct from diffuse to many small aggregate-like structures. If this mutation has a similar effect on the full-length FYCO1 this may perhaps affect the transparency of the lens of carriers of this mutation.

Abbreviations

aa	amino acid(s)
Ab	Antibody
APS	Ammonium peroxodisulfat
Atg	autophagy- related genes
CMA	Chaperone- mediated- autophagy
DMEM	Dulbecco′s Modified Eagle′s Medium
E.coli	Escherichia coli
ER	endoplasmic reticulum
FBS	Fatal bovine serum
FM	Full growth Medium
FYCO1	FYVE and coiled-coli domain containing protein 1
FYVE	Fab1p,YOTB, Vac1p and EEA1
GOI	Gene of interest
GOLD	Golgi dynamics
GST	Glutathione S- transferase
IP	Immunoprecipitation
IPTG	Isopropyl-β-D-thiogalactopyranoside
LB	Luria-Bertani
MEM	Minimum Essential Medium Eagle
ON	Overnight
PBS	Phosphate Buffered Saline
PFA	Paraformaldehyde
RT	Room temperature
RTL	Reticulocyte lysate
SDS-PAGE	Sodium Dodecyl Sulfate Polyacrylamide Gel Electrophoresis
SOC	Super optimal broth with Catabolite repression
TE	Tris-EDTA
TEMED	Tetramethylethylenediamine
WB	Western Blot

Table of contents

1 Introduction

1.1 The cytoskeleton

Eukaryotic cells are composed of a dynamic network of protein filaments known as the cytoskeleton. The cytoskeleton is important for cellular shape, motility and spatial organization of cytosolic components. It is divided into three major classes: actin filaments, microtubules (MT) and intermediate filaments (Fletcher and Mullins, 2010, Bershadsky and Vasiliev, 2012). Actin filaments are helical polymers of actin protein. They are highly concentrated beneath the plasma membrane, and are important for cellular shape and movement (Blanchoin et al., 2014). MT are long, hollow cylinders made of tubulin protein (*α-tubulin* and *β-tubulin*), which assembles into linear protofilaments. MT are highly dynamic structures due to their ability to quickly become polymerized and depolymerized. MT are polar structures that have plus and minus ends with differing polymerization and depolymerization rates. They are crucial for neural polarity (Conde and Caceres, 2009) as well as for intracellular transport of organelles (Vale et al., 1985). The transport along MT requires motor proteins and two set of motor proteins: kinesins and dyneins. Actin filaments and MT can both bind and hydrolyze nucleoside triphosphates and generate a force by assemble head-to tail polarization, which contribute to the movements (Conde and Caceres, 2009, Mourino-Perez et al., 2016). The intermediate filaments are ropelike fibers, made of intermediate filament proteins. Intermediate filaments are linked to adhesive structures, such as desmosomes (connects cells together) and provide mechanical strength (Herrmann and Aebi, 2004)

1.2 Vesicle and organelle movement by motor proteins on MT

Intracellular vesicles and organelles are transported along MT by the motor proteins kinesins and dyneins (Hirokawa, 1998). Movement along MT is dependent on a cycle of association and dissociation of ATP. Most kinesins transport vesicles and organelles along MT in a plus-end manner (*anterograde* transport), and move along MT at a steady and slow rate. Kinesin-1 is a plus-end heterotetramer with two heavy chains and two light chains, whit each heavy chain containing an N-terminal nucleotide-binding motor domain (Cardoso et al., 2009). Two light chain dyneins are minus-end directed MT motor proteins and interact with dynactin to start the transportation. Dyneins are the largest and the fastest among the known molecular motor proteins and move through association and dissociation of ATP (Allan, 2011). Motor proteins are involved in vesicular transport, which is important for cellular homeostasis.

1.3 Rab GTPase family

Rab proteins are master regulators in the endocytic pathway, regulating transport between organelles of endocytic- and secretory pathways with high specificity. The small monomeric G proteins (guanine nucleotide binding proteins) are Ras like GTPases, that mediate endosome targeting, by regulating docking and tethering. Through the Rab proteins intrinsic GTPase activity, they function as molecular switches by hydrolyzing guanosine-5` triphosphate (GTP) to guanosine-5 diphosphate (GDP (Stenmark, 2009). Rab proteins are important for linking membranous compartments to molecular motor proteins allowing for long distance transport of organelles along microtubule or actin tracks (Hammer Iii and Wu, 2002). A link has been discovered between different Rab proteins and autophagosomes in the regulation of autophagy (Ao et al., 2014).

1.3.1 Regulation of autophagosome maturation by Rab GTPases

The fusion- and transporting mechanisms of autophagosomes are regulated by Rab GTPases (Ao et al., 2014). One of the Rabs involved in autophagy is Rab7. It has been shown to regulate autophagosome formation (Lin et al., 2012) and maturation (Hyttinen et al., 2013). Rab7 is present on both late endosomes and autophagosomes. Rab7 is important for the fusion process via its binding to the homotypic fusion and protein sorting (HOPS) tethering complex. HOPS promotes tethering of membranes such as endosomes, vacuoles, autophagosome and lysosomes (Wang et al., 2011).

Rab7 regulates MT transport direction through recrutment of effectors such as FYVE and coiled-coil domain containing 1 (FYCO1) (Pankiv et al., 2010) and oxysterol-binding protein related protein 1L (ORP1L)/ Rab-interacting lysosomal protein (RILP) (Cantalupo et al., 2001, van der Kant et al., 2013). The vesicles transported along MT in a plus- end-direction are bound to kinesin through FYCO1s coiled-coil (CC) region, and are regulated through the FYCO1 interaction with Rab7 (Pankiv et al., 2010, Raiborg et al., 2015). In contrast, vesicles transported along MTs in a minus-end direction, are controlled and regulated by the production of the single multiprotein complex composed of dynein and HOPS complex. Through a combination of regulation and recruitment of HOPS complex and dynein motor proteins, MT minus- end transport and fusion can be regulated by the multiprotein complex, Rab7-RILP-ORP1L (van der Kant et al., 2013).

1.4 Cellular degradative systems

Cellular homeostasis is obtained by degradation systems regulating the quality and the quantity of cytosolic components, such as organelles and proteins. Eukaryotic cells have two main intracellular degradation systems: the proteasome and the lysosomal pathway (Pickart and Cohen, 2004, Saftig and Klumperman, 2009). Proteasomal degradation serves as a protein quality control. Short-lived and misfolded proteins are ubiquitinated and transported into the proteasomes, by chaperones, where they are degraded (Adams, 2003). Protein aggregates are degraded by the lysosomal degradation pathway. Lysosomes are the terminal part of the endocytic pathway, and contain high levels of acidic content in addition to hydrolytic enzymes. Damaged or surplus proteins and organelles from the intracellular space are targeted for lysosomal degradation, as well as macromolecules obtained from the extracellular space (Saftig and Klumperman, 2009). Autophagy is the main intracellular degradation system and targets proteins and organelles for lysosomal degradation (Mizushima and Komatsu, 2011). There are three major classes of autophagy: macroautophagy, microautophagy and chaperone-mediated-autophagy (CMA) (Figure 1.1). Macroautophagy is the major and most studies category of autophagy. Macroautophagy degrades proteins and organelles through the fusion of the double membrane autophagosome with the lysosome (Mizushima and Komatsu, 2011). In microautophagy, cytoplasmic components are engulfed by the lysosome through invagination of the lysosomal membrane (Li et al., 2011). In chaperone-mediated autophagy, substrates are directly translocated into lysosomes by the chaperone protein Hsc70 (heat shock cognate 70) and the lysosomal transmembrane protein, Lamp- 2A (Orenstein and Cuervo, 2010).

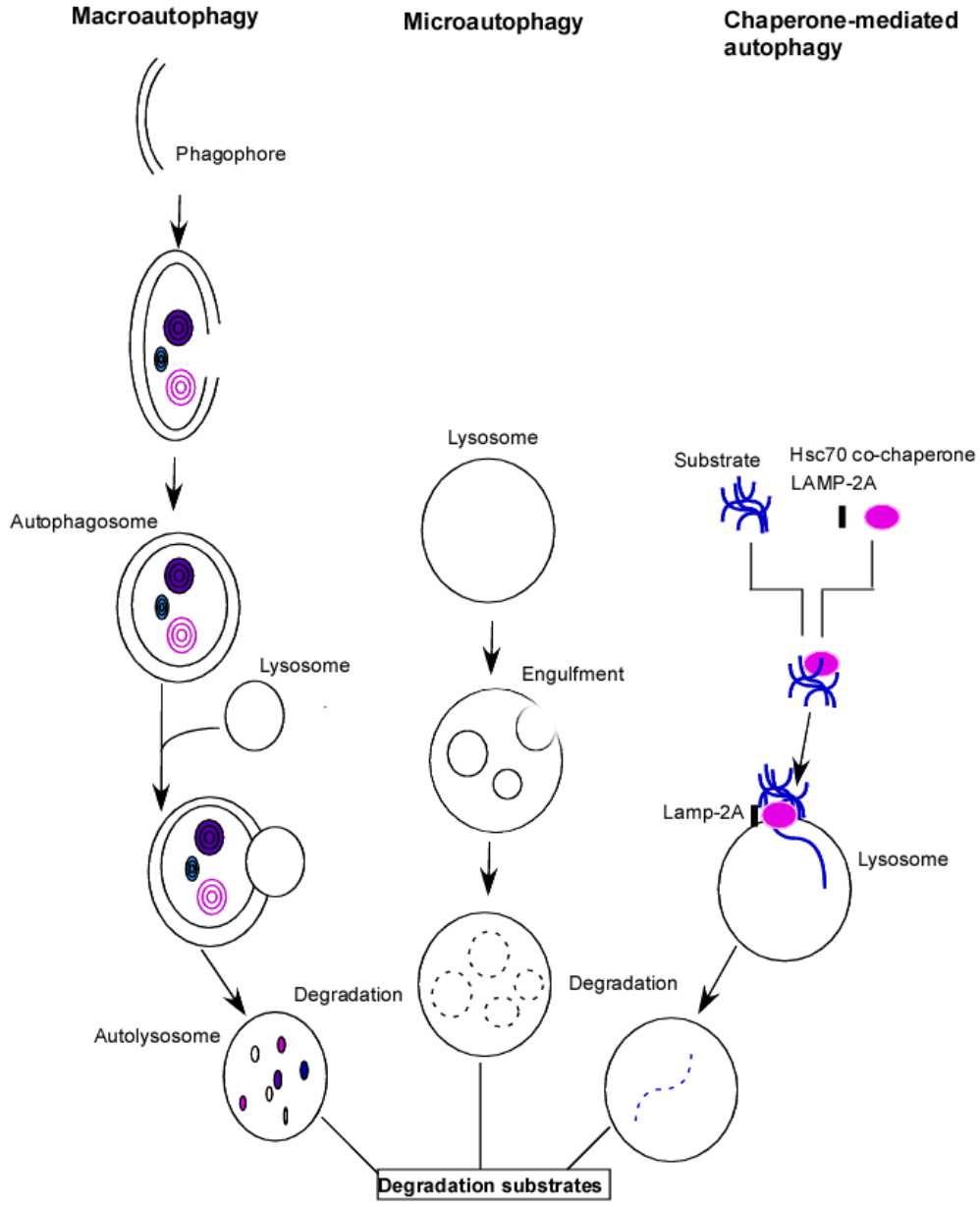

Figure 1.1: Autophagy classification. Autophagy is divided into three major classes: macroautophagy, microautophagy and chaperone-mediated-autophagy (CMA). Macroautophagy creates a double membrane structure (autophagosome) around the substrate, which is marked for degradation, by an autophagy receptor (i.e p62, NBR1). Degradation initiates once an autophagosome fuses with a lysosome. In microautophagy, the lysosome itself engulfs substrates, where it becomes degraded. Chaperone-mediated- autophagy (CMA) degrades ubiquitin-marked substrates, which becomes delivered into the lysosome with the help from chaperone-protein Hsc70 (Heat shock protein 70) and lysosomal transmembrane protein (Lamp-2A). All three autophagy classes produce degradation products such as, amino acids, which is used in anabolic processes. Figure adopted from (Mizushima and Komatsu, 2011).

1.4.1 Macroautophagy (hereafter autophagy)

Autophagy is an evolutionary conserved degradation pathway, where damaged or surplus cytosolic components are degraded through the lysosomal system. The degrading process is vital to maintain homeostasis, turnover and quality control of cellular compartments, and in avoiding accumulation of damaged and surplus compartments and proteins, which can become toxic for the cell. Nutrient deprivation, hypoxia, reactive oxygen species, damaged DNA, protein aggregates, damaged organelles, or intracellular pathogens are stress factors that can induce the autophagy process to reduce toxicity. Autophagy serves as a dynamic recycling system. It is important during starvation for the formation of new cellular building blocks (Mizushima and Komatsu, 2011). Autophagy sequesters marked substrates by enclosing them into a double-membrane vesicle called an autophagosome. The vesicle contents then become degraded through fusion with a lysosome. Autophagy can be both selective and unselective. In unselective autophagy, the bulk degradation process is important for cell energy homeostasis, whereas selective autophagy is important in organelle and protein quality control, in the defense against microbes, and for innate immunity and antigen presentation (Johansen and Lamark, 2011, Mizushima and Komatsu, 2011). Autophagy is a multistep process requiring transcriptional and translational regulation to start initiation and formation of autophagosomes that matures and becomes degraded.

1.4.2 The molecular machinery of autophagosome formation

The autophagic process is divided into initiation-, formation-, maturation- and degradation (Figure 1.2) (Mizushima et al., 2011, Mizushima and Komatsu, 2011). The autophagic process is regulated of autophagy-related (ATG/Atg) proteins. The ATG/Atg proteins are essential for the autophagic process. So far, at least 35 ATG genes have been identified, through yeast genetic studied, and 15 of these are core ATG genes, which are essential for the different autophagy pathways (Nakatogawa et al., 2009). Atg proteins are activated by different stress factors and make up different complexes.

The autophagosome formation is regulated by different signaling pathways, including growth factors, such as IGF1, and hormones. These signals further regulate the proteins in the pathway. For example, the mammalian target of rapamycin complex 1 (mTORC1) is known to inhibit the autophagy initiation. mTORC1 and AMPK regulates autophagy by phosphorylating of the ULK1 kinase,. They do this by directly phosphorylating ULK1 at different positions, which induces different effects. AMPK phosphorylates and activates ULK1, while mTORC1 phosphorylates and inactivates ULK1 (Kim et al., 2011). The autophagosome transport and

fusion is dependent on different regulators, which regulate adaptor proteins to bind to membranes and motor proteins.

In figure 1.2 the autophagy process is described for the mammalian system. Induction of the phagophore begins with the activation of the Unc-51- like kinase (ULK) complex 1/2. ULK 1/2 is activated together with FIP200, Atg13 and Atg101. This complex regulates the class III phosphatidylinositol 3-kinase (PI3K) complex (Vps34, Vps15, Beclin1, Atg14L and Ambra-1). Vacuolar protein sorting protein 34 (Vps34) produces phosphatidylinositol 3-phosphate (PI3P) by phosphorylating the phosphatidylinositol's. PI3P serves as an affinity membrane binding tag and recruits PI3P binding motifs (e.g.FYVE, Phox (PX) or PROPPIN- domains) (Lemmon, 2008). The formation of PI3P by PI3K initiates the nucleation step and formation of a cup-shaped double-membrane structure, known as the phagophore. The phagophore is established from either endoplasmic reticulum (ER), mitochondria, the Golgi apparatus or the plasma membrane (Tooze and Yoshimori, 2010, Mizushima et al., 2011, Hailey et al., 2010, Ravikumar et al., 2010). PI3Ps recruits different effectors, such as WIPI 1/2 (WD-repeat PI3P effector protein). WIPI2 binds directly to Atg16L, which is bound to the conjugate Atg5-Atg12 (Dooley et al., 2014). The Atg12 conjugation system (Atg12, Atg7, Atg10, Atg5 and Atg16) interacts with the LC3 conjugation system (LC3A/B/C or GABARAP; GABARAPL1 and GABARAPL2/GATE-16) (Atg8 in yeast). LC3 becomes processed by Atg4 (cysteine protease) and the E2-like protein Atg3 is recruited by the Atg12 conjugate system, and lipidated LC3-I to LC3-II. LC3-II is conjugated to the lipid phophatidylethanolamine (PE) by the E1-like enzyme Atg7, which binds to the phagophore (Mizushima et al., 2001) (formation step). This conjugation results in the LC3 insertion into the inner and outer phagophore. LC3 serves as a receptor for selective autophagic receptors (i.e SQSTM1/p62 and NBR1) (Noda et al., 2010). These receptors direct marked substrates for degradation by their interaction with LC3. The phagophore become closed into an autophagosome. This autophagosome becomes fused with the lysosome and becomes an autolysosome (Johansen and Lamark, 2011)(maturation step). The substrates are degraded by lysosomal hydrolases, and are subsequently recycled back to the cytoplasm by permeases (Johansen and Lamark, 2011, Mizushima et al., 2011) (degradation step).

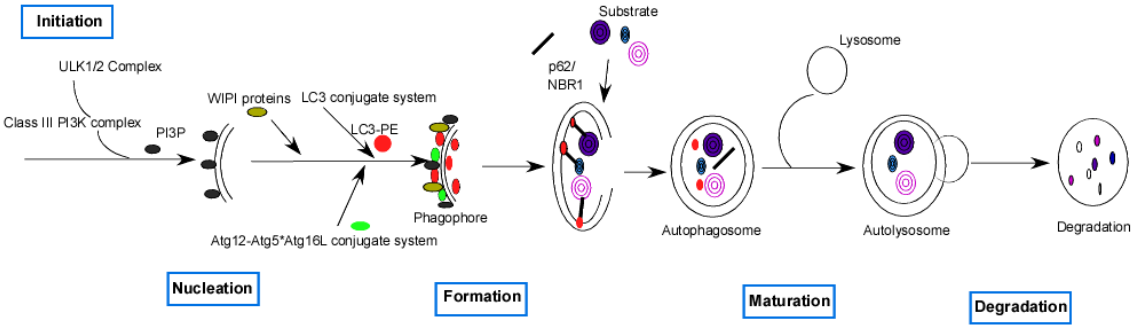

Figure 1.2: The overall mechanism of the mammalian autophagy process. Unc-51- like kinase (ULK) complex 1/2 becomes initiated by different stress factors and regulates the Class III phosphatidylinositol 3-kinase (PI3K) complex. Class III PI3K complex induces the formation of the nucleation site where the phosphatidyl-inositol becomes phosphorylated to PI3P. The formation of double membrane structure, phagophore, develops and WIPI proteins can be recruited. LC3 from the LC3-cpnjugation system attaches to the outer and inner side of the phagophore. Atg12--Atg5-Atg16L conjugate systems continues the formation of the phagophore. Derivative substrates are subsequentlys delivered to autophagy receptor, such as p62 or NBR1, which bind to LC3 on the inner side of the phagophore. The phagophore closes and becomes the autophagosome. The matured autophagosome fuses with the lysosome, and becomes the autolysosome. Here, all substrates become degraded.

1.5 FYVE and coiled- coil domain containing 1 (FYCO1)

FYCO1 is found as a single copy gene in humans, located in the putative tumor suppressor region on chromosome 3p21.3, called the"common eliminated region 1 ", C3CER1 (Kiss et al., 2002) is 1478 amino acids (aa) long and contains an N-terminal RUN (RPIP8, UNC-14, and NESCA) domain, a long coiled-coil (CC) region, a FYVE (Rab1, YOTB, Vac1 and EEA1) domain, a LIR (LC3 interacting Region) region, and a C-terminal GOLD (Golgi dynamics) domain (Figure 1.3) (Pankiv et al., 2010).

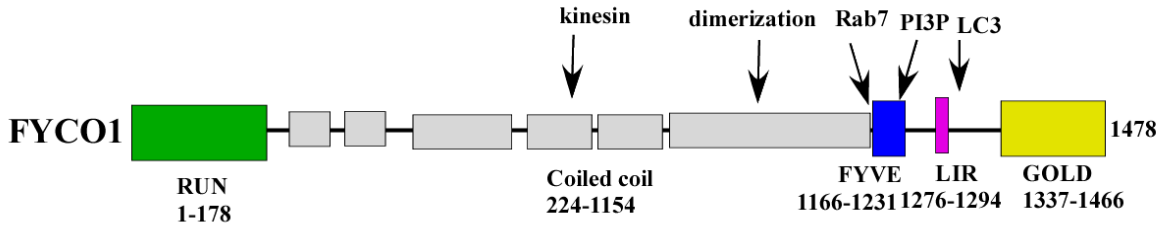

Figure 1.3: Domain architecture of human FYCO1. FYCO1 is divided into RUN-, Coiled-coli-, FYVE-, LIR region and GOLD domain. Kinesin- 1 binding requires the Coiled-coil, Rab7 requires the N-terminal part of FYVE-domain, PI3P requires the FYVE domain and LC3 binds to FYCO1`s LIR domain between amino acids 1276-1394.

There are proteins that share domain similarity with FYCO1 (Figure 1.3), and these proteins share similarities with their domain architecture as well. Two asuch proteins are presented in figure 1.4: the RUN and FYVE domain contain proteins (RUFY) and Early Endosome Antigen1 (EEA1) (Figure 1.4) (Rose et al., 2005). These are both associated with vesicles (Kitagishi and Matsuda, 2013). The PI3P lipid-binding domain (FYVE domain) on the C-terminus of the central 850aa CC region is common for all three proteins (Gaullier et al., 1998).

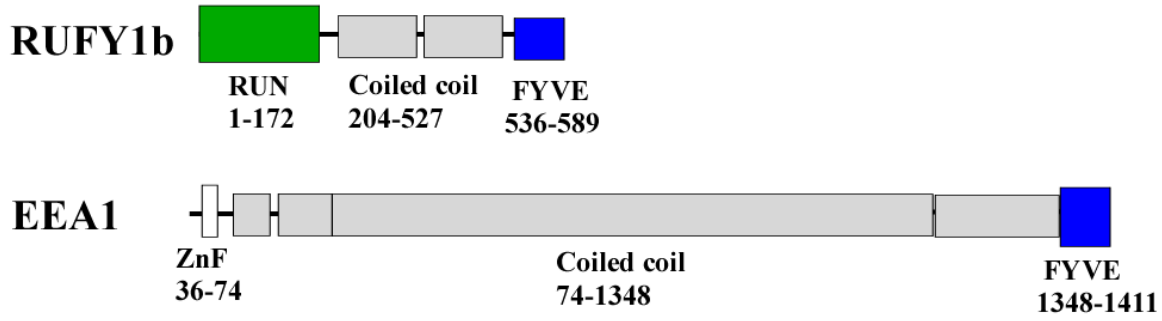

Figure 1.4: The alignment of the two homologue proteins of FYCO1. RUN-domain, RUN and FYVE domain contain protein 1(RUNFY1) and Early Endosome Antigen1 (EEA1). Recreated from Pankiv et al (Pankiv et al., 2010).

1.5.1 The functional role of FYCO1

Previous study of FYCO1 revealed its role in transport of vesicles such as late endosomes (LE), autophagosomes and autolysosomes (Pankiv et al., 2010). The function of its RUN domain is still unknown, however it is predicted, through knowledge about similar proteins (RUFY 1-4), that it may facilitates interaction between FYCO1 proteins and Rab, and Rap proteins (Callebaut et al., 2001, Recacha et al., 2009). The RUN-domain of RUFY proteins have been suggested to be involved in membrane trafficking and cell polarity. This could suggest that proteins containing a RUN- domain can interact with filamentous networks, such as actin or MT (Kitagishi and Matsuda, 2013). FYCO1 dimerizes by its long CC region (Pankiv et al., 2010). The FYVE domain interacts with PI3P, which is essential for its membrane recruitment (Gaullier et al., 1998). In addition, the C-terminal part of the CC region ($FYCO1_{990\text{-}1233}$) (adjacent to FYVE domain) is found to interact with Rab7, which is responsible for LE and lysosome membrane recruitments (Pankiv et al., 2010). These vesicles contain p62/SQSTM1, which co-localizes with the lysosome marker LAMP1 and Atg5. This reveals the presence of FYCO1 on the outer membrane of autophagosomes and autolysosomes (Pankiv et al., 2010). The LIR region of FYCO1 (1276-1294 amino acids) was found to be essential for LC3B

interactions (Pankiv et al., 2010). FYCO1 was previously thought to have membrane tethering functions, and a mechanism for its selective autophagosomal membranes recruitment. However, more recently, FYCO1 was identified as an LC3 and Rab7 effector protein, which enables the MT plus-end directed transport of vesicles (Figure 1.5) (Pankiv et al., 2010).

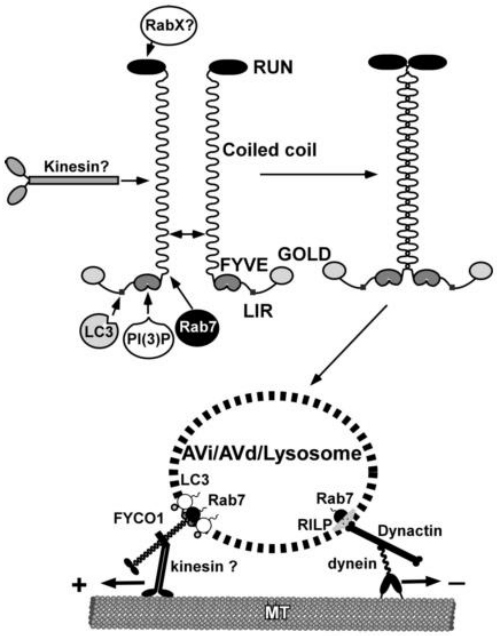

Figure 1.5: Illustration of the supposed role of FYCO1. A model of the proposed function of FYCO1 in vesicle trafficking along microtubule. The figure is obtained from Pankiv et al (Pankiv et al., 2010).

Congenital cataracts (CC) is the cause of vision loss in approximately one third of infants born blind (Robinson et al., 1987). Interestingly, mutations in FYCO1 have been identified, which could be a cause of autosomal-recessive congenital cataracts (arCC). Most of the mutations resulted in truncated forms of the protein and caused termination of the peptide chain before the GOLD domain. One of these mutations is a homozygous single base change from leucine to proline in exon 16, position 1376, which is located in the GOLD domain. This mutation was identified to affect the transparency of the lens. This highlights a role for FYCO1 in human lens development and transparency (Chen et al., 2011). Another study revealed a direct recruitment of FYCO1 to Dectin-1 phagosomes by LC3 (Ma et al., 2014). FYCO1 co-localize with LC3B to Dectin-1 phagosomes and facilitates the maturation of early $p40phox^{+}$ (early endosome marker) phagosomes into $LAMP1^{+}$ phagosomes (Ma et al., 2014). Interestingly, FYCO1 is found to be working together with the ER-protein, protruding, in mediating microtubule-dependent transport of LE via ER-endosome contact sites, which results in cell protrusions and neurite outgrowth (Raiborg et al., 2015). In the same year, Olsvik showed that FYCO1 contains a C-terminal LIR domain. This LIR domain contains an acidic residue on position 8 and a hydrophobic residue on position 9, which were found to be important for its efficient binding

to LC3B. Therefore this LIR-domain facilities the efficient maturation of autophagosomes during basal autophagy conditions (Olsvik et al., 2015). In previous studies, the expression of FYCO1 resulted in accumulation of lysosomes at the cell periphery, which is part of the indication of its lysosomal transport abilities (Johnson et al., 2016). Today, the function of the GOLD domain of FYCO1 is still unknown, but further studies may hopefully reveale its role.

1.5.2 The GOLD domain

The Golgi complex plays a key role in the modification and sorting of proteins received from the ER. Several eukaryotic golgi- and lipid-traffic proteins are involved in these processes and have a GOLD (Golgi dynamics) domain. The size of the GOLD domain is between 90 and 150 amino acids long and is conserved in other proteins, as such as p24 family proteins, Sec14-like proteins and GCP60 (Anantharaman and Aravind, 2002). The predicted structure of the GOLD domain of FYCO1 was obtained from Phyre^2 database (Kelley et al., 2015) was showed to be composed of six to seven compact all- β-strands (Figure 1.6) (Anantharaman and Aravind, 2002).

Figure 1.6: Graphic illustration of the GOLD domain of FYCO1. A graphic illustration over the two dimensional structure of the β-barrell strands of the GOLD domain, obtained from Phyre^2 (Kelley et al., 2015)The predicted structure of the GOLD domain of FYCO1 was showed to be composed of six to seven compact all- β-strands.

GOLD domain containing proteins

p24 family proteins are highly conserved type 1 transmembrane proteins (TMED1), containing a GOLD domain (Schuiki and Volchuk, 2012). The p24 family consists of heterotetramer proteins, which contain a GOLD domain in their N-terminus, next to the CC-region. Ten p24 proteins have been identified in in most vertebrates (whereas one is a pseudogene in humans) and they are divided into the four subclasses: p24α, β, γ and δ (Strating et al., 2009, Schuiki and Volchuk, 2012). They have a central role in protein transport from ER to Golgi. In addition to retrieval of escaped cargo and recycling of essential components via the retrograde pathway (Schuiki and Volchuk, 2012). The GOLD domain of p24γ_2 was thought to interact with

glycosylphosphatidylinositol-anchored proteins (GPI-AP). However, recent studies showed that the GOLD domain is not involved in GPI recognition. Instead, the motifs in the membrane-adjacent α-helical region of p24γ_2 were found to be involved in the integration of these proteins into coat protein complex II-coated transport vesicles. These findings suggest that the function of the GOLD domain still is unclear for p24 (Theiler et al., 2014).

The GOLD domain has been identified in other proteins, such as Sec14-like proteins, Transmembrane emp24 domain containing protein 1 (TMED1/p24 family protein gamma-1) and Golgi adaptor acyl coenzyme A (acyl-CoA) binding domain protein 3 (ACBD3/GCP60). A multiple sequence alignments from Clustal Omega (Sievers et al., 2011, Goujon et al., 2010) shows which amino residues are conserve through their GOLD domain (Figure 1.7). The amino acids composition of the different GOLD domains differs from each of the proteins. These GOLD domain proteins are often found together with fatty acid -, lipid- or sterol binding domains such as CRAL-TRIO, FYVE, pleckstrin homology (PH), acetyl CoA- and oxysterol binding domain (Anantharaman and Aravind, 2002).

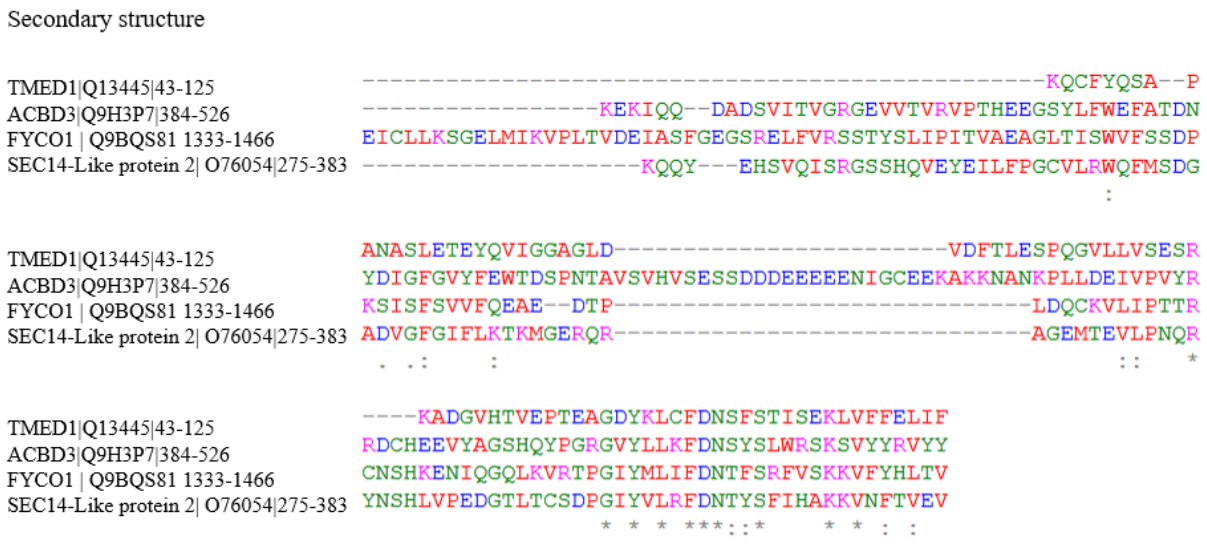

Figure 1.7: Alignment of the protein sequences of GOLD domain containing proteins. A multiple alignment was obtained from Clustal Omega (Sievers et al., 2011, Goujon et al., 2010). The sequence alignment is of the GOLD domain of FYCO1, SEC14-like protein 2, ADCBD3/ GCP60 and TMED1 (type 1 transmembrane proteins, p24 family). * (asterisk) indicates positions which have a single, fully conserved residue. . (period) indicate conservation between groups with weakly similar properties-scoring ≤0.5 in the Connet PAM 250 matrix and : (colon) indicates conservation between groups of strongly similar properties - scoring > 0.5 in the Gonnet PAM 250 matrix. Color description of the residues: The magenta are basic-H residues, the red are small (small + hydrophobic and aromatic) residues, blue are acidic residues, green are hydroxyl + sulfyfryl + amino residues and grey are unusual amino/imino acids(European Bioinformatics Institute (EMBL-EBI), 2016).

Sec14-like proteins are involved in secretion. SEC14-like domain of supernatant protein factor (SPF) are involved in the sterol endo-synthesis. SPF is found in complex with 2,3-oxidosqualene. This ligand binding was enabled by the removal of its GOLD domain. These results suggest that its GOLD domain acts as a regulator (Christen et al., 2015). The GCP60 protein is a peripheral protein, which interacts with the cytoplasmic C-terminal part of the Golgi integral membrane protein Giantin (Sohda et al., 2001).

The functional role of the GOLD domain

The complete function of the GOLD domain is still unknown, but a protein-protein interaction function was identified in some GOLD domain containing proteins (Anantharaman and Aravind, 2002).

Previous studies have shown that the GOLD domain functions as a cargo binding site and that the GOLD domain is involved in more than only protein-protein interactions. There is evidence that GOLD domain containing proteins are involved in assembly of membrane-associated complexes and regulate the cargo assembly into membranous vesicles, as revealed by Anantharam and Aravind (Anantharaman and Aravind, 2002). The GOLD domain was previously observed in sugar- and lipid-binding proteins (Gaskell et al., 1995).

Therefore, it was predicted that the GOLD domain function of FYCO1 is related to the GOLD domain function of other similar proteins. However, the GOLD domains can have different functions due to their composition of the amino acids, and where it is located inside the protein. The multiple sequence alignment (Figure 1.7) showed that GOLD domains are not identical in their amino acids distribution.

1.5 Mass spectrometry as a tool for protein identification

Proteomics is defined as the large-scale study of the structure and function of proteins. Mass spectrometry (MS) has become one of the most used methods for identification and analysis of complex protein samples. MS-based proteomics has become easier to use for protein study, due to the ability to use gene and genome sequence databases (Aebersold and Mann, 2003). MS groups individual ions according to their mass and their total charge, carried out on ionized analyte in a gas-phase, and consists of an ion source, a mass analyzer and a detector (Figure 1.8).

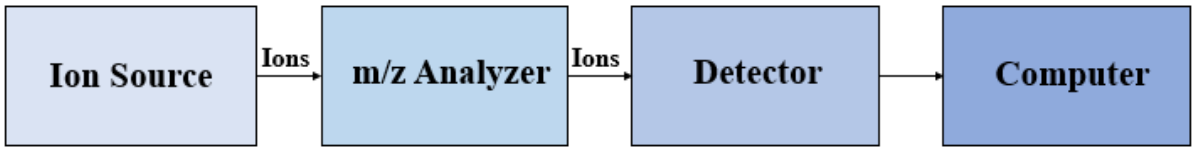

Figure 1.8: Illustration of the major components of a mass spectrometer. The ionization starts at the ion source, where the ions are transferred through the m/z analyzer, the detector and then the mass-to-charge-ratio is calculated in the computer.

The entire system works in a vacuum. Before applying the protein samples for identification, all proteins have to be digested into small peptide fragments. This digestion is done by proteases most commonly trypsin. Trypsin is a serine protease that specifically cleaves peptide bonds at the C-terminal side of lysine- and arginine-residues (Olsen et al., 2004). These peptides are fractionated by a liquid-chromatograph (LC) and can be ionized by an electrospray ionization (ESI) (Fenn et al., 1989). The soluble protein sample is converted into a gas phase when it is sent into MS. The liquid-chromatography-MS (LC-MS) is used to measure the mass of each protein peptide. LC-MS/MS (Tandem MS) fragment peptides through collision-induced dissociation (CID) or high energy collision dissociation (HCD) (Vogeser and Parhofer, 2007). LC-MS/MS is used as an analytical tool to identify protein-sequences based on the molecular mass of the particle and/or fragments in a complex sample, and is today the most used method in MS-based proteomics to analyze complex peptide mixture (Aebersold and Mann, 2003).

Protein identification is generally done through the use of already known protein sequences from a protein databases. Universal protein resource (UniProt) (Consortium, 2015) was used as the database for protein identification in the current study (UniProt, 2016). Each MS/MS spectrum uses their fragment spectrums to identify a specific protein. All of these spectrums have to correlate with the same protein. The value of the confidence depends on the correlation with the peptide amounts. The high heterogeneity produced by MS/MS data makes up for the limitation of its protein identification. Peptide fragments are identified through a database that compares the peptide fragments and a software is subsequently used to collect the protein data and develop a list over all protein candidates identified by LC-MS/MS. In the current study, Proteome Discover 2.1 Software (Thermo Scientific™) was used for protein identification.

1.6 Aims of study

The initial aim of this study was to reveal and identify new protein interaction candidates for the RUN- and the GOLD domain of FYCO1. This would give us a greater insight over the complete function of FYCO1. However, RUN domain was excluded, because of technical problems and time limitations. Therefore, the GOLD domain became the major focus. A mutation in the GOLD domain (L1376P) was observed in patients with autosomal-recessive congenital cataracts. We were interesting if this mutation affected the expression level and the cellular localization of the isolated GOLD domain.

By addressing the following questions, we hope to obtain a better understanding and determination of the full-length FYCO1s ability to interact with other proteins through its GOLD domain and how the mutation affects the localization and expression of the isolated GOLD domain in cells.

- Is the GOLD domain involved in protein-protein interactions?
- Which proteins do the GOLD domain interact with?
- Are these direct or indirect interactions?
- Does the transiently transfected GOLD domain redistribute some of the co-transfected putative protein partners?
- How does the L1376P mutation affect the expression and localization of the isolated GOLD domain?

2. Materials and methods

2.1 Materials

Table 2.1: Plasmids and expression constructs

Vectors	Description	Source
Gateway cloning vectors		
pDest-EGFP-C1	Mammalian EGFP fusion expression vector; CMV promoter, Ampicillin resistant. Located at the N-terminal end.	(Lamark et al., 2003)
pDest-mCherry-C1	Mammalian mCherry fusion expression vector; backbone as pDest-EGFP-C1 Ampicillin resistant. Located at the N-terminal end.	(Pankiv et al., 2007)
pDest-myc-C1	Mammalian myc-tag fusion expression vector; CMV promoter ant T7 promoter, Ampicillin resistant. Located at the N-terminal end.	(Lamark et al., 2003)

Vectors	Description	Source
cDNA constructs made by site-directed mutagenesis and Gateway® LR reaction		
pENTER-FYCO1 (1333-1478)	Gateway® Entry vector for the GOLD domain of FYCO1	(Pankiv et al., 2010)
pENTER-FYCO1 (1333-1478) L1376P	Made by site-directed-mutagenesis of pENTER- FYCO (1333-1478)	In this study
pDONOR221-RUVBL2	Gateway® Entry vector	Harvard Plasmid Repository
pDONOR221-TUBA4	Gateway® Entry vector	Harvard Plasmid Repository
pDONOR221-DNAJA	Gateway® Entry vector	Harvard Plasmid Repository

pDONOR221-ARF4	Gateway® Entry vector	Harvard Plasmid Repository
pDONOR221-TXNDC5	Gateway® Entry vector	Harvard Plasmid Repository

Vectors	**Description**	**Source**
Other vectors		
pDestEGFP-VPS4		(Bishop and Woodman, 2000)
pDest-Myc-MO1B		In this study
pDest-Myc-GBAS		In this study
pDest-Myc-NIPSNAP1		In this study
pDestEGFP-FYCO1(1-1478)	Full-length FYCO1	(Pankiv et al., 2010)
pGEX-4T-1	Bacterial GST fusion expression vector with a tac promoter. Used as an control	In this study
EGFP-KDEL	ER marker	In this study

Table 2.2: cDNA constructs made by Gateway® LR reaction (this study)

Vectors	**Description**
cDNA construct used in this study, made by Gateway® LR reaction	
pDest-15-FYCO1(1333-1478)	From pENTR- FYCO1(1333-1748)
pDest-EGFP-FYCO1(1333-1378)	From pENTR- FYCO1(1333-1748)
pDest-EGFP-FYCO1(1333-1378) L1376P	From pENTR- FYCO1(1333-1748) L1376P
pDest-mCherry-FYCO1(1333-1378)	From pENTR- FYCO1(1333-1748)

pDest-mCherry-FYCO1(1333-1378) L1376P	From pENTR- FYCO1(1333-1748) L1376P
pDest-myc- RUVBL2	From pDONOR221-RUVBL2
pDest-myc-TUBA4A	From pDONOR221-TUBA4A
pDest-myc-DNAJA1	From pDONOR221-DNAJA1
pDest-myc-TXNDC5	From pDONOR221-TXNDC5
pDest-myc- ARF4	From pDONOR221-ARF4
pDest-mCherry-RUVBL2	From pDONOR221-RUVBL2
pDest-mCherry-TUBA4A	From pDONOR221-TUBA4A
pDest-mCherry-TXNDC5	From pDONOR221-TXNDC5

Table 2.3: Primers for site-directed mutagenesis

cDNA clone	**Primer name**	**Sequence**
pENTER-FYCO1 (1333-1478) L1376P	pENTER-FYCO1 (1333-1478) L1376P primer forwar	5`-CCAGCACCTACAGCCCGATCCCCATCACTGTGG-3`
	pENTER-FYCO1 (1333-1478) L1376P primer reverse	5`-CCACAGTGATGGGGATCGGGCTGTAGGTGCTGG-3`

Note: In this study all plasmid constructs made by site-directed mutagenesis or gateway® LR reaction were verified by restriction digestion and/or DNA sequencing.

Table 2.4: Sequencing primers

Primer name	Primer sequence	Information
M13 Forward	5`-GTTTTCCCAGTCACGACGTTGTA-3`	Used in this study to sequence inserts in pDONOR221
M13 Reverse	5`-GCGGATAACAATTTCACACAGGA-3`	Used in this study to sequence inserts in pDONOR221
ENTR 3`	5`-GATTTTGAGACACGGGCCA-3`	Used in this study to sequence inserts in pENTR223
ENTR 5`	5`-GTTAGTTACTTAAGCTCGG-3`	Used in this study to sequence inserts in pENTR223
GST-C1	5`- CATGGTCCTGCTGGAGTTCGTG-3`	Used in this study to sequence inserts in pDest-EGFP

Table 2.5: Restriction enzymes

Enzyme name	Recognition sequence (5`-3`)	Concentration (U/ml)	Reaction buffer	Supplier
BsrGI	TGTACA	10.000	Neb 2.1	New England Biolabs
HindIII- HT	AAGCTT	20.000	Cutsmart	New England Biolabs
SacI	GACGCTC	20.000	Cutsmart	New England Biolabs

Table 2.6: Antibodies (Ab) used for Immune fluorescence and IP

	Antibody	Supplier	Dilution
Primary Ab	Rabbit anti- GFP (#ab-290)	Abcam	1:2000
	Mouse anti-γ-tubulin #T6557	Sigma	1:2000
	Mouse anti- myc #MM-0169	Medimabs	1:200
	DRAQ5™	BioStatus	1:2000
Secondary Ab	Alexa Fluor® 647	Life technology	1:1000

	Goat-anti mouse		
	Alexa Fluor® 555 Goat-anti mouse	Life technology	1:1000

Table 2.7: Bacteria strains and growth medium

Bacteria strains	
Escherichia. coli	**Description**
DH5α	E.coli strain used for storage of plasmids
SoluBL21 (DE3)	Strain used for protein expression

Table 2.8: Concentration of antibiotic in bacterial growth medium

Antibiotic	**Concentration (µg/ml)**
Ampicillin (amp)	100
Kanamycin (kan)	50
Spectinomycin	50
Gentamycin	10

Table 2.9: Cell lines and their growth medium and buffers

Cell line	Description	Full Growth medium (FM)
HEK 293 Flp-In™ T-REx cells (Invitrogen # R78007)	Human embryonic kidney cells with Flp-In™ T-REx system. This cell line is design for rapid generation of a stable expression of a protein of interest by an Flp-In™ expression vector and a tetracycline-inducible expression of a gene of interest from a specific genomic location (Invitrogen, 2010).	Dulbecco′s Modified Eagle′s Medium (DMEM) (Sigma,D6046) 10% Fetal bovine serum (FBS) (Merck) 100 µg/ml Pencillin 100 µg/ml Streptomycin
HEK 293 Flp-In ZnF-FYCO1 #12	Human embryonic kidney cells These cells are knockout for full-length FYCO1 by Zink finger system. Published in our recent JBC paper (Olsvik et al., 2015)	Dulbecco′s Modified Eagle′s Medium (DMEM) (Sigma,D6046) 10% Fatal bovine serum (FBS) (Merck) 100 µg/ml Pencillin 100 µg/ml Streptomycin
HEK 293 Flp-In ZnF-FYCO1 #12 GFP-FYCO1	Human embryonic kidney cells These cells are stably expressing GFP-FYCO1 controlled by tetracycline. .Tetracycline turn on the GFP-FYCO1 expression.	Dulbecco′s Modified Eagle′s Medium (DMEM) (Sigma,D6046)

	Published as above	10% Fetal bovine serum (FBS) (Merck) 100 µg/ml Pencillin 100 µg/ml Streptomycin
HeLa (ATCC® CCL-2™)	Human cervical carcinoma cells	Minimum Essential Medium Eagle (MEM) (Sigma, M4655) 10% Fetal bovine serum (FBS) (Merck) 100 µg/ml Pencillin 100 µg/ml Streptomycin
B-3 (ATCC® CRL-11421™)	Human lens cells	Minimum Essential Medium Eagle (MEM) (Sigma, M4655) 20% Fetal bovine serum (FBS) (Merck) 100 µg/ml Pencillin 100 µg/ml Streptomycin

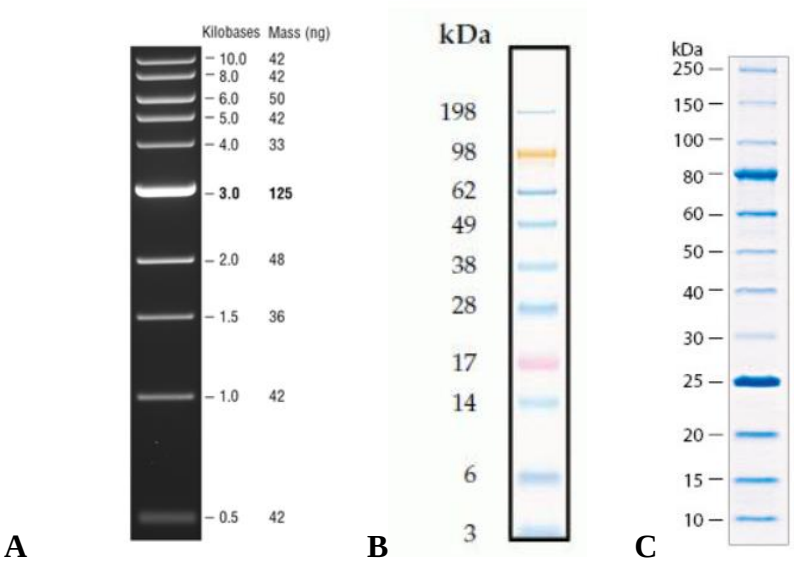

A **B** **C**

Figure 2.1: Molecular weight ladder for DNA and proteins: **A:** 1 kb DNA ladder (Neb, #N3232L). **B:** SeeBlue®Plus2 Pre- Stained Protein Standard (Thermofisher scientific, # LC5925) for visualize proteins on SDS-PAGE gel. **C:** Unstained protein ladder (10-250 kDa) (Neb, # P7703S) for 10- 20% SDS-PAGE.

2.2 Methods

2.2.1 Overview of the study

In the first part of the project, we sought to identify protein interactors binding to the GOLD domain of FYCO1 (amino acids 1333-1478), using affinity purification coupled to mass spectrometry (MS). Recombinant GOLD domain (1333-1478) of FYCO1 fused with a GST-tag was expressed in competent *E.coli* strain, soluBL21™ (AMS Biotechnology). The GST-GOLD domain was purified through pulldown with Glutathione sepharose beads. The interaction study was done using extracts from HeLa and HEK293 Flp-In T-REx cells. These cells were grown in full media, and lysed for *in vitro* pulldown assay. The pulldown assay was done with GST-bound GOLD domain to detect protein-interactors. The possible protein-interaction-candidates were obtained by proteomics studies. In the second part of the study, these possible new protein-interaction-candidates were further studied through *in vivo* and *in vitro* study.

2.2.2 Transformation of competent bacteria cells

Bacteria transformation is the genetic alternation of bacteria, where competent bacteria take up naked DNA from the extracellular environment. This DNA becomes integrated into the genome or maintained as a plasmid. Transformation can occur naturally by closely related bacterias, but this process occurs at a slow rate. Certain bacteria can become competent by chemical or mechanical exposure. This treatment weakens the cellular membranes, which increases the efficiency of DNA uptake. Competent cells can be prepared through calcium chloride ($CaCl_2$) or rubidium chloride (RbCl) treatment. Bacterias used in the current study are $CaCl_2$ competent and prepared by laboratory technicians.

The transformation procedure can be done by two commonly used methods, by either electroporation or heat shock. Both methods make pores in the plasma membrane for DNA uptake. In this current study, the heat shock procedure was used.

Two different E.coli strains were used during this study: DH5α (Bethesda Research Laboratories Inc.) and SoluBL21 (DE3) (AMS Biotechnology (AMSBIO) (see description in the table 2.7).

Bacteria transformation procedure

1. Competent bacteria cells were thawed on ice.
2. 50 µl bacteria cells were mixed together with 100-150 ng plasmid (DNA of interest). The tubes were flicked 4-5 times to mix (do not vortex).
3. The transformation mixture was held on ice for 20-30 minutes.
4. The transformation mixture was incubated at 37^0C (water bath) for 2 minutes.
5. The transformation mixture was held on ice for 2 minutes.
6. 500 µl catabolite repression (SOC) (room temperate) medium was added to the transformation mixture and incubated at 37^0C for 1 hour with shaking.
7. LB-agar plates (with required antibiotics) was moved from 4^0C to room temperature.
8. 250 µl of the transformation mixture were plated into the LB-agar plates with appropriate antibiotic and grown overnight at 37^0C.
9. The following day, three colonies were transferred into three cylinders with 5 ml LB media with appropriate antibiotics and regrown overnight for plasmid purification. Freezing stocks were made from these overnight cultures.

Procedure for freezing down bacteria cells

1. One colony was transfer to 5 ml pre-warmed LB medium with appropriate antibiotics and incubated overnight at 37^0C.
2. 1.2 ml overnight bacteria culture was mixed with 300 µl sterilized 50% Glycerol (Sigma). This was divided into tubes and store at -70^0C. Always keep on ice.

Super optimal broth with Catabolite repression (SOC) media
20 g Bacto Trypton
5 g Bacto yeast extract
10 ml 250mMKCl
5 g $MgCl_2$
20 mM glucose
dH_2O to 1 L
pH adjusted to 7.5 with NaOH

LB (Luria-Bertani)- agar plate
10 g Bacto Trypton
5 g Bacto yeast extract
10 g NaCl
15g Agar
dH_2O to 1 L
pH adjusted to 7.5 with NaOH

LB medium
10 g Bacto Trypton
5 g Bacto yeast extract
10 gNaCl
dH_2O to 1 L
pH adjusted to 7.5 with NaOH
Antibiotic:
100 µg/ml Ampicillin
50 µg/ml Kanamycin

2.2.3 Plasmid purification

Plasmids from bacteria cells were purified by GenElute™ Plasmid Miniprep system (Sigma, #PLN350). Through this purification system, plasmid DNA is purified by an alkaline denaturation of high molecular weight chromosomal DNA, wherein the closed circular plasmid DNA remains double stranded, and through neutralization it becomes a part of the supernatant. The chromosomal DNA renatures and remains as pellet in the tube, while small and large plasmid DNA in the supernatant is extracted (Birnboim and Doly, 1979). The plasmid DNA is absorbed onto a silica membrane in the presence of high salts, where it is washed. After washing, the bound plasmid DNA becomes eluted in a Tris-EDTA buffer (Sigma).

Procedure for GenElute™ Plasmid Miniprep kit (Sigma Aldrich)

1. Cells were pelleted from 1-3 ml overnight culture by centrifuge at ≥12.000xg for 1 minute. The supernatant was discarded.
2. Cells were suspend cells inn 200 µl resuspension Solution by pipetting.
3. 200 µl Lysis solution was added and the tubes were invert gently to mix. The reaction mixture were incubated for ≤ 5minutes.
4. 350 µl Naturalization Solution (S3) was added to the solution.
5. The cell solution was pelleted by centrifugation at ≥12.000xg for 10 minutes.
6. 500 µl Column preparation Solution was added to the binding column in a collection tube. It was centrifuged at ≥12.000xg for 10minute. The flow- through was discarded.
7. The cleared lysate from step 5 was transferred into the binding column.
8. The binding column was centrifuged for 1minute. The flow- through was discarded.
9. For optimal ($EndA^+$ strains only) wash: 500µl Optional Wash Solution was added to the binding column. Centrifuged for 1 minute. The flow- through was discarded.
10. 750µl Wash Solution was added to the binding column. Centrifuged for 1 minute. The flow- through was discarded.
11. The empty binding column was centrifuged for 1-3minute
12. The purified plasmid DNA was eluted by transferring binding column into a new collection tube.
13. 50-100µl Elution Solution was added to the binding column. The tube were incubated for 1-5minutes. Centrifuged for 1 minute.
14. The DNA concentration was measured.

2.2.4 Measurement of DNA concentrations

DNA concentration (ng/µl) from the DNA purification was measured by a *Nanodrop 2000/2000c Spectrophotometer* (Themo scientific). Elution buffer was set as blank. The absorbance spectrum for nucleic acids are at 260 nm, and therefore the DNA concentration was quantified at this absorbance. However, proteins have absorption at 280nm, and peptide bonds absorbs at 230 nm. Protein and peptide bonds contaminate DNA samples and therefore the purity indication of the DNA samples are measured by the 260/280 nm and 260/230 nm ratios. DNA samples are pure when the ratio 260/280 nm is between 1.7-1.9 and the ration of 260/230 is between 2.0-2.2.

2.2.3 Agarose gel electrophoresis to identify DNA Agarose gel electrophorese separates DNA fragments based on their size. A 6X loading buffer is added to the DNA samples. The loading buffer makes the DNA sink into the well and their viability when they migrates through the gel. DNA fragments migrate through the agarose gel matrix, composed of agarose (here used 0.7%), a linear polysaccharide (originally extracted from seaweed), which together polymerizes into a compact network with different size of the pores (depending on the agarose concentration). These pores alter the migration speed of each DNA fragment. This migration is depend on the ions in the minigel-buffer, which carries the current through the electric field. This current creates the movement of DNA through the gel. DNA fragment migrates toward the positive pole (anode), due to their negative charge. The degree of migration depends on the size and the conformation of DNA fragment, but also together with the agarose concentration and the voltage. DNA fragment becomes visualized by a GelRed™ Nucleic Acid Gel stain (10000X) (Biotum) and the use of UV trans-illuminator UVP (BioDoc-it™ imaging system).

Agarose gel Procedure

0.7% agarose gel solutions was made by adding 0.7g SeaKem® LE Agarose (Lonza) in 100 ml minigelbuffer (1X), this solution was microwaved and gently shaken until all agarose powder were dissolved. The solution was poured into a chamber and the wells were placed into the solution. The solution was incubates for around 30 min at room temperature. The solution became polymerized and transformed into a gel. The gel was transferred into a tray, with minigelbuffer (1X) covering the gel.

Minigelbuffer (1X)
193.76 g Tris
27.33 g NaOAc
14.9g EDTA
dH_2O to 2 liters
pH adjusted to 8.0 with acetic acid

6X gel loading buffer
0.25% Bromphenol Blue (Merck)
60 mM EDTA pH 8.0
0.6% SDS
40%(W/v) sucrose
Sterile filtered

2.2.5 Restriction enzyme digestion

Restriction enzyme digestion is used to verify the DNA insert after DNA cloning. Recognition cutting of restriction sites on each side of the DNA insert is done to verify that the right insert has been cloned into the vector of interest. According to the restriction sites, one or two restriction enzymes are used for this approach. One restriction enzyme linearizers the vector. The band size that appear on the gel can be compared with the band size of vector without the insert. However, the insert can be cut out by two restriction enzymes. These two enzymes cut on each side of the insert or in a known site inside the insert. The verification is done when the digestion mix is run on an agarose gel, where the DNA construct and vectors is separated by size. If the band size correlates with the known size of the given insert appears, the cloning procedure has been successful.

Restriction enzyme digestion protocol

1. The following components of the reaction digestion mixture were mixed in a 1.5 ml Eppendorf tube:
   700 ng DNA construct
   1.5 µl Restriction buffer (From table 5)
   0.5 µl of each restriction enzyme (From table 5)
   dH_2O to a final volume of 20 µl
2. The digestion mixture was incubated a 37 ^{0}C for 1 hour.
3. The reaction was inactivated by adding 4 µl of 6X loading buffer and run on a 0.7% agarose gel.
4. Bands were visualized by GelRed™ Nucleic Acid Gel stain (Biotum).

6X gel loading buffer
0.25% Bromphenol Blue (Merck)
60 mM EDTA pH 8.0
0.6% SDS
40%(W/v) sucrose
Sterile filtered

2.2.6 Polymerase chain reaction (PCR)

Polymerase chain reaction (PCR) is used for cloning and amplifies the DNA sequences of interest. This method can be used in many different arrays of biochemical processes. Some of these can be DNA amplification, real-time quantification of nucleic acids, mutagenesis, sequencing, microRNA analysis, single nucleotide polymorphism (SNP) genotyping and viral quantification.

The basis for every PCR reaction is the heat stabile DNA polymerase, free deoxynucleotides (dNTPs), DNA- primers and a suitable buffer. The PCR reaction consist of different steps. The first step break and denatures the double stranded DNA (dsDNA) helix by a heat shock (94-98 ^{0}C). In the second step, the temperature is lowered (50-60 ^{0}C) and the primers can anneal to the 5`end of the single stranded DNA (ssDNA) (the temperature is depended on the melting temperature of the primer). In the third step, the temperature is raised to the optimum temperature (around 70 ^{0}C) of the DNA polymerase. The DNA polymerase binds to the ssDNA and extends the ssDNA through the primers from 5`to 3` and attaches complementary dNTPs to the original DNA strand as a template. Step 1 to 3 are repeated multiple times and the target sequence is amplified at an exponential manner. The temperature is then lowered (4 ^{0}C), as the final reaction step.

2.2.6.1 PCR based Site-direct mutagenesis

PCR based site- direct mutagenesis is a technique used to create mutations in the DNA sequence by PCR reaction. The designed primers contain a desired mutation. These primers are used as template for synthesizing the complementary strand with the mutation. Throughout this work the QuickChange® Site-Directed Mutagenesis Kit, instruction manual (Stratagene, #200518) was used to insert the wanted mutation.

Site-directed mutagenesis protocol

1. The following were added in a PCR tube and mixed:

1.5 µl of 10X reaction buffer

1 µl (10ng) of dsDNA template (pENTER- FYCO1(1332-1478))

0.5 µl DMSO (sigma)

1 µl (10 µM) Primer forward (From table 3)

1 µl (10 µM) Primer revers (From table 3)

2.5 µl dNTP mix (Sigma)

dH_2O to a final volume of 25 µl

2. 0.5 µl *pfuTurbo* DNA polymerase (2.5U/ µl) (Agilent Technologies, #600254-52) were added to the mixture
3. The reaction was placed in a PCR cycler (Eppendorf AH diagnostics) with the following PCR program (Table 2.10).

Table 2.10: PCR program for target with a size of 4kb.

Numbers of Cycles	**Temperature (^{0}C)**	**Time**
1	96	30 seconds
18	96	30 seconds
	55 (primer T_m - 5^{0}C)	1 minute
	68	2 minutes/kb
Hold	4	∝

10X Reaction Buffer
100nM KCl
100mM $(NH_4)_2SO_4$
200mM Tris-HCl (pH 8.8)
20mM $MgSO_4$
1% Triton® X-100
1 mg/ml nuclease-free bovine
serum albumin (BSA)

2.2.6.2 PCR based DNA sequencing

DNA sequencing is used to verify the precise order of nucleotides in the DNA, often used after cloning and mutagenesis. BigDye®3.1 kit (Applied Biosystems) was used with different primers according to their vectors.

Procedure

1. The following reagents were mixed into PCR tubes and held on ice.
   200-500 ng Plasmid
   1 µl BigDye Terminator v3.1 mix
   2 µl of 5X BigDye sequencing buffer
   1 µl Sequence primer (From table 4)
   dH_2O to final volume of 10 µl
2. The reagent mix were placed into a PCR cycler and run with following PCR program (Table 2.11).
3. The finished reagent mix was delivered to the core sequencing facility.

Table 2.11: PCR program for DNA sequencing

Numbers of Cycles	**Temperature (^{0}C)**	**Time**
1	96	1 minute
33	96	30 seconds
	50	15 seconds
	60	4 minutes
Hold	4	∝

2.2.7 Sodium Dodecyl Sulfate Polyacrylamide Gel Electrophoresis (SDS-PAGE)

SDS PAGE is a technique used to separate and identify proteins according to their size. These proteins are treated with an anionic detergent, SDS. SDS denatures secondary structures and non- disulfide liked tertiary structures and unfolding proteins (Shapoiro et al. 1976, weber and Osborn 2969). It also applies negative charge to the proteins, which makes them migrate towards the positive field. It is the glycerol in the SDS- loading buffer that enables the samples to sink into the well. Smaller proteins run longer than larger proteins.

10% acrylamide gel procedure

The following components were mixed in each Erlenmeyer flask.

10% Separation gel (protein size identification for proteins between 25 kDa to 80 kDa).

1. 4.9 ml dH_2O
2. 2.5 ml 40% Acrylamid (Applichem)
3. 2.5 ml 4X Separation gel buffer
4. 100 µl APS (Ammonuium peroxidsulfate) (Merck)
5. 10µl TEMED (N,N,N',N'-Tetramethylethylenediamine) (Sigma)

4 % concentration gel

1. 6.4 ml dH_2O
2. 1.0 ml 40% Acrylamid (Applichem)
3. 2.5 ml 4X concentration gel buffer
4. 100 µl APS (Merck)
5. 10µl TEMED (Sigma)

4X Separating gel buffer
181.65 g Tris- base
4g SDS
dH_2O to 1 liter
pH adjusted to 6.8 with HCl

4X Concentrating gel buffer
60.55 g Tris- base
4g SDS
dH_2O to 1 liter
pH adjusted to 6.8 with HCl

2.2.7.1 Coomassie blue staining for polyacrylamide gels

Coomassie blue (also known as brilliant blue) stain is used to visualize proteins after separation by SDS-PAGE. It creates electrostatic interactions with protonated basic amino acids and hydrophobic associations with aromatic residues inside polyacrylamide gels. This staining is compatible for MS.

Procedure

1. SDS- PAGE gel was removed out of the electrophoresis apparatus and into a 15cm plate.
2. Fix solution was added for 10 minutes, discard fix solution.
3. Staining solution (Coomassie Brilliant Blue R-250 (Thermo Scientific™) was added for 1 hour. Coomassie Brilliant Blue R-250 was poured back to its tube.
4. Destaining solution I was added for around 20 min. Destaining solution I was collected in a flask.
5. Destaining solution II was added until adequately destained.

Fix solution
400 ml MeOH
100 ml Acetic acid
500 ml dH_2O

Staining solution
62.5 ml Stain stock (2 g Coomassie Brilliant Blue R-250)
250 ml MeOH
50 ml Acetic acid
dH_2O to 500 ml

Destaining solution I
500 ml MeOH
100 ml Acetic acid
dH_2O to 1 liter

Destaining solution II
50 ml MeOH
70 ml Acetic acid
dH_2O to 1 liter

2.2.8 GATEWAY cloning technology

Gateway® cloning technology is a cloning technique where the gene of interest (GOI) is clone into a vector, by recombination. The gateway cloning technique is based on the site-specific recombinant properties of bacteriophage lambda in *E.coli*, with the properties of switching between a lytic and a lysogenic life cycle. The site- specific integration of phage lambda into the host genome is gone in the latter life cycle (Hartley et al., 2000). These properties enables fast in-frame cloning. There are recombinant sequences called Gateway attachment (att) sites, where the GOI can be inserted. Two set of registered enzyme mixes are used in this cloning technique. These are called BP Clonase and LR Clonase. This Gateway method is divided into two steps. First, generation of Gateway entry clones. Here are specific Gateway attB1 and attB2 sequences added to the 5` and 3`end of a GOI. These sequences are produced by a gene specific PCR primers. This sequence is inserted into a special Gateway plasmid called donor vector, done by BP Clonase enzyme mix. This mix catalyses the recombination and insertion of the attB sequence PCR product into the attP recombinant site in the Gateway donor vector called Gateway entry clone (pENTR, used for storage of gene constructs) which contain a Gateway attL recombinant site. In the second step, the gene cassette in the Gateway entry vector can be transferred into a Gateway destination vector (pDest) by LR Clonase enzyme mix. This pDest vector contain a Gateway attR recombinant sequence and other elements, as promoters and/or epitope tags, which alter the gene properties.

LR reaction procedure

The reaction mix was made in a 1.5 ml Eppendorf tube.

1. The following components were mixed and incubated at 25^0C (water bath) overnight or (2-3 hours):
   100 ng pENTER cDNA construct
   150 ng pDest vector
   0.5 µl LR (enzyme) (Invitrogen)
   TE buffer was added up to a total volume of 10 µl
2. LR mixture was incubated with 1µl protease K (Biolabs) at 37^0C for 10 minutes.
3. 5 µl of the gateway mix was transformated into DH5α chemically competent *E.coli* cells for plasmid amplification and purification.

All gateway constructs were verified by restriction digestion and runned on an agarose gel electrophoresis to identify the right construct.

Tris-EDTA (TE) buffer

10mM Tris/HCl, pH 7.4 (adjusted with HCl)

1mM EDTA pH 8.0

2.2.9 GST pull-down assay

Glutathione S-transferase (GST) pull-down assay is a method used to study protein-protein interactions. These interactions are based on the proteins capability to bind to protein of interest. In this assay, the protein of interest must be linked to a GST-tag. GST-tagged proteins are expressed in large amount in *E.coli* by DNA recombinant technology (section 2.2.9.1*).* These proteins have high affinity for glutathione and can be purified by affinity chromatography on glutathione-Sepharose™ 4 Fast Flow beads (GE Healthcare). Their interaction partners can be studied by an incubation of the GST-protein of interest together with a complex putative protein mixture. Any protein-interaction complexes can be recovered by centrifugation and washing and resolved by SDS-PAGE (Vikis and Guan, 2004). Verification of the putative protein interaction partners can be done by MS analyzation. Protein bands are cut-out and sent to the MS facility core for identification. However, *in vitro* translation of putative interaction partners by TNT® T7 Coupled Reticuloyte Lysate System (Promega) with radioactively labeled (e.g. [^{35}S]-methionine) can be verified by autoradiography. Additional, unlabeled putative interaction partners can be verified by immunoprecipitation (IP) assay.

During this study, GST pulldown- assay were done with both *in vitro* and *in vivo* translated protein interaction partners for the GOLD domain of FYCO1 (amino acids 1333-1478) fused to a GST-tag.

2.2.9.1 Production of GST-fused proteins in *E.coli*

The GOLD domain of FYCO1 was cloned into a pDest15- vector. This resulted in a GST-tag (220 amino acids) on the N-terminal part of the GOLD domain. pDest15 vector is a gateway vector for construction of GST fusion proteins. It contains a glutathione S-transferase- tag (GST-tag) and T7 promoter. SoluBL21 (DE3) *E.coli* strains are improved strains for producing soluble proteins with GST-tag under control of a T7 promoter. The transcription of the gene is induced upon adding isopropyl-β-D-thiogalactopyranoside (IPTG). IPTG inhibits a repressor (Lac repressor), which is bound to the T7 promoter. This repressor will fall off when IPTG bind. The T7 promoter becomes available for the T7 RNA polymerase, which binds and transcribes the target gene.

Protein expression procedure

SoluBL21 (DE3) cells containing the required plasmid were plated out on an agar- plate with the required antibiotic. Each plasmid contains an antibiotic resistant gene, which enables the cells to grow on antibiotic plates.

1. One colony was inoculated into 5 ml pre-warmed LB-media with amp and grown over-night (approximately 16 hours).
2. The over- night bacteria culture was transferred into 100 ml pre-heated 2xYT-media with ampicillin and grown for 2-3 hours at 37^0C with shaking until it had an OD_{600nm} value between 0.6-0.9.
3. This pre-culture was induced by 50 µl 1M IPTG (Promega)
4. The culture was incubated for 3-4 hours at room temperature (approximately 25^0C) with shaking.
5. The culture was pelleted by centrifugation at 5000 xg for 10minutes at 4^0C.
6. The supernatant was discard, and the bacteria pellet was kept on ice
7. 4 ml of lysis buffer was added to the bacteria pellet.
8. 10 % Triton X-100 (Sigma) was added and the bacteria solution was divided into tubes before they were frozen down at -70^0C, to the next day.

LB medium
10 g Bacto Trypton
5 g Bacto yeast extract
10 gNaCl
dH_2O to 1 L
pH adjusted to 7.5 with NaOH
Antibiotic:
100 µg/ml Ampicillin
50 µg/ml Kanamycin

2xYT medium
16 g Bacto trypon
5 g Bacto yeast extract
5 g NaCl
dH_2O to1 lire
pH adjusted to 7.5 with NaOH
20 mM glucose
Supplemented with appropriate antibiotics

Lysis buffer
50mM Tris- HCl pH 8
250nM NaCl
1mM EDTA
1mM DTT
0.35 mg/ml lysozyme

NETN buffer
20mM Tris-HCl pH8.0
100mM NaCl (2M)
0.5% NP40 (Nonidet p 40
Substrate) (sigma) (10%)
1mM EDTA (0.5M)
dH_2O to final volume

Protein harvesting procedure

1. The tubes with the lysed bacteria were thawed on ice.
2. The cells were sonicated (Vibra-cell™, Sonics) at 40% amplitude, 3 times for 20 seconds with 10 seconds pause in between.
3. The sonicated solution was centrifuge at high speed for 10 minutes.
4. The supernatant (periplasmic components, containing soluble proteins) was kept for protein purification

2.2.9.2 Protein purification by GST-pulldown assay

In this study, the pDest15-GOLD domain was bound to glutathione-sepharose beads by affinity chromatography. GST has a very strong affinity for glutathione and results in a strong binding between GST-fusion proteins and Glutathione Sepharose™ 4 Fast Flow beads (GE healthcare). Glutathione Sepharose™ 4 Fast Flow beads (GE healthcare) are dissolved in 20 % ethanol.

Procedure

1. 200 µl of Glutathione Sepharose™ 4 Fast Flow beads (GE healthcare) were taken out.
2. The ethanol was discarded and the beads were washed three times with cooled NETN buffer.
3. Protein lysate were added together with the beads and incubate the mix at 4^0C for 1hour, rotating.
4. The beads were spanned down and washed three times with 1X PBS (10X # 70011-050 pH 7.4, Gibco /life technologies).
5. The concentration of beds were adjusted to 50 % with 1X PBS (10X # 70011-050 pH 7.4, Gibco /life technologies)
6. The beads were stored in 50% NETN buffer.
7. 10 µl protein beads were taken out for verification by SDS-PAGE.

2.2.9.3 GST-pulldown assay for examine new protein interaction candidates for the GOLD domain

Through this GST-Pulldown assay, protein interaction candidates from HEK293 T-REx Flp-In - and HeLa cell lysates (section 2.2.10.4) were investigated. These cells were incubated together with both GST-GOLD proteins– and GST (negative control) bound to glutathione-sepharose beads.

Procedure

1. Cell lysate from HEK293 Flp-In T-REx- and HeLa cells ($\sim 10^6$-10^7 cells) (section 2.2.10.4) were incubated together with 15 µl empty and washed glutathione-sepharose beads (50:50 NETN buffer) for 30 minutes at 4^0C, rotating.
2. The cell lysate were transferred to 15-20 µl washed (two times with NETN buffer) GST-GOLD protein beads and GST beads and incubated for ~3 hours at 4 ^{0}C, rotating.
3. The GST-GOLD and GST beads were washed 5-6 times with NETN buffer. Discard buffer.
4. 15 µl SDS-loading buffer were mixed with the beads and boiled for 3-5 minutes and centrifuged by a table centrifuge. SeeBlue®Plus2 Pre- Stained Protein Standard (Thermo Scientific™ # LC5925) ladder was used (Figure 1B).
5. The protein samples were separated by a SDS-PAGE (section 2.2.7).
6. All protein bands were cut and sent to mass spectrometry (section 2.2.15)

2.2.9.4 In vitro transcription and translation of proteins coupled to a GST-pulldown assay

Direct protein-protein interaction using TNT™ T7 Coupled reticulocyte Lysate System (RTL) (Promega) where the *in vitro* transcribed and translated proteins were radioactive labeled, [^{35}S]-methionine). Here, direct interaction between the *in vitro* translated protein-interaction candidates and GST-GOLD were tested.

Procedure from the Promega kit:

The components of the reaction mixture (Promega kit) were mixed in a 1.5 µl eppendorf tube. One reaction mixture is enough for five samples. The reaction mixture was multiplied when more samples were made.

1. Following components (Promega kit) for one reaction mixture were mixed:
   25 µl reticulocyte lysate

   4 µl TNT buffer

1µl amino acids mix minus methionine

1µl [^{35}S] - Methionine

1µl TNT polymerase T7

2. 1 µg DNA and dH_2O were added to the total reaction mixture (32 µl) to the total of 50 µl.
3. The reaction mixtures were incubated at 30^{0}C for 60-90 minutes.
4. To verify the translation, 3 µl of the *in vitro* translation were taken out for each sample, mixed with 18 µl 2X SDS- loading buffer with 10 % DTT (1M) and boiled for 3-5 minutes (Input).
5. The rest of each *in vitro* translated protein sample were pre-incubated with 15 µl of empty GST-beads (washed with cooled NETN buffer) together with 100 µl of cooled NETN (containing protease inhibitor) for 30 minutes at 4 ^{0}C, rotating.
6. ~100 µl of each *in vitro* translated protein samples were incubated with 15-20 µl 50% GST-GOLD beads (washed with cooled NETN buffer) for 1 hound at 4 ^{0}C, rotating.
7. The beads were centrifuged by a table centrifuge, and washed five times with cooled NETN buffer.
8. All of the NETN buffer were discard and 15 µl of 2X SDS- loading buffer with 10 % DTT (1M) (Sigma) were added. The samples were boiled for 3-5 minutes.
9. 15 µl of the GST-pulldown and 3.5 µl of the pre-incubation (5 % input) reaction mixture was loaded on a 10% thin SDS-PAGE gel.

2.2.9.4.1 Autoradiography: Detection of radioactive proteins in polyacrylamide gels

The SDS-PAGE gel was transferred on a filter paper, covered with a sheet of plastic foil and dried in a GelDryer (BioRad, Model 583) at 80^{0}C for 45`-1 hour. The dried gel was transferred inside a film cassette with a phosphor imaging plate (Fujifilm Science Lab) on top. The film was scanned the next day with FUJI BAS-5000. All images were detected by Image Gauge V.4.0 (Fujifilm Science Lab).

NETN buffer
20mM Tris-HCl pH8.0
100mM NaCl (2M)
0.5% NP40 (Nonidet p 40
Substrate) (sigma) (10%)
1mM EDTA (0.5M)
dH_2O to final volume

Protease inhibitor:
1 Complete protease inhibitor
cocktail tablet (Roche) in 10 ml
NETN buffer

2.2.10 Mammalian cell culture

Throughout this study putative protein interaction for the GOLD domain of FYCO1 were studied by use of mammalian cells from human cervix HeLa cells, human embryonal kidney (HEK) 293 Flp-In T-rex cells and human lens cells (B-3) (Table 2.9).

2.2.10.1 Growth condition

All mammalian cell cultures were grown in their full medium (FM) (Table 2.9) and kept in incubators with a temperature of 37^0C, 95% air and 5% Carbon dioxide (CO_2).

2.2.10.2 Cell splitting

Mammalian cells were kept in their full growth medium (FM), passage every third day (with a confluence between 80%), by dividing them 1/5, 1/10 or 1/20 (depends on the next splitting event)* into new flasks. The optimal confluence for transfection, freezed down or before pulldown assay is 70%. New cells were taken up after passage number 10 and 20, according to the cell-type.

Cell passage procedure

1. The FM of the cells were discarded.
2. The cells were washed with room temperature 1X PBS (10X # 70011-050 pH 7.4, Gibco /life technologies) one time. Discard PBS.
3. 0.5-1.5 ml pre-heated Trypsin-EDTA (Sigma) was added to the cells and incubated at 37^0C for 3-5 minutes. Or until they are detached to the surface.
4. 5 ml pre-heated FM was added to the cells. The cells were suspend 5-10 times.

5. Cells were transferred to a new flask with pre-heated FM. Split cells in a relation of 1:2, for each incubation day.

*Alternation: B3 cells grow slower than the other cell lines and therefor have to split 1:5.

2.2.10.3 Taking up cells and freeze them down

Uptake of mammalian cell procedure

All cells are stored in liquid nitrogen. Cells were taken up from the nitrogen tank and thawed gently. They were added into pre-heated FM in 75cm^2 flask. They were either spanned down or incubated between 3-4 hours, before the FM was changed. This was done to avoid DMSO (sigma) to affect the cells (DMSO is toxic for the cell). Cells were incubated at normal condition and spitted with a confluence of 80%.

2.2.10.3.1 Freezing down mammalian cells

Cells were freezed down with a confluence of 70%. Important to keep the cells on ice during the procedure.

Procedure:

1. Cells were passage to get a less confluence than normal passage procedure.
2. Cells were spanned down and re-suspended gently the pellet with cold freezing mixture (10% DMSO (Sigma) and 90%FBS (Merck))
3. The cells were divide into 2 ml freezing tubes and stored in the nitrogen tank.

2.2.10.4 Mammalian cell lysis

4 x 10^6 cells/ml were seeded out on 15cm plates. 2ml of the lysed cells were incubated into the GST-pulldown assay. Cells were seeded out in a density and lysed to obtain all proteins for pulldown assay. The lysed cells were added together with beads containing bound GOLD domain.

Cell lysis procedure

1. The cells were washed two times in 1X PBS (10X # 70011-050 pH 7.4, Gibco /life technologies) 1ml cold cell lysisbuffer (with protease and phosphatase inhibitors) were added to the 15cm cell-plates. The plates were incubated for 20 minutes at 4^{0}C, shaking.
2. The cells were scraped and the lysates were transferred to a 2 ml Eppendorf tubes. Centrifuge it at 16000xg at 4^{0}C.
3. The clear lysates were transferred /used in a pulldown assay.

Cell Lysisbuffer
20mM Tris-HCl pH8.0
100mM NaCl (2M)
0.5% NP40 (Nonidet p 40
Substrate) (sigma) (10%)
1mM EDTA (0.5M)
dH_2O to final volume
In 10 ml buffer
1 tablet complete EDTA-free
protease inhibitor (Roche)
1:100 phosphatase cocktail sett II
inhibitor (Calbiochem®)

2.2.10.5 Mammalian cell transfection

Cell transfection can be done by different transfection reagent. Transit®-LT1 (Mirus) and Metafectene®Pro (Biontex) were used in this study and are both liposome based transfection reagents. These reagents containing lipids, which capsulate DNA. The lipid capsulated DNA is taken up by the cell through endocytosis.

Transfection procedure

Cells were counted by a Bûrkner counting chamber. 7000-10 000 cells were seeded out into 8 wells plates for microscopy one day before the transfection. The cell confluency were around 70% before transfection. Cells were transfect the next day with the transfection mixture. 0.1µg DNA/well were added into the transfection mixture and incubate for 15-20 minutes at room temperature. FM were changed and 200 µl transfection mix were added to the wells. The cells were incubated at 37^0C, with 95% air and 5% Carbon dioxide (CO_2) over night. Cells were Fixated the next day with 100% MeOH.

Transfection mixture:

26µl DEM/ well (÷p/s, ÷ FBS) and 0.5µl Transit®-LT1 (Mirus) / Metafectene®Pro (Biontex)/ well were mixed and incubate for 3-5 minutes at room temperature.

2.2.11 Fluorescence microscope

A fluorescence microscope is an optical microscope, which uses fluorescence to study organic or inorganic substances. Fluorescence is define as an atoms ability to absorb light energy (excited) from a specific wavelength. The electron jumps to a higher energy level, a short-lived excited state. Here, the electron loose energy and goes back to the ground state, thereby emitting a photon. The emitted fluorescence can be used to generates an image (Lichtman and Conchello, 2005).A confocal microscope is one type of fluorescence microscope.

2.2.11.1 Confocal microscope

Confocal microscopes are specialized fluorescence microscope, which have high sensitivity, high signal to noise ratio and great specificity in excitation and emission detection. In addition, the lateral and vertical resolution is higher than in normal fluorescence microscope. The features are obtained by spatial filtering techniques, which eliminate out- of focus light and increase the brightness in fluorescence image of thick specimens. Thick specimens can be optically sliced and be used to construct a 3D image. Confocal microscope employs point-by-point illumination or point scanning.Two pinholes eliminates the out- of focus fluorescence emission light, and together with the point scanning generates images with great optical resolution. In laser scanning confocal microscopy (LSCM) the light source is a laser. LSCM is widely used today as an essential tool for biomedical imagining applications. This laser passes first through the first pinhole, called light source pinhole aperture. This pinhole is situated in a conjugate plane (confocal), with a scanning point on the specimen. A dichromatic mirror reflect the excited light rays, which becomes focused by the objective lens before it reaches the specimen in a focal plane. The fluorescence light becomes emitted from the specimen and passes through the objective lens, where it becomes focused. The focused light passes back through the dichromatic mirror and focused as a confocal point at the detector pinhole aperture. The light becomes detected by the photodetector (Wright and Wright, 2002).

2.2.12 Cell fixing and staining

Cell preparation for confocal microscopy is important and cells can be fixed by either methanol, acetone, ethanol, paraformaldehyde (PFA) or formalin. Methanol fixation was used during this study and is a more sensitive fixation and lower the risk to destroy specific cellular structures (e.g. ER).

Methanol fixation procedure

1. Cells were fixed in -20^{0}C methanol (100%) for 10 minutes. Collect the methanol.
2. The cells were washed 3 times with ice-cold 1X PBS (10X # 70011-050 pH 7.4, Gibco /life technologies).
3. The cells were stored in 1X PBS (10X # 70011-050 pH 7.4, Gibco /life technologies)

2.2.12.1 Immunofluorescence staining procedure

1. 200 µl block solution (3% goat serum in 1X PBS (10X # 70011-050 pH 7.4, Gibco /life technologies) were added onto the cells on the confocal wells.
2. Incubate the cells with the blocking solution for minimum 30 minutes shaking at room temperature.
3. 150 µl of the primary Antibody (Ab) (in 1% goat serum in 1X PBS (Gibco /life technologies # 70011-050 pH 7.4)) solution were added to each confocal well and incubated for minimum 30 minutes, shaking at room temperature.
4. Wash the wells 6 times with ice-cold 1X PBS (Gibco /life technologies # 70011-050 pH 7.4)
5. 150 µl of the secondary Ab (in 1% goat serum in 1X PBS ((Gibco /life technologies # 70011-050 pH 7.4)) (corresponding alexa-flour) solution were added into each confocal cell and incubated for minimum 30minutes, shaking at room temperature. It were keep dark.
6. Keep the cells with 1X PBS (Gibco /life technologies # 70011-050 pH 7.4) at 4^{0}C.

2.2.13 GFP- trap /Immunoprecipitation

Green fluorescent protein (GFP) tags are used to study proteins localization and dynamics. In addition, GFP fused proteins can be used for immune precipitation assays, enzyme activity measurements, ChIP analysis and MS, through a GFP –trap® system (Chromtek). This assay is used to analyze GFP proteins and their interaction candidates. GFP-Trap is composed of GFP binding proteins coupled to monovalent matrix (e.g. magnetic agarose beads, agarose beads, 96-multiwell plate or magnetic particles). However, agarose beads were used in this study.

GFP –Trap and immune precipitation Procedure

1. HEK294 Flp-In ZnF FYCO1 #12 and HEK294 Flp-In ZnF FYCO1#12 GFP-FYCO1 cells were seeded out with a density of ~320.000 cells/ 6cm well.
2. The cells were transfected with 4 µl Metafect® pro (Biontex) together with 300 µl DMEM (minus FBS and antibiotics), overnight.
3. The gene expression of GFP- FYCO1 from the HEK294 Flp-In ZnF FYCO1 #12 GFP-FYCO1 cells were induced by 1 µg/ml Tetracycline (Sigma).
4. Harvest cells, all FM was aspirated and the cells were washed with 1X PBS.
5. The cells were lysed by adding 300 µl RIPA buffer (+ inhibitors). Cells were incubated at 4^0C, shaking for ~30 min.
6. The cells lysate were scraped and centrifuged at 500g for 5 minutes.
7. The cell lysate supernatant were kept on ice.
8. 15 µl of supernatant were taken out as the input sample. Add 2X SDS-loading buffer (10% 1M DTT) to the input. Boil for 3-5 minutes.
9. 12 µl 50% GFP-Trap® Agarose beads were prepared by washing them in 1X RIPA buffer.
10. Each cell lysate supernatant were loaded on to 12 µl 50% GFP-Trap® Agarose beads and incubated for 2 hour at 4 ^{0}C, rotating.
11. The beads were washed 3 times with 1X RIPA buffer.
12. 15 µl 2X SDS-loading buffer were added to the beads and boiled for 3-5 minutes.
13. The bound proteins from the beads were loaded onto a SDS- PAGE.

2.2.14 Western Blot (WB)

WB is a method where proteins are transferred from a gel to a membrane (e.g. nitrocellulose or polyvinylidene fluoride (PVDF)) by using an electric field. First, proteins are separated by SDS-PAGE. Next, proteins are blotted to the membrane. After the blotting, the membrane is blocked with 5% milk to prevent any unspecific binding of antibodies to the surface of the membrane. Lastly, the membrane become incubated with primary antibodies, which is specific for the protein of interest. Next, the membrane is incubated with a secondary antibody (e.g. Fluorescence dye), to recognize the protein of interest.

WB Procedure

1. The PVDF membrane was first sought in transfer buffer before the SDS-PAGE gel was added. The protein gel was blotted to the membrane by Trans-Blot® Turbo™ (BioRad).
2. After the blotting, the membrane were blocked with a blocking buffer (5% milk (Normilk AS) in TBST for 1 hour at room temperature.
3. Primary antibody was incubated overnight.
4. The membrane was washed 3 times for 10 minutes each time with TBST buffer
5. The secondary antibody were incubated for 1 hour at room temperature and washed 3 times for 10 minutes each time with TBST buffer.
6. The membrane signals were detected by a Lumi-Imager F1™ (Boehringer Mannheim), which captures the chemiluminescent image.

RIPA buffer	**TBST buffer**	**Transfer buffer**
50mM Tris pH 7.5	10 mM Tris pH8	1.88 g Tris base
150mM NaCl	150 mM NaCl	23.25 g Glycin
1mM EDTA	1 mL Tween-20	150 ml methanol (100%)
1% NP40	dH_2O to total 1 L	850 ml dH_2O
0.25 % Triton- X100		

2.2.15 Protein identification by Liquid chromatography-tandem mass spectrometry (LC-MS/MS)

The identification of new protein-interaction for the GOLD domain of FYCO1 were tested by cell lysate pulldown assay followed by protein-identification by MS. Recombinant GOLD domain fused to GST was expressed in *E. coli* and bound to GST-beads. A pulldown assay with cell lysate from HeLa and HEK293 T-REx Flp-In cells were incubated together with the GST-GOLD domain- and GST protein beads (section 2.2.9.3).

Procedure

1. Proteins from the GST-pulldown assay were resolved on SDS-PAGE (10% acrylamide gel) to the bands are in the separation gel (15-20 minutes at 30mA).
2. The buffer was poured from the container, leaving the gel in the tray.
3. All gel bands containing proteins were exited with a scalpel. Be careful for contamination of keratin.
4. The gel piece were transferred to a protein LoBind Eppendorf tube.
5. The protein gel-pieces were delivered to our proteomic core facility, Tromsø University Proteomics Platform (TUPP).

   TUPP prepared the protein gel-pieces for analysis. These protein gels were subjected in a gel reduction, alkylation and trypsin digestion (6 ng/µl trypsin (V511A, Promega, Wisconsin, USA). OMIX C18 tips (Varian, Inc., Palo Alto, CA, USA) were used for sample clean-up and concentration. 0.1% formic acid was added to the peptide mixture and loaded onto a Thermo Fisher Scientific EASY-nLC1000 system and EASY- Spray column (C18, 2 µm, 100 Å, 50 µm,50 cm). Next, peptides became fractionated through a 2-100% acetonitrile gradient in 0.1% formic acid over 50 minutes at a flow rate of 200 nl/min (Shevchenko et al., 2007). Lastly, peptides become fragmented through a Q-Exactive™ Hybrid Quadrupole-Orbitrap™ Mass Spectrometer (© 2015 Thermo Fisher Scientific Inc) (Figure 2.2).

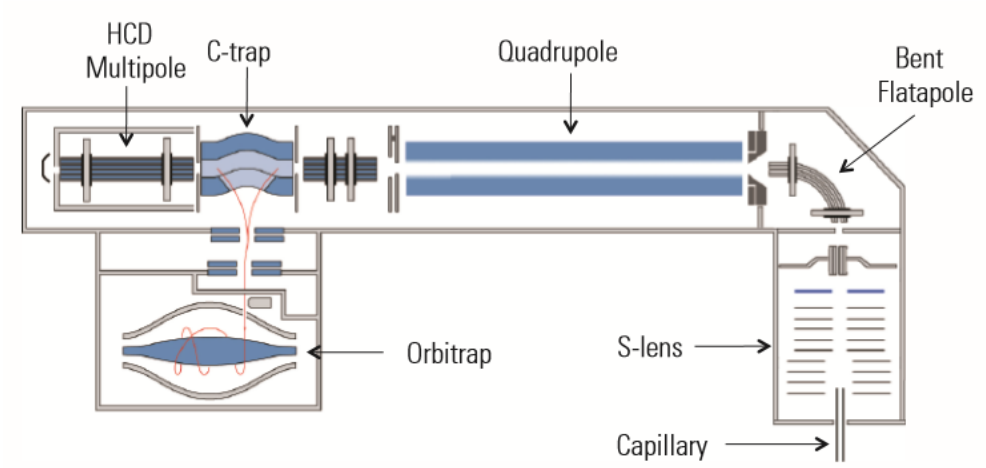

Figure 2.2: Illustration of the Q-Exactive™ Hybrid Quadrupole-Orbitrap™ Mass Spectrometer (© 2015 Thermo Fisher Scientific Inc). The LC- eluate is loaded and travels through the capillary, S- lens, bent flatapole, the quadrupole further through the C-Trap, where the ions goes up to the orbitrap, where the ions are trapped and analyzed Each peptide fragment of interest is sent into the HCD, where they return to C-trap and ends up in orbitrap, where the peptides becomes fragmented and produces MS/MS spectrums (Michalski et al., 2011).

2.2.15.1 Protein identification and processing of the peptide-fragment spectrums

Data from the *Q-Exactive™ Hybrid Quadrupole-Orbitrap™ Mass Spectrometer* (Thermo Scientific™) was collected in data dependent mode using a Top10 method. Next, these data were processed through *Proteome Discoverer™ software* (Thermo Scientific™), which is a software used for identification of peptide spectrums obtained from MS. All fragmented peptide-spectrums were searched up against already known protein sequences from *Homo Sapiens.* This was done through the proteomic database, Uniprot (Consortium, 2015, UniProt, 2016) using the Sequest HT program. The fragment mass tolerance was set to 0.02 Da and the peptide mass tolerance used in this search were 10ppm. First, peptides were filtrated and identified through a false discovery rate (FDR) set to 1%. Next, peptides bound to unspecific to GST proteins (negative control), where excluded. Lastly, keratin proteins were excluded. Keratin is one of the most normal contaminations in MS.

3 Results

3.1 Establishing the GST-pulldown assay followed by MS, to identify putative protein interaction partners for the GOLD domain of FYCO1

The idea was to perform an unbiased GST pulldown-MS study in order to identify putative interaction proteins for the GOLD domain of FYCO1. An overview of the study is illustrated in figure 3.1. As a starting point we had a plasmid ready for bacterial expression of the GOLD domain (amino acids 1333-1478 of FYCO1) fused to GST (we named this plasmid pDest15-GOLD). This plasmid contains a T7 promoter (Figure 3.2). This T7 promoter makes the plasmid able to be transcribed by the viral RNA polymerase. Therefore GST-GOLD became expressed in *E.coli* strain containing a viral T7 RNA polymerase.

The GST-GOLD was further purified from *E.coli* extract using glutathione-sepharose beads. GST-GOLD bound to beads was then incubated with mammalian cell extracts and GST pulldown experiments performed to isolate putative GOLD interaction proteins. HEK293 T-REx Flp-In- and HeLa cells were used for this approach. The GOLD domain interacting proteins were separated by SDS-PAGE and identified by LC-MS/MS (Figure 3.1). The experiment was repeated eleven times and the results are therefore highly representative.

Next, cDNA for Specific putative GOLD interaction proteins were ordered and cloned into different desired vectors. Interacting abilities were tested by *in vitro* and *in vivo* pulldowns and by confocal imagining.

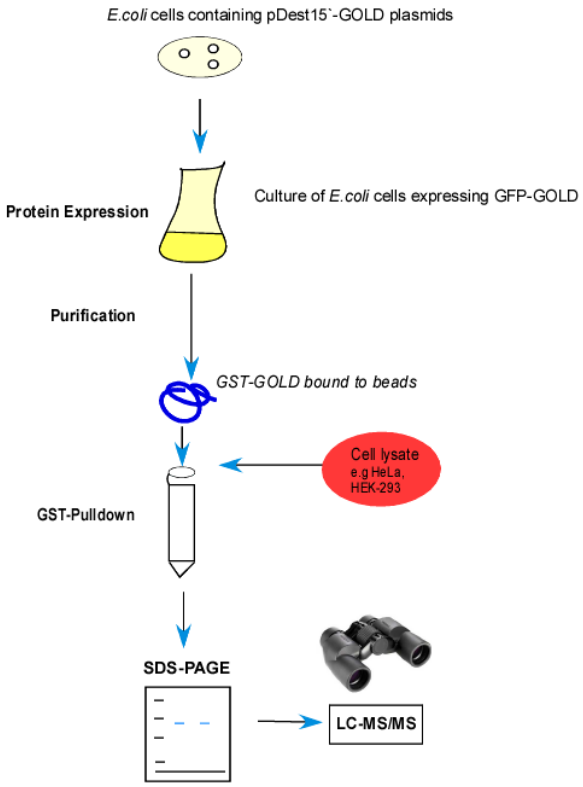

Figure 3.1: An illustration of the work-flow over the different steps to LC-MS/MS.

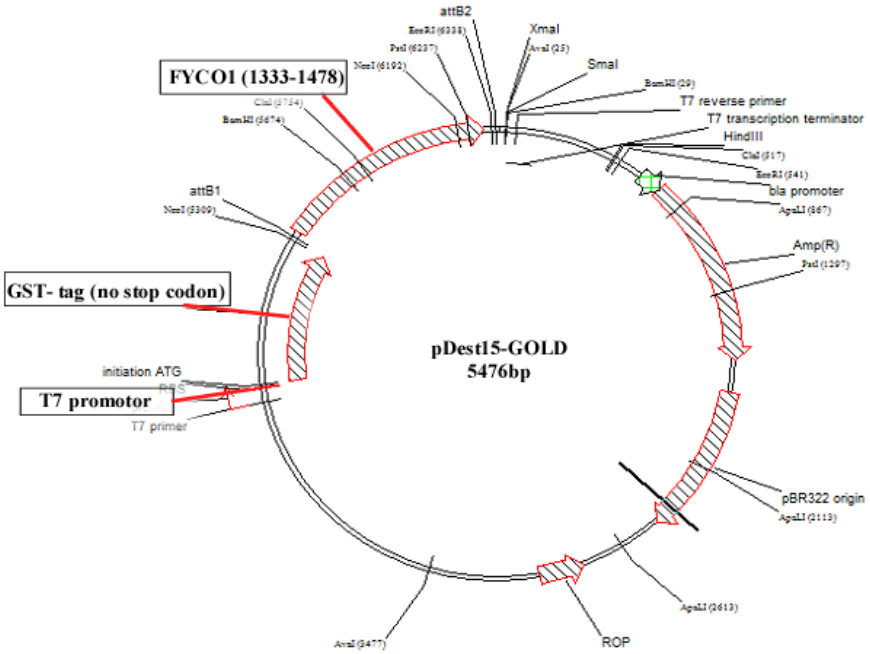

Figure 3.2: A plasmid map over pDest15`- GOLD. In this plasmid the GOLD domain of FYCO1 fused to GST is expressed from T7RNA polymerase promoter.

3.2 Identification of the GOLD domain interaction candidates

The GST-tag on the GOLD domain was used for the purification, through its affinity for glutathione-sepharose beads. The GST-GOLD was produced and purified. GST-GOLD is located as a 40 kDa band, without any other unspecific bands. The same was true for GST (25 kDa) (Figure 3.3).

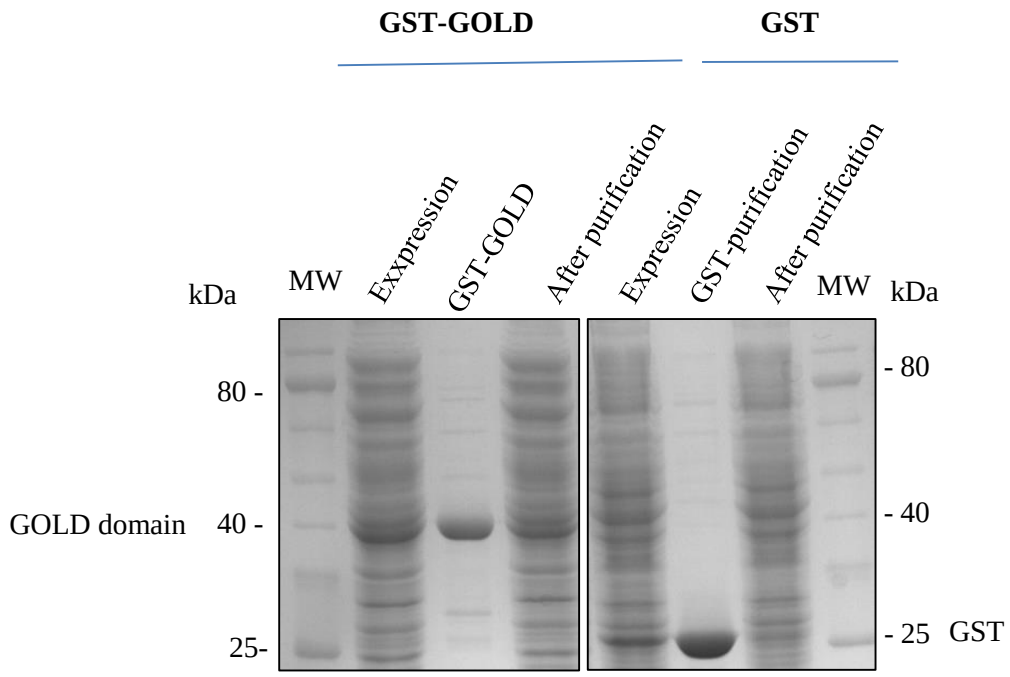

Figure 3.3: Affinity purification of GST-GOLD with glutathione-Sepharose™ 4 Fast Flow beads (GE Healthcare). Glutathione S-transferase (GST) pull-down assay were used to purify the GST-GOLD domain (40 kDa) and GST (25 kDa). Protein samples before expression and protein after the purification were loaded on an SDS-PAGE. Unstained protein ladder (10-250 kDa) (Neb, # P7703S) was used as the Molecular Weight (MW) ladder.

Next, a GST-pulldown experiments were performed where ~10^7 cells (HEK293 Flp-In T-REx and HeLa cells) were incubated with the GST or GST-GOLD protein-beads. Protein interaction candidates were co-precipitated together with GST-GOLD domain. These protein candidates were loaded onto LC-MS/MS and the protein identification was done using Proteome Discoverer™ 2.1 software *(*Thermo Scientific™). This software is a search engine, which uses the obtained mass spectrometry data to identify proteins from peptide sequence database (Perkins et al., 1999). In the current study UniProt (Consortium, 2015, UniProt, 2016) was used as the peptide sequence database.

The identified proteins from all the eleven experiments were run in parallel with GST, as a negative control, to exclude unspecific binding. All of the obtained protein candidates were filtered by specific criteria's (Table 3.1). From these eleven experiments, all protein peptides were sorted into protein groups. In total, 182 proteins were identified (Appendix). How representative their co-precipitations were according to their obtained PSM value. #PSM is the match between our obtained spectrum and the highest-scoring peptide. In addition, 22% of the protein groups were only identified in HEK293 T-Rex Flp-In cells. However, 28% of the protein groups were only identified in HeLa cells. These results shown us that the protein distribution between these two cell lines were relative the same and the experiments were therefore merged. The cellular localization of each protein were obtained by the ProteinCenter software in the *Proteome software Discovery* program (Thermo Scientific™*)*. The data shows that a highly number of the proteins were known to interact with membranes (22.8%) (Figure 3.4). These proteins were of high interesting, due to FYCO1s membrane interacting function. In addition, some of these proteins were also found distributed in the nucleus, the cytoplasm, Golgi apparatus, mitochondrion and endoplasmic reticulum (ER) (Figure 3.4).

Table 3.1: Protein filtration criteria's in Proteome software Discovery (Thermo Scientific™**).**

Criteria's	**Description**
False discovery rate (FDR), below 1%	The ratio between false PSM and the number of PSM obtained above the score threshold (1%).
Not bound to GST-beads	Proteins are not co-precipitated with GST-beads
Keratin excluded	Keratin is one of the most normal contaminations in MS and were here excluded.

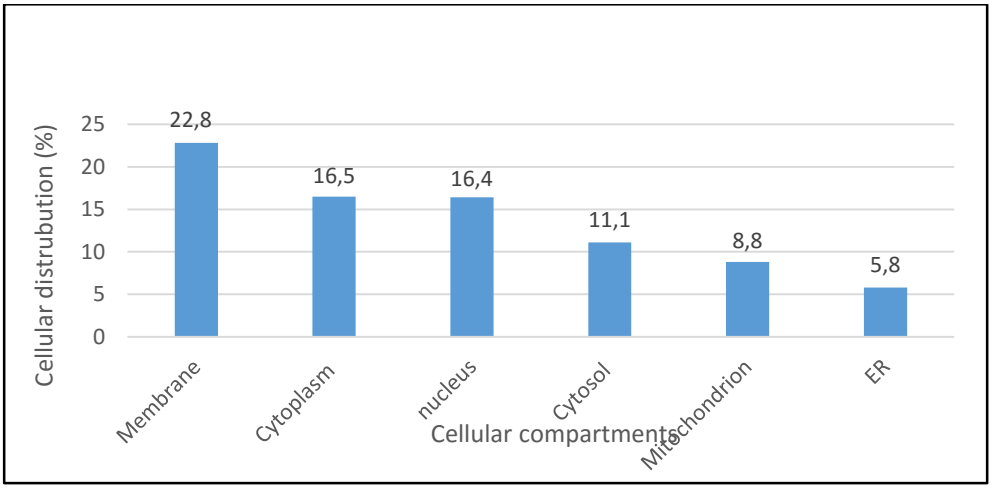

Figure 3.4: The known distribution (%) of protein interaction candidates in different cellular components. Distribution (%) of the protein-interaction candidates in different cellular compartments: membrane, nucleus, cytoplasm, cytosol, Golgi apparatus, mitochondrion, endoplasmic reticulum (ER) and in other components were calculated by the 182 proteins obtained from the ProteinCenter software from Proteome software Discovery (Thermo Scientific™).

Next, a cut-off value for the 182 interaction candidates were set. All protein candidates should be co-precipitated in at least six of the eleven experiments. From the cut-off, 30 putative interacting proteins were selected from how many times they were co-precipitated together with the GOLD domain of total eleven experiments (Table 3.2). These were also sorted according to their peptide spectrum matches (#PSM), since #PSM is a relative indication of the number of identified peptide spectrum matches for each protein and describe the identification of the incident level of a protein interaction (Figure 3.5).

Table 3.2: Putative interacting proteins (30) were separated according to the number of positive identifications throughout the eleven experiments.

Protein name	Gene ID	Number of positive identified/ total experiments	# PSM
Tubulin, alpha-4A chain	TUBA4A	11/11	338
DnaJ homolog subfamily A member 1	DNAJA1	10/11	212
ADP/ATP translocase 2	SLC25A5	10/11	199
Thioredoxin domain-containing protein 5	TXNDC5	9/11	123
DnaJ homolog subfamily A member 2	DNAJA2	9/11	116
ATP synthase subunit alpha, mitochondrial	ATP5A1	9/11	109
Pyrroline-5-carboxylate reductase 2	PYCR2	9/11	97
Carbamoyl-phosphate synthase, mitochondrial	CPS1	9/11	71
Guanine nucleotide-binding protein subunit beta-2-like 1	GNB2L1	9/11	58
Protein NipSnap homolog 1	NIPSNAP1	8/11	73
DnaJ homolog subfamily A member 3, mitochondrial	DNAJA3	8/11	36
D-3-phosphoglycerate dehydrogenase	PHGDH	8/11	35
DnaJ homolog subfamily B member 11	DNAJB11	8/11	31
2',3'-cyclic-nucleotide 3'-phosphodiesterase	CNP	8/11	28
ATP synthase subunit gamma, mitochondrial	ATP5C1	8/11	26
Cytochrome b-c1 complex subunit 2, mitochondrial	UQCRC2	8/11	23
60kDa heat shock protein, mitochondrial	HSPD1	7/11	34
Mitochondrial import inner membrane 50	TIMM50	7/11	27
RuvB-like 2	RUVBL2	7/11	9
Delta(24)-sterol reductase	DHCR24	7/11	8
Calcium-binding mitochondrial carrier protein Aralar 2	SLC25A6	6/11	169
Cytochrome c1, heme protein, mitochondrial	CYC1	6/11	34
Heterogeneous nuclear ribonucleoprotein U	HNRNPU	6/11	32
ADP- ribosylation factor 4	ARF4	6/11	31
Protein NipSnap homolog 2	GBAS	6/11	18
Vacuolar protein sorting-associated protein 4A	VPS4A	6/11	18
Heterogeneous nuclear ribonucleoproteins A2/B1	HNRNPA2B1	6/11	14
Lysophosphatidylcholine acyltransferase 1	LPCAT1	6/11	12
DNA eplication licensing factor MCM7	MCM7	6/11	11
Ras-related protein Rap-1b	RAP1B	6/11	8

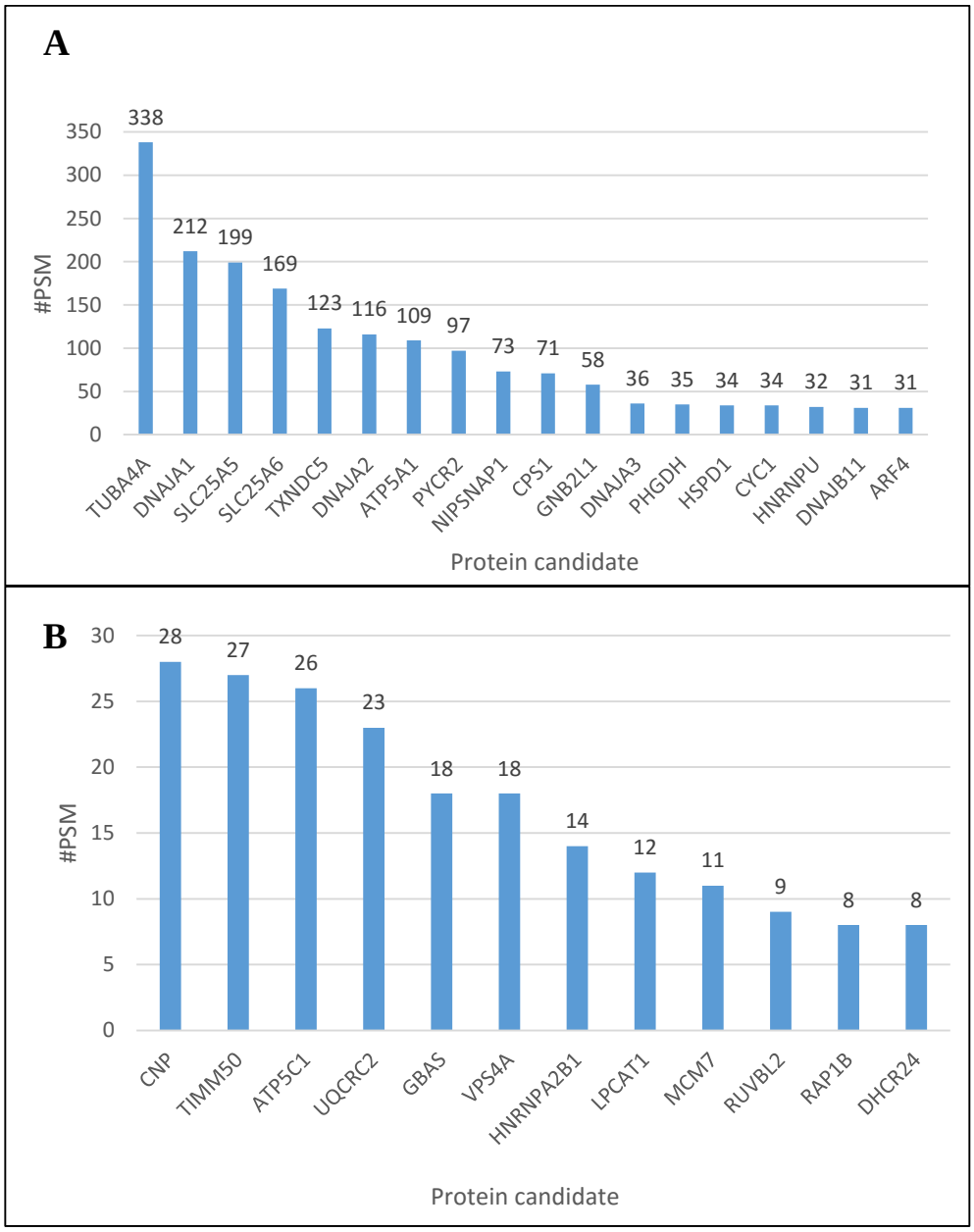

Figure 3.5: The 30 selected protein-interaction candidates arranged by their #PSM. These candidates are sorted by their #PSM value, from highest to lowest. **A:** Tubulin, alpha-4A chain (TUBA4A), DnaJ homolog subfamily A member 1 (DNAJA1, ADP/ATP translocase 2 (SLC25A5), Calcium-binding mitochondrial carrier protein Aralar2 (SLC25A6), Thioredoxin domain-containing protein 5 (TXNDC5), DnaJ homolog subfamily A member 2 (DNAJA2), ATP synthase subunit alpha, mitochondrial (ATP5A1), Pyrroline-5-carboxylate reductase 2 (PYCR2), Protein NipSnap homolog 1 (NIPSNAP, carbamoyl-phosphate synthase, mitochondrial (CPS1), Guanine nucleotide-binding protein subunit beta-2-like 1 (GNB2L1), DnaJ homolog subfamily A member 3, mitochondrial (DNAJA3), D-3-phosphoglycerate dehydrogenase (PHGDH), 60kDa heat shock protein, mitochondrial (HSPD1), Cytochrome c1, heme protein, mitochondrial (CYT1), Heterogeneous nuclear ribonucleoprotein U (HNRNPU), DnaJ homolog subfamily B member 11 (DNAJB11) and ADP-ribosylation factor 4 (ARF4). **B:** 2',3'-cyclic-nucleotide 3'-phosphodiesterase (CNP), Mitochondrial import inner membrane (TIMM50), ATP synthase subunit gamma, mitochondrial (ATP5C1), Cytochrome b-c1 complex subunit 2, mitochondrial (UQCRC2), Vacuolar protein sorting-associated protein 4A (VPS4A), Protein NipSnap homolog 2 (NipSnap2/GBAS), Heterogeneous nuclear ribonucleoproteins A2/B1(HNRNPA2B1), Lysophosphatidylcholine acyltransferase 1 (LPCAT1), DNA eplication licensing factor MCM7 (MCM7), RuvB-like 2(RUVBL2), Delta(24)-sterol reductase (DHCR24) and Ras-related protein Rap-1b (RAP1B).

3.3 Comparison of this study with a previously reported IP-MS study with full-length FYCO1

An unbiased interaction study of full-length FYCO1 has previously been published by Christian Behrends in 2010 (Behrends et al., 2010). In this study, proteins from HEK293 cell lysates were tested for their interacting capabilities for full-length FYCO1 by immune-precipitation and LC-MS/MS identification. This study sought to create an organized network of the human autophagy system. A list of 333 putative interaction candidates for full-length FYCO1 were here identified (Behrends et al., 2010). The result from this study was compared with our results. Ten protein interaction candidates for the GOLD domain were overlapping with the protein candidates from the Behrends list (Figure 3.6). The proteins are arranged by their obtained #PSM from our study. Seven of the ten proteins showed a high PSM value. The remaining three have lower PSM values, but were ranged higher in Behrends list (Figure 3.6).

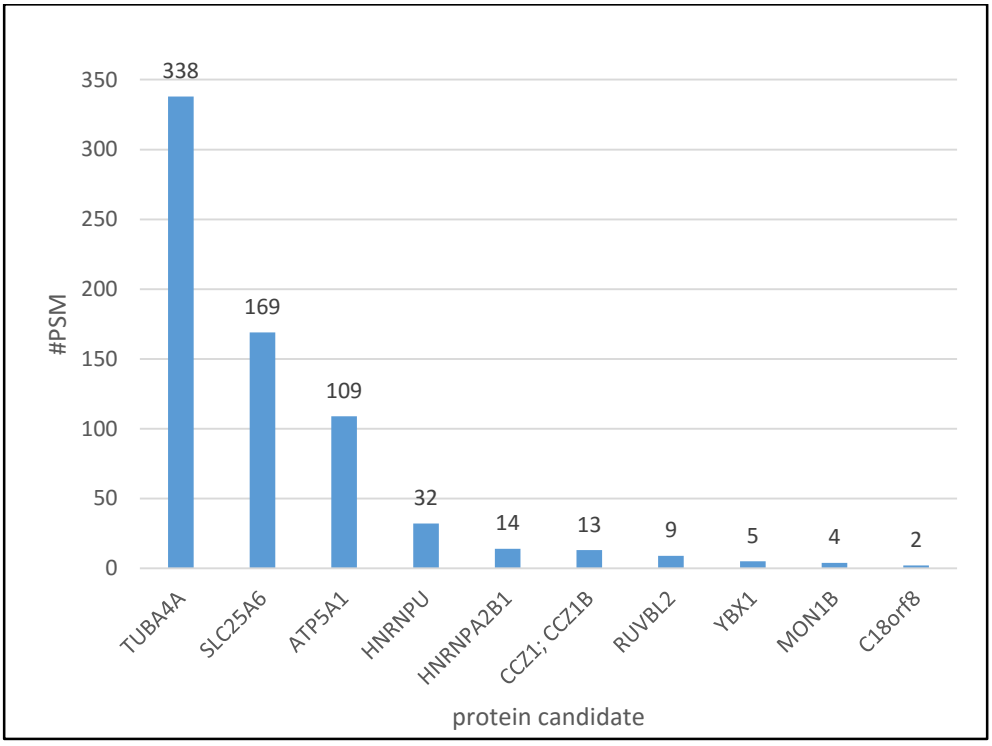

Figure 3.6: Ten protein interaction candidates identified in experiments with immunoprecipitation of full-length FYCO1 and the GST pulldown with the isolated GOLD domain. These protein candidates were found in the co-precipitation with both full-length FYCO1 and for the GOLD domain. They are here arranged according to their #PSM obtained in our study. These putative proteins are: Tubulin, alpha-4A chain (TUBA4A), ADP/ATP translocase 3 (SLC25A6), ATP synthase subunit alpha, mitochondrial (ATP5A1), Heterogeneous nuclear ribonucleoprotein U (HNRNPU), Heterogeneous nuclear ribonucleoproteins A2/B1 (HNRNPA2B1), Vacuolar fusion protein CCZ1 homolog B (CCZ1B), RuvB-like 2 (RUVBL2), nuclease-sensitive element-binding protein 1 (YBX1), Vacuolar fusion protein MON1 homolog B (MON1B) and Uncharacterized protein C18orf8 (C18orf8).

3.4 Selection of nine potential GOLD domain interacting proteins for further studies

From the 30 protein interaction candidates, nine proteins were selected for further studies (Table 3.3). These nine candidates were chosen according to the reported function and localization, but also based on other reasons related to activities within our research group and if cDNA were available or not. Further verification assays were used to look at their level of direct and indirect interactions to the GOLD domain.

Tubulin, alpha-4A chain (TUBA4A)

TUBA4A was pulled down in all eleven LC-MS/MS experiments and had the highest #PSM value (338) among the 30 selected candidates. For this reason, TUBA4A was chosen for further studies. However, Crapome (a database used to identify the distribution level of proteins form other proteomics experiments) identified TUBA4A as a protein frequently co-precipitated in different affinity interaction assays (e.g. immune precipitation with GST-, FLAG- epitope tags) (data not shown). It is showento be distributed in the cytoplasm, cytoskeleton, cytosol and extracellular environment (information obtained by ProteinCenter software (Thermo Scientific). MT are composed of α- and β- tubulin. Here TUBA4A is one of the isoforms of α-tubulin. MT are involved in intracellular transport, cell motility, mitosis and maintain of cell polarity and shape (Conde and Caceres, 2009). FYCO1 is known to interact with MT through motor proteins (Raiborg et al., 2015, Pankiv et al., 2010). The GOLD domain can have an interaction towards TUBA4A.

DnaJ homolog subfamily A member 1 (DNAJA1)

DNAJA1 was pulled down in ten of eleven (91%) LC-MS/MS experiments. Its high #PSM value (212) makes it one of the best interaction candidates for the GOLD domain. In addition, DNAJA1 is not often co-precipitated in protein interaction studies (Crapome database) (data not shown). This increases its chance to be involved in the interaction with the GOLD domain. DNAJA1 is distributed in the cytoplasm, cytosol, ER, on membranes, mitochondrion and in the nucleus (information obtained by ProteinCenter software (Thermo Scientific). It is known to work as a co-chaperone of heat shock protein 70 (Qiu et al., 2006).

Thioredoxin domain-containing protein 5 (TXNDC5)

TXNDC5 was pulled down in nine of eleven (82%) LC-MS/MS experiments. It makes a good putative interaction candidate by having one of the best identification rates and a high #PSM value (123). In addition, TXNDC5 is not often seen to co-precipitate in protein-interaction studies (Crapome database) (data not shown). TXNDC5 is present in ER and in the plasma membrane (information obtained by ProteinCenter software (Thermo Scientific) and is found to interact with the insulin-sensing receptor, AdiporR1. This suggest that TXNDC5 is involved in adiponectin receptor biology and signaling (Charlton et al., 2010).

NipSnap homolog 1 (NIPNSNAP 1) and NipSnap homolog 2 (NIPSNAP2 /GBAS)

NIPSNAP1 and GBAS are homologs of each other and share similarities in structure and function. NIPSNAP1 was pulled down in eight of eleven (73%) LC-MS/MS experiments and GBAS was pulled down in six of eleven (54%) LC-MS/MS experiments. The chance of interaction to the GOLD domain is higher for NIPSNAP1 than GBAS. This is due to a higher #PSM value for NIPSNAP1 (73) than GBAS (18). The protein function and localization is still debated, however it is thought to either be in the matrix or in the inner membrane of the mitochondrion. The possibility for interaction with the GOLD domain is reduced, if they are localized inside the mitochondria. Although, the proteins may interact with the full-length FYCO1 through its GOLD domain before or during their transport into the mitochondrion. NIPSNAP1 and GBAS has also been examined in our research group, and were therefore included in this study.

RuvB-like 2 (RUVBL2)

RUVBL2 was pulled down in seven of eleven (63%) LC-MS/MS experiments with a #PSM value of 9. It was included due to the interest of our research group. It is also interesting that it was found to co-precipitate together with TUBA4A (Biogrid[3.4] (thebiogrid.org)) and that it came down together with mTOR by affinity capture-MS (Biogrid[3.4] (thebiogrid.org)). It is an ATPase DNA helicase and involved as a regulator of ER stress-induced gene transcription (Marza et al., 2015). However, it is localized on membranes and in the cytoplasm (information obtained by ProteinCenter software (Thermo Scientific), which can make it available for FYCO1.

Vacuolar protein sorting-associated protein 4A (VPS4A)

VPS4A was pulled down in six of eleven (54%) MS experiments with a #PSM value of 18. It was included due to the interest of our research group, and because of its function.VPS4A is known to interact with Ras-binding proteins and ESCRT-III complex (Zheng et al., 2012), and is involved in intracellular protein trafficking, as the transport of LE proteins (Scheuring et al., 2001). These features gives VPS4A an interesting opportunity to interact with the full-length FYCO1, and from our results, through the GOLD domain.

ADP- ribosylation factor 4 (ARF4)

ARF4 was also included as one of the nine interaction candidates, being pulled down in six of eleven (54%) LC-MS/MS experiments and got a #PSM value of 30. Its identification rate and #PSM value makes it a likely interaction candidate. Since ARF4 already has been used in our laboratory, it could easily be tested against the GOLD domain. In addition, ARF4 is rarely identified in different affinity interaction assays (e.g. immune precipitation with GST-, FLAG-epitope tags) (Crapome database) (data not shown). ARF proteins belong to the Ras superfamily of small GTPases, which regulate vesicle traffic and organelle structures. Regulation of organelle structure has been shown to be done by recruiting coat proteins, modulating structure of actin at the membrane surfaces and to regulate phospholipid metabolism (D'Souza-Schorey and Chavrier, 2006). ARF proteins may work together in the ER–Golgi system and at the plasma membrane (Donaldson and Jackson, 2011). These functions increase the chance for ARF proteins to interact with the FYCO1, and therefore the GOLD domain.

Vacuolar fusion protein MON1 homolog B (MON1B)

According to our result, by its low interaction rate (9%) and low #PSM value (4), MON1B is not one of the high interaction candidates for the GOLD domain. However, MON1B was included as a possible interaction candidate, due to its already known putative interaction against the full-length protein, FYCO1 (Behrends et al., 2010) and the interest of our research group. It is known that MON1B creates a complex with CCZ1. This complex functions as a GEF for Rab7. Rab7 becomes activated and associates strongly to PI3P positive membranes (Cabrera et al., 2014) and is shown to interact with the FYCO1 (Pankiv et al., 2010). MON1B is therefore a biased putative interaction candidate, which can have an interaction with full-length FYCO1 through FYCO1s GOLD domain**.**

Table 3.3: Putative protein interaction candidates (9) for the GOLD domain selected for further study

Protein name	Gene ID	Number of positive identified/ total	#PSM	Size (kDa)	Localization*
Tubulin alpha-4A chain	TUBA4A	11/11	338	49.9	- Cytoplasm - Cytoskeleton - Cytosol
DnaJ homolog subfamily A member 1	DNAJA1	10/11	212	44.9	- Cytoplasm - Cytosol - ER - Membrane - Mitochondrion - Nucleus
Thioredoxin domain-containing protein 5	TXNDC5	9/11	123	47.6	- ER - Organell lumen
Protein NipSnap homolog 1	NIPSNAP1	8/11	73	33.3	- Membrane - Mitochondrion
RuvB-like 2	RUVBL2	7/11	9	51	- Cytoplasm - Membrane - Nucleus
Protein NipSnap homolog 2	GBAS	6/11	18	33.7	- Membrane - Mitochondrion
ADP-ribosylation factor 4	ARF4	6/11	31	20	- Cytoplasm - Cytosol - Golgi - Membrane - Nucleus
Vacuolar protein-assosiated protein 4A	VPS4Q	6/11	18	48.8	- Cytoplasm - Cytosol - Endosome - Membrane - Nucleus - Vacuole
MON1 homolog B	MON1B	1/11	4	59	- Cytoplasm

** Information obtained from ProteinCenter software from Proteome software Discovery 2.1 (Thermo Scientific™)*

3.5 According to the *in vitro* pulldown assay, DNAJA1 may be the strongest direct interaction candidate for the GOLD domain

Behrends and his co-workers showed earlier that TUBA4A, RUVBL2 and MON1B were observed to precipitate together with full-length FYCO1 (Behrends et al., 2010). Interestingly, these came also down in our interaction study, with the isolated GOLD domain of FYCO1. To examine their direct interaction abilities towards the GOLD domain, these proteins and the six other protein candidates were obtain through cDNA from our own plasmid archive (ARF4, GBAS, NIPSNAP1, MON1B and VPS4A) or ordered from the Harvard PlasmID collection (Harvard, 2016) (TUBA4A, DNAJA1, TXNDC5 and RUVBL2).The gateway pENTR cDNA plasmid constructs were obtained for five of the nine proteins chosen for further studies. These five, TUBA4A, DNAJA1, RUVBL2, ARF4 and TXNDC5 cDNAs were cloned into pDest-Myc vector, which contains a T7 promoter and a myc-tag (Lamark et al., 2003). GBAS, NIPSNAP1 and MON1B were already cloned into this pDest-Myc vectors. VPS4A was not available as a pENTR construct, Due to time limitations, VPS4A was not tested. However, the eight candidates were *in vitro* transcribed and translated in a reticulocyte lysate System (Promega) together with radioactive ^{35}S- methionine. First, these *in vitro* transcribed proteins were incubated with empty glutathione-Sepharose beads, to exclude unspecific binding. Next, their protein interacting abilities for the GOLD domain were tested by a GST-pulldown assay. This was performed by incubating them together with GST-GOLD bound on glutathione-Sepharose beads. In parallel, these protein candidates were incubated with GST-beads, to exclude their unspecific binding to GST (bound to glutathione-Sepharose beads). GST works here as a negative control. Their interactions were identified by measuring their radioactive methionine content. The binding intensity is due to the measured radioactive methionine, which is shown as dark bands on the autoradiography. The strength is dependent on the interaction-strength towards the GST-GOLD domain. Unspecific interactions were excluded by the GST control.

The data presented in figure 3.7 shows the *in vitro* binding between the bacterial expressed GST-GOLD domain and *in vitro* translated protein candidates. The bands on the autoradiography indicating 5% input indicate an efficient *in vitro* translation of most of the candidates, except for TXNDC5. TXNDC5 gave no *in vitro* translationand product. (Figure 3.7C). Interaction against GBAS, MON1B and ARF4 were all tested three times. These data are therefore more significant than the other. NIPSNAP1, TUBA4A, DNAJA1 and RUVBL2 were all tested once and additional experiments must be included to make any conclusion about their direct interaction to the GOLD domain.

Two strong bands were observed in most of the inputs. These two bands, are two different forms of the protein. The ribosome can bind to more than one start codon and make a truncated form of the protein, which makes these two bands. The largest band (upper) is the full-length form of the protein fused to myc-tag, whereas the smaller (lower band) is most likely a product without a myc-tag or a truncated form (Figure 3.7A). Therefore all bands found in the input were included in the interaction strength quantitation (Figure 3.8). Additional bands found only after the pulldown (not found in the input) as seen for DNAJA1, can be due to cleaved proteins (Figure 3.7C).

Figure 3.8 shows the quantification of the interaction intensity towards the GOLD domain. In total, all interacting toward the GOLD domain were below 5 % (compared to the 5 % input). An interaction value below 5 % is define as a very weak interaction. However from our quantification results (Figure 3.8), regarding to the GST-control and comparing with the 5% input, DNAJA1 seems as the protein with the best interaction toward the GOLD domain. This was also observed in the autoradiograph (Figure 3.7C). GBAS is quantified as the second best interaction candidate. RUVBL2 and TUBA4A did not show any unspecific interaction against GST, which can make their observed weak binding specific (Figure 3.7C). While, NIPSNAP1, ARF4, MON1B were not observed to have a direct interaction against the GOLD domain.

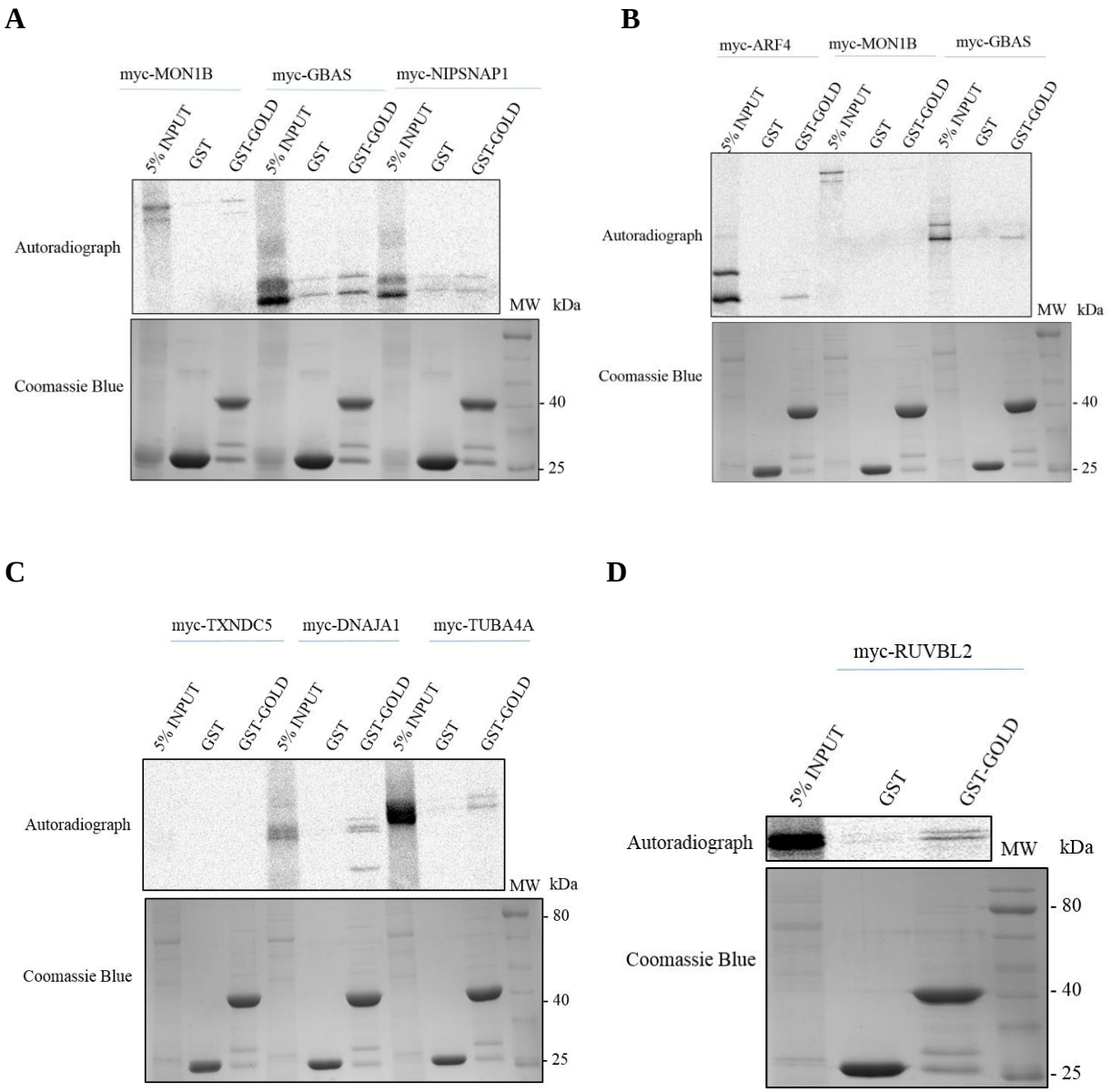

Figure 3.7: *In vitro* interaction study of the protein-interaction candidates, MON1B, GBAS, NIPSNAP1, ARF4, TXNDC5, DNAJA1, TUBA4A and GBAS. Autoradiograph of the GST pulldown assay between the GOLD domain fused to GST and immobilized on glutathione-sepharose beads and myc-tagged -MON1B, -GBAS, -NIPSNAP1, -ARF4, -TXNDC5, -DNAJA1, -TUBA4A and -RUVBL2 produced by in vitro translation in presence of ^{35}S-methionine. The in vitro translated proteins were incubated together with GST immobilized on glutathione- sepharose beads to exclude unspecific binding. The interaction/binding between GST-GOLD and in vitro translated protein-candidates are in regarding to a 5 % input and are resolved by SDS-PAGE, stained by coomassie blue and detected by autoradiography (Fuji BAS-5000). Unstained protein ladder (10-250 kDa) (Neb, # P7703S) was used as the Molecular Weight (MW) ladder **A:** Autoradiograph of GST-GOLD and *in vitro* translated MON1B, GBAS and NIPSNAP1. **B:** Autoradiograph of GST-GOLD and *in vitro* translated ARF4, MON1B and GBAS. **C:** Autoradiograph of GST-GOLD and *in vitro* translated TXNDC5, DNAJA1 and TUBA4A. **D:** Autoradiograph of GST-GOLD and *in vitro* translated RUVBL2.

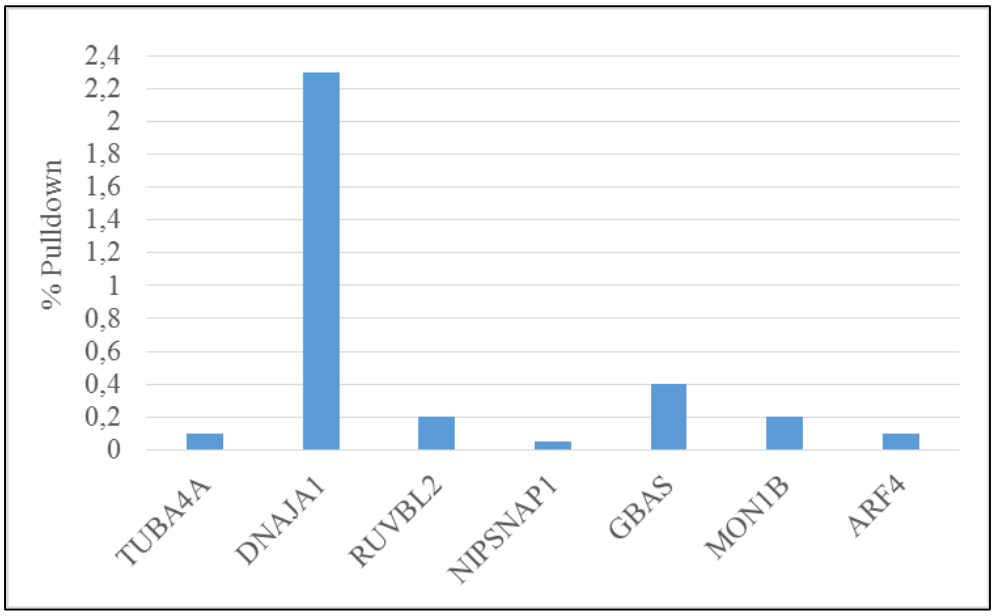

Figure 3.8: Quantitation of binding to GST-GOLD domain in *in vitro* GST-pulldown assay. The percentage (%) pulldown values (y-axis) are the mean values from each of the interaction bands from the *in vitro* translated proteins pulled down (x-axis). The quantifications are relative to the GST control and the results were developed by using Image Gauge software 4.0 (Fuji).

3.6 TXNDC5 precipitates together with the GOLD domain *in vivo*

Next, an indirect interaction study was done by an *in vivo* GFP-Trap assay with immune-precipitation against the myc-tagged protein candidates (Figure 3.9). Due to time limitations, only five of the interaction candidates, cloned into a myc-vector, were tested. These five were, RUVBL2, TUBA4A, TXNDC5, DNAJA1 and MON1B. This experiment was only done once. Each of these interaction candidates were transiently co-transfected together with the GOLD domain fused to a green fluorescent protein (GFP) into HEK293 Flp-In ZnF-FYCO1 knockout for FYCO1 #12 (HEK293 Flp-In ZnF-FYCO1 #12) by METAFECTENE® PRO system (Figure 3.9A) (Olsvik et al., 2015). In addition, HEK293 Flp-In ZnF-FYCO1 #12 cells, stably expressing GFP-FYCO1, were transiently transfected with the same five Myc-tagged protein candidates (Figure 3.9B). In regard to the unspecific binding, the results showed TXNDC5 as the only possibly candidate that showed an interaction with the GOLD domain (Figure 3.9A). However, as previously known, Behrends showed earlier that endogenous TUBA4A, RUVBL2 and MON1B were observed to precipitate together with full-length FYCO1 (Behrends et al., 2010). Through our previous *in vitro* pulldown experiments, none of these seems to have a strong direct interaction towards the GOLD domain. This is true for their interaction in the IP as well. In this *in vivo* pulldown experiment relative to the unspecific binding, none of these candidates were observed to precipitate together with the GOLD domain. However, MON1B precipitate together with the full-length FYCO1 (Figure 3.9B).

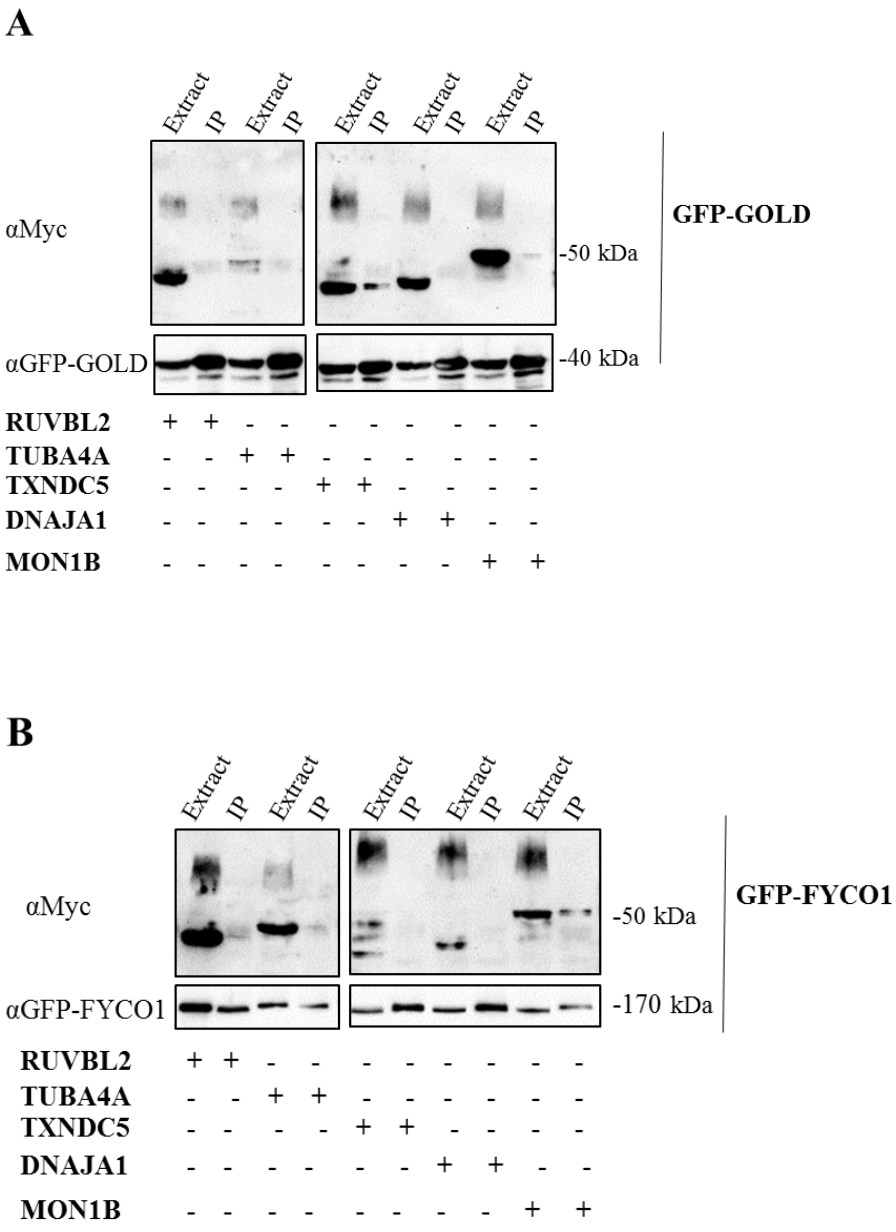

Figure 3.9: Immune-precipitation of GFP-tagged GOLD domain and FYCO1 co-expressed with Myc- tagged -RUVBL2, -TUBA4A, TXNDC5, -DNAJA1 and –MON1B. Unstained protein ladder (10-250 kDa) (Neb, # P7703S) was used as the Molecular Weight (MW) ladder. Signals were detected by Lumi-ImagerF1™ (Boehringer Mannheim) **A:** HEK293 Flp-In ZnF-FYCO1 #12 lysates were pulled down with GFP-GOLD (GFP-trap). Myc-tagged proteins were immuno-precipitated with Myc-antibodies (upper panel). GFP-tagged GOLD domain (lower panel) was immune precipitated with GFP antibodies. **B:** HEK293 Flp-In ZnF-FYCO1 #12 stably expressing GFP-FYCO1 lysates were pulled down with GFP-FYCO1 (GFP-trap). Myc-tagged proteins were immuno-precipitated with Myc-antibodies (upper panel). GFP-tagged FYCO1 domain was immune precipitated with GFP antibodies (lower panel).

3.7 Expression of the GOLD domain in cells reveals a diffuse localization pattern

Next, the cDNA for the GOLD domain was gateway-cloned into a pDest-mCherry-C1 tagged vector. This vector express the GOLD domain as a fusion with the red fluorescent protein mCherry. The GOLD domain has previously been cloned into a pDestEGFP-C1 with a GFP-tag, so this was not done in this study. To examine differences in the expression level between the empty mCherry- and GFP vectors, these were transiently transfected into HEK293 Flp-In ZnF-FYCO1 #12 cells and examined by confocal microscopy. These were compared with the transiently transfected mCherry-GOLD and GFP-GOLD constructs (Figure 3.10). All cell-transfections were performed using TransIT®-LT1 reagent (Mirusbio) system. Cells were fixed with methanol (100%) for 24 hours after transfection. Live cell imaging was done the following day after the transfection. All images were taken using laser scanning confocal microscope 780 (LSM780) (Zeiss).

In figure 3.10 the expression of the wildtype GOLD domain was compared tp the expression of the empty pDestEGFP (EGFP/GFP) - and pDest-mCherry (mCherry)-vectors. GFP and mCherry alone are diffusely expressed throughout the cell, with no specific structures seen. However, the GOLD domain is also diffusely expressed over the whole cell, but with somewhat stronger perinuclear localization. The perinuclear localization is shown as a “line” around the nucleus. This may indicate ER structures, but have to stain for this structure. In addition we looked at the expression level and localization of full-length FYCO1 in HEK293 Flp-In ZnF-FYCO1 #12 cells stably expressing GFP-FYCO1. FYCO1 makes clear rings, both perinuclear and in the peripheral part of the cell (Figure 3.10).

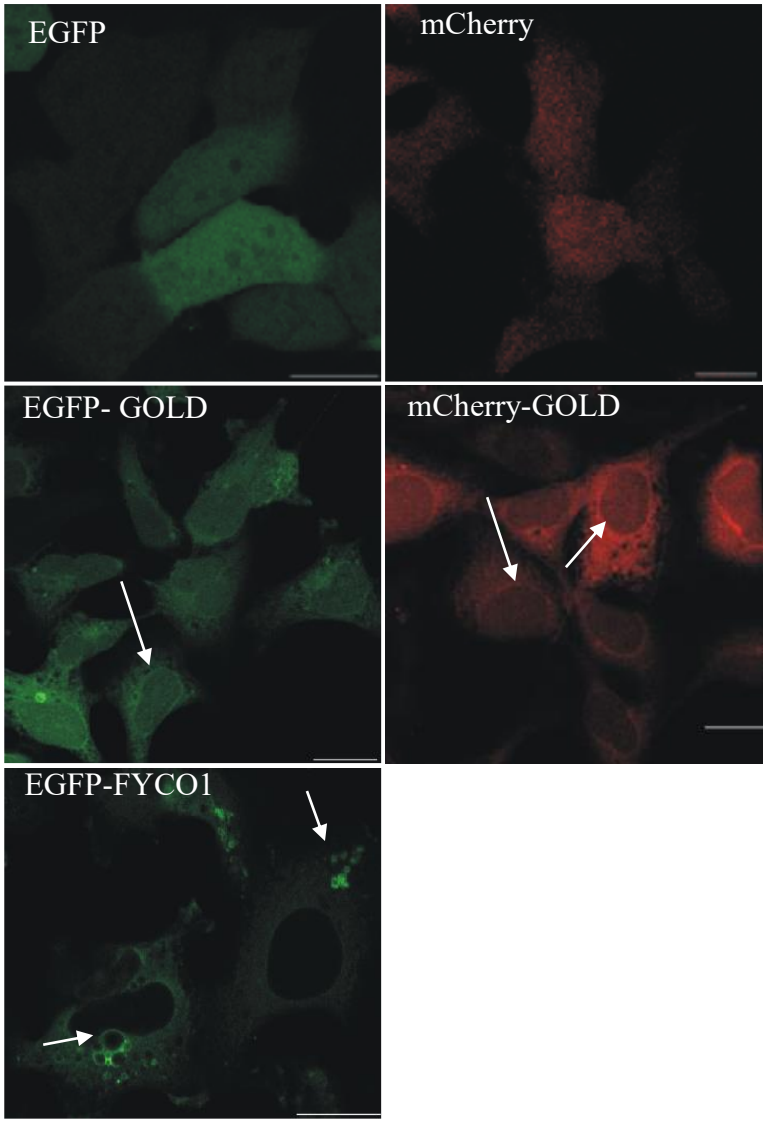

Figure 3.10: Examine the expression differences between the empty EGFP- and mCherry- tags and the EGFP-GOLD domain, mCherry-GOLD domain and full-length GFP-FYCO1. HEK293 Flp-In ZnF-FYCO1 #12 cells were transiently transfected with EGFP- and mCherry-tags, EGFP-GOLD domain, mCherry-GOLD domain and full-length GFP-FYCO1.The empty GFP- and mCherry –tag are both totally diffused expressed (upper image). EGFP-GOLD and mCherry-GOLD shoes both diffuse expression throughout the cell. The arrows point out structures which may be ER structures, found around the nucleus (middle images). The GFP-FYCO1 was observed to make ring structures (marked as arrows), both perinuclear and in the peripheral (lower image). All cells were fixed with methanol (100%). Scale bar 20µm.

3.8 Generally difficult to examine co-localization together with the GOLD domain, because of its diffuse localization.

Confocal microscopy was used to check for co-localization of the GOLD domain and putative interaction partners in cells. To examine these protein interactions by confocal microscopy, all proteins were expressed in a fluorescent tag or a myc-tag capable for labeling with an antibody, which can be visualized by an antibody. In this study, three of the protein interaction candidates (TUBA4A, RUVBL2, TXNDC5) were first gateway-cloned into mCherry-C1 vectors. The other candidates were expressed with a myc-C1 tag (MON1B and DNAJA1) or a GFP-C1 tag (VPS4A). All the tags were expressed on the N-terminal part of the proteins. NIPSNAP1 and GBAS have their N-terminus end processed before it becomes inserted into the mitochondrial membrane. Therefore, they need to be cloned into a C-terminal mCherry-tag. NIPSNAP1 and GBAS were therefore not included due to time limitation. ARF4 is another protein that was depend on its N-terminal end. ARF4 normally become myriosylated on its N-terminus, which is important for its binding capabilities to membranes (Antonny et al., 1997). ARF4 was not cloned into a vector containing a C-terminal fluorescence tag. Therefore, NIPSNAP1, GBAS and ARF4 were not included in this assay.

Next, protein interaction candidates were either transiently transfected alone or transiently co-transfected together with the GOLD domain in HEK293 Flp-In ZnF-FYCO1 #12 cells (TUBA4A, TXNDC5, RUVBL2, VPS4A, MON1B and DNAJA1). In addition, some of the protein interaction candidates (TUBA4A, TXNDC5, RUVBL2 and MN1B) were co-transfected into HEK293 Flp-In ZnF-FYCO1 #12 cells stably expressing GFP-FYCO1. All cells were kept in their full growth medium (Dulbecco′s Modified Eagle′s Medium (DMEM) (Sigma, D6046), 10% FBS (Merck), 100U/ml Penicillin and100g/ml Streptomycin), seeded out with a cell concentration of ~ 7000 cells/ well. The transient transfection was done the following day. The expression of FYCO1 in HEK293 Flp-In ZnF-FYCO1 #12 cells stably expressing GFP-FYCO1 was induces by tetracycline. Fixed with methanol (100%) was done the day after transfection.

Several of the protein interactions were examine for their co-localization with the GOLD domain or with the full-length FYCO1 by confocal microscope. The results showed still a diffused cellular expression and localization of GFP- and mCherry- GOLD domain for most of the co-transfected experiments. These co-localizations were examined by a line-plot measurement (Zen Blue software, Zeiss). The local co-localization can be measured through this type of plot, where an arrow through a structure can measure the intensity of the color channels (EGFP (green lines) and mCherry (red lines) (see Table 2.6) and the graphs can be examined by comparing their intensity.

TUBA4A redistributes the GOLD domain to the centrosomes

TUBA4A was identified by MS as one of the highest ranked protein interaction candidates to the GOLD domain. In addition, it is shown to be a protein interaction candidate for the full-length FYCO1 (Behrends et al., 2010). HEK293 Flp-In ZnF-FYCO1 #12 cells was transiently co-transfected with mCherry-TUBA4A and EGFP-GOLD domain (Figure 3.11). When expressed alone, TUBA4A was observed diffusely through the cell, with a large perinuclear puncta/aggregate perinuclear at the centrosome (Figure 3.11A and C). However, when expressed alone, the GOLD domain does not associate with centrosomes (Figure 3.11B). When the GOLD domain was co-expressed together with TUBA4A, TUBA4A redistributed the GOLD domain to the centrosome. They were observed to be localizes on centrosomes by staining for anti-γ –tubulin, which is a centrosome marker (Figure 3.11C). These co-localizations were verified by a line-plot measurement (two lower images) (Figure 3.11C). This suggests an interaction between TUBA4A and the GOLD domain in cells. In addition, full-length FYCO1 co-expressed with TUBA4A showed structures that could be observed to co-localize with what likely are the centrosome. This must, however, be verified by centrosome staining. However, the localization and distribution of TUBA4A was observed to be changed after the co-expressing with full-length FYCO1. TUBA4A is shown to locate to similar rings as FYCO1 (Figure 3.11D).

A

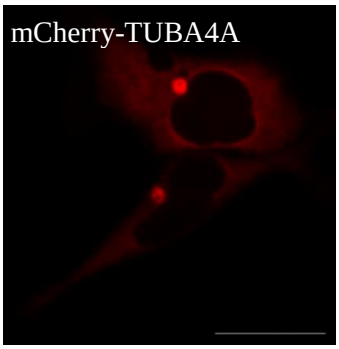
mCherry-TUBA4A

B

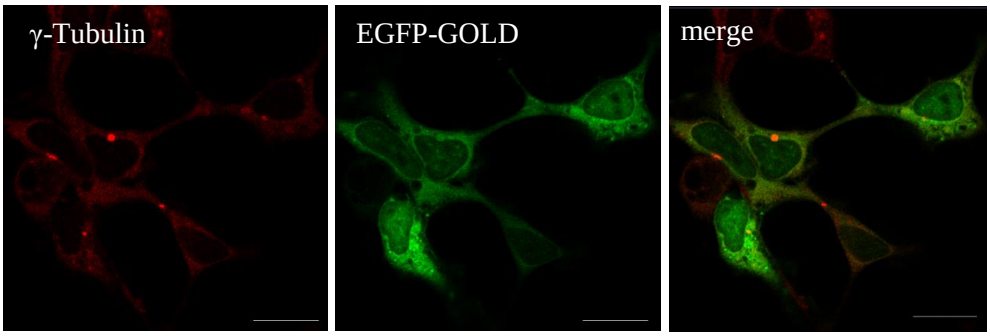
γ-Tubulin
EGFP-GOLD
merge

C

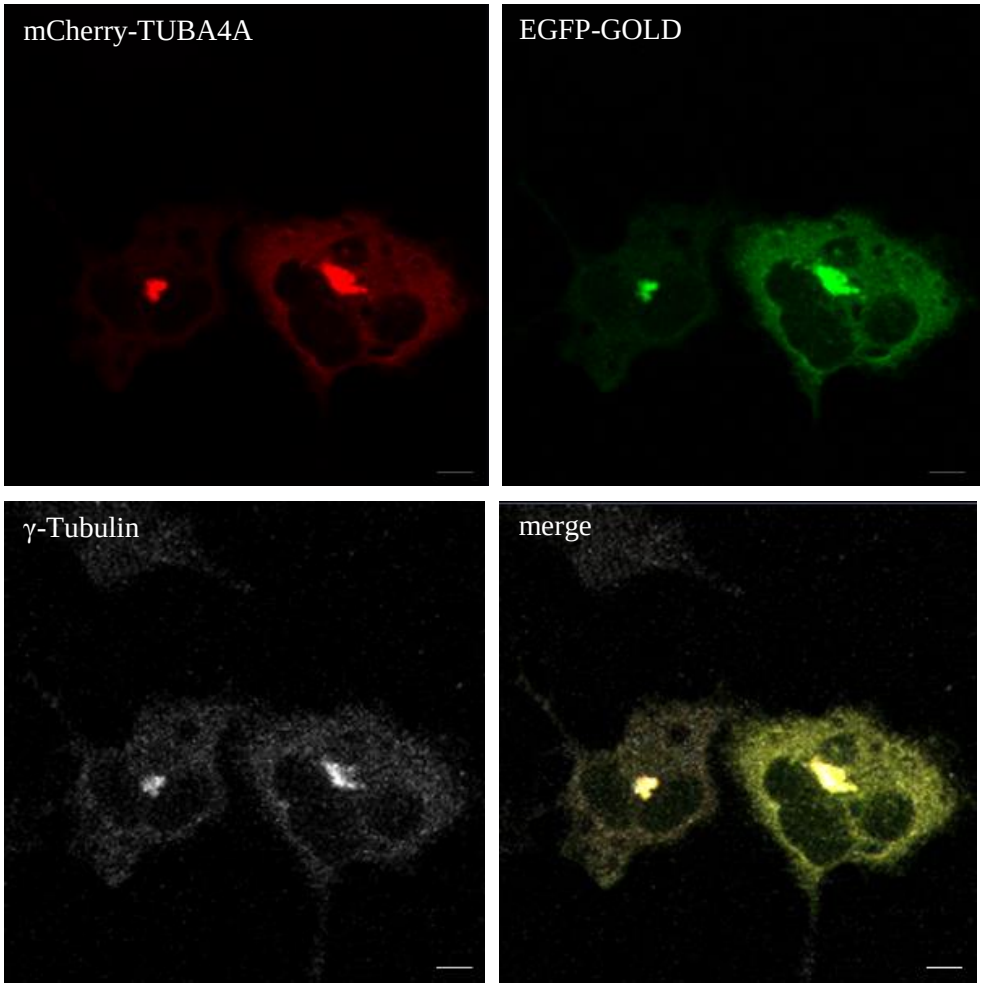
mCherry-TUBA4A
EGFP-GOLD
γ-Tubulin
merge

C (Continue)

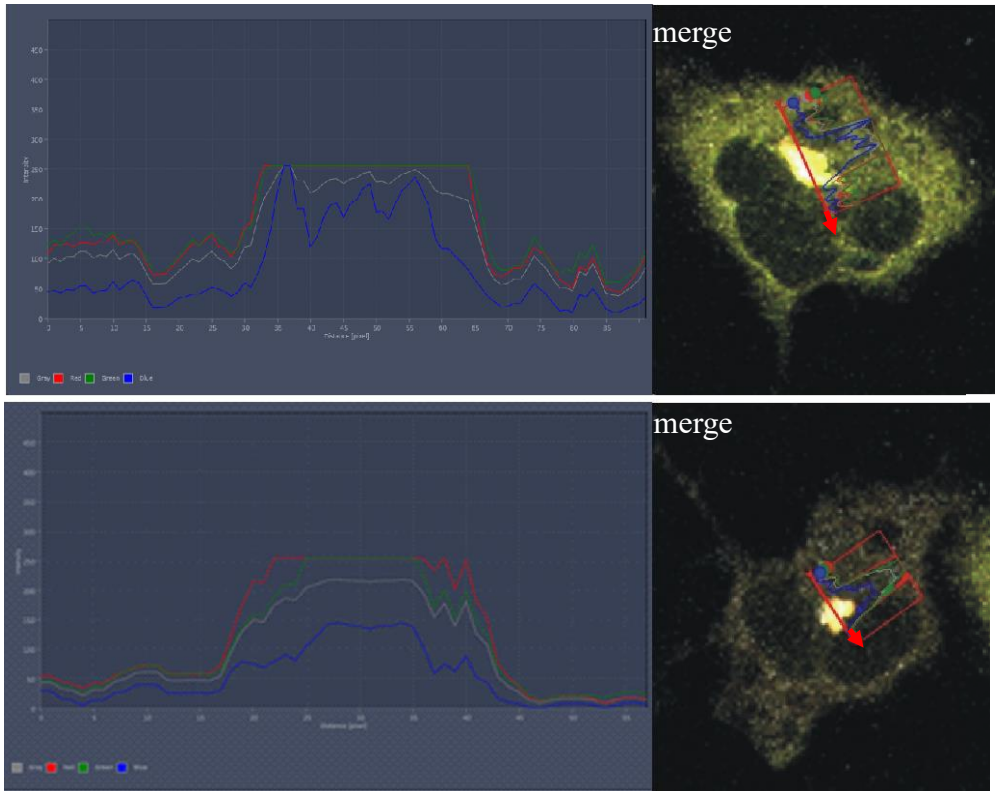

D

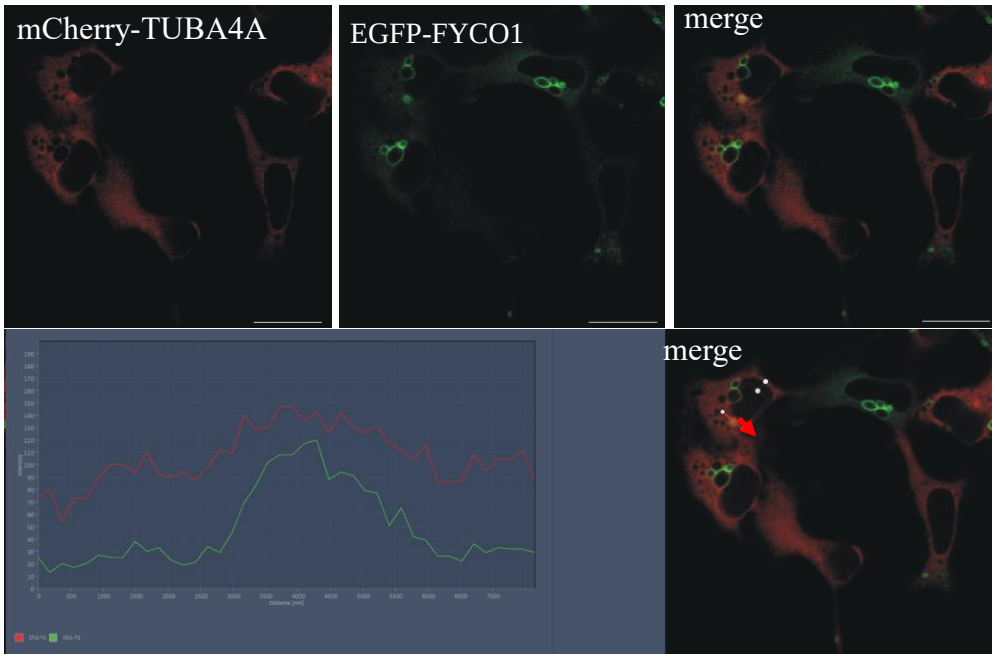

Figure 3.11: TUBA4A redistributes the GOLD domain to the centrosomes

A: HEK293 ZnF-FYCO1 #12 cells were transiently transfected with mCherry-TUBA4A. Scale bare 20 µm **B:** HEK293 ZnF-FYCO1 #12 cells were transiently transfected with EGFP-GOLD and stained for anti- γ-Tubulin. Scale bare 20 µm. **C:** HEK293 ZnF-FYCO1 #12 cells were transiently co-transfected with mCherry-TUBA4A and EGFP-GOLD. The cells were stained for anti- γ-Tubulin. Scale bare 5 µm. Co-localization is measured by a line-plot (lower image), where the intensity of EGFP (green line), mCherry (red line) and anti-Tubulin (grey line) were compared. **D:** HEK293ZnF-FYCO1 #12 cells stably expressing GFP-FYCO1 were transiently transfected with mCherry-TUBA4A. Scale bare 20 µm. Co-localization is measured by a line-plot (lower image) where the intensity of EGFP-FYCO1 and mCherry-TUBA4a were compared. All cells were fixed with methanol (100%).

TXNDC5 seems to be concentrated on ring structures formed by FYCO1

HEK293 Flp-In ZnF-FYCO1 #12 cells were transiently transfected with mCherry-TXNDC5, EGFP-KDEL and EGFP-GOLD (Figure 3.12A-C). When expressed alone, TXNDC5 is diffusely expressed over the whole cell and EGFP-KDEL shows clear ER structure (Figure 3.12A). KDEL is a C-terminal Lys-Asp-Glu-Leu ER retention signal sequence fused to GFP, and is used as an ER marker (Figure 3.12A) (Munro and Pelham, 1987). Human Protein Atlas (Uhlen et al., 2015) was used to identify the location of TXNDC5, TXNDC5 are known to be localized to ER structures (ProteinAtlas). The co-expression of TXNDC5 together with KDEL does not change the distribution of TXNDC5 or KDEL. ER structures can easily be damaged and the cell structures were examined in live cells. TXNDC5 is dynamic, but does not have the same dynamics as the KDEL structures (data not shown) (Figure 3.12B). TXNDC5 does not co-localize with KDEL. This was also observed by the line-plot (Figure 3.12B). In figure 3.12C the HEK293 Flp-In ZnF-FYCO1 #12 cells are fixed. The fixation influenced the KDEL structures, and it was not possible to see the KDEL expression. However, TXNDC5 is observed to be localized perinuclear as a line around nucleus. This is a similar localization as the GOLD domain (Figure 3.10). TXNDC5 is not as much localized in the nucleus as it was observed in the live cells. TXNDC5 share same cytosolic distribution as the GOLD domain (Figure 3.12C). Through the observation and the line-plot measurements, TXNDC5 is partial associated with the GOLD domain (Figure 3.12C). TXNDC5 was co-expressed in HEK293 Flp-In ZnF-FYCO1 #12 cells stably expressing GFP-FYCO1 (Figure 3.12D).The result shows us that TXNDC5 is making clear rings where FYCO1 is located (Figure 3.12D).

A

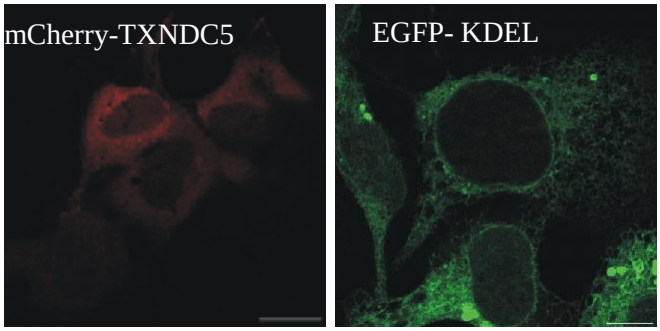
mCherry-TXNDC5
EGFP- KDEL

B

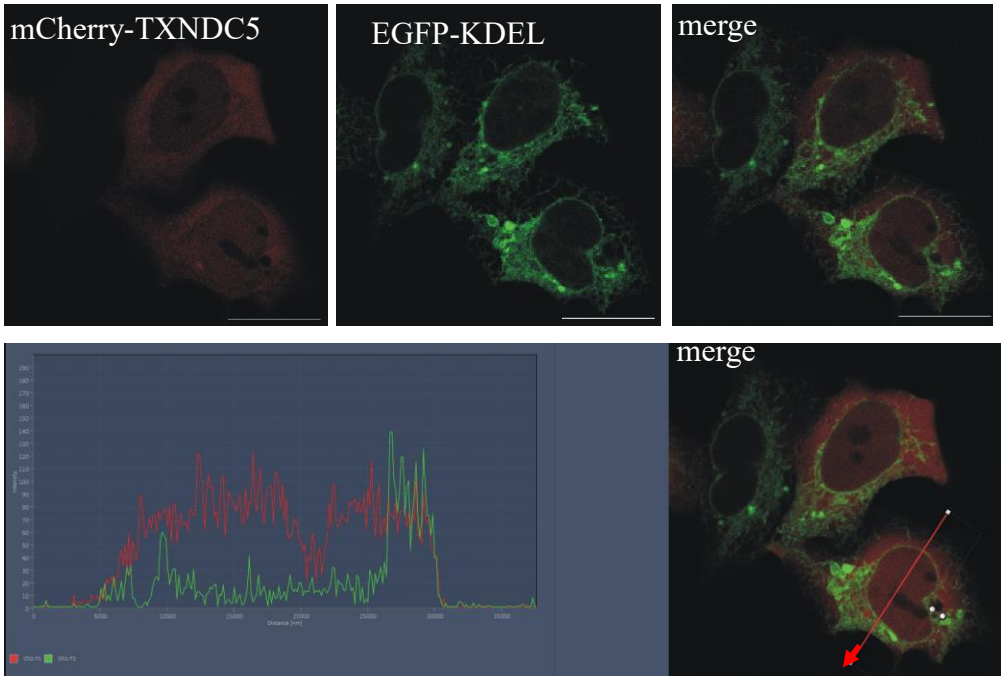
mCherry-TXNDC5
EGFP-KDEL
merge
merge

C

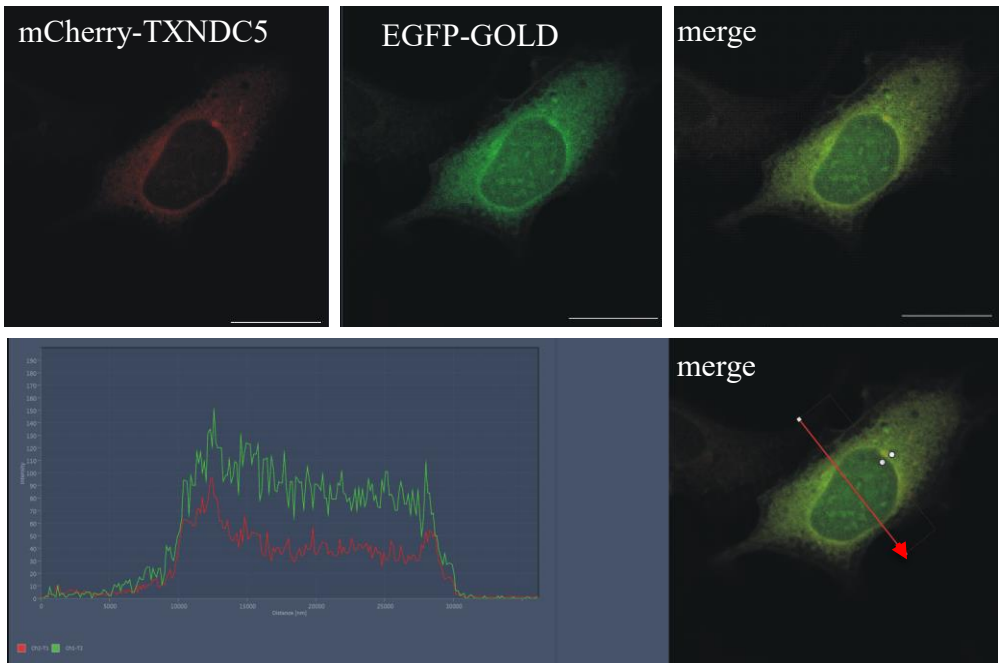

D

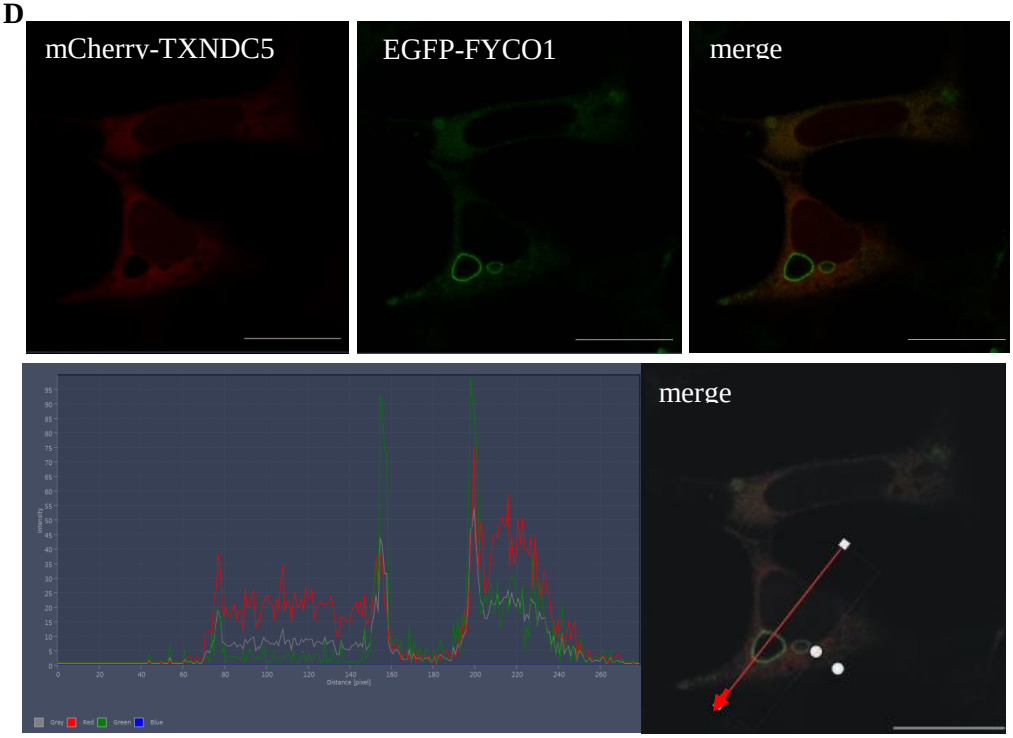

Figure 3.12: TXNDC5 seems to be concentrated on ring structures formed by FYCO1
A: HEK293 ZnF-FYCO1 #12 cells are transfected with mCherry-TXNDC5 (left) and with GFP-KDEL (right). These images are of live cells. Scale bar 20µm. **B:** HEK293 ZnF-FYCO1 #12 Co-transfection with mCherry-TXNDC5 and EGFP-KDEL. These images are of live cells. The co-localization in measured by a line-plot (lower image), where the intensity of EGFP (green line) and mCherry (red) were compared. Scale bare 20µm **C**: Co-transfection with mCherry-TXNDC5 and the EGFP-GOLD domain. These cells are fixed with methanol (100%). The co-localization in measured by a line-plot (lower image), where the intensity of EGFP (green line) and mCherry (red line) were compared. Scale bare 5µm. **D:** HEK293 Flp-In ZnF-FYCO1 #12 cells stably expressing GFP-FYCO1 Transfected with mCherry- TXNDC5. The co-localization in measured by a line-plot (lower image), where the intensity of EGFP (green line) and mCherry (red line) were compared. These cells are fixed with methanol (100%). Scale bar 20µm.

RUVBL2 is diffuse, but has a similar perinuclear distribution as the GOLD domain

HEK293 Flp-In ZnF-FYCO1 #12 cells were transiently transfected with RUVBL2 and the GOLD domain (Figure 3.13). When expressed alone, RUVBL2 is distributed mainly in the cytoplasm, but also observed in the nucleus (Figure 3.13A). When the GOLD domain was expressed together with RUVBL2, RUVBL2 seems to get a more early ER structure, and less localized in the nucleus (Figure 3.13B). RUVBL2 is diffuse, but has a perinuclear distribution similar to the GOLD domain. The line-plot shows a co-localization between RUVBL2 and the GOLD domain (lower image) (Figure 3.13B).

This is due to the diffuse expression of both the GOLD domain and RUVBL2. In addition, RUVBL2 became transfected into HEK293 Flp-In ZnF-FYCO1 #12 cells stably expressing GFP-FYCO1. This result shows that RUVBL2 are distributes in the cytosol and makes clear rings where FYCO1 is observed. According to the line-plot, the association between RUVBL2 and FYCO1 is not clear (Figure 3.13C).

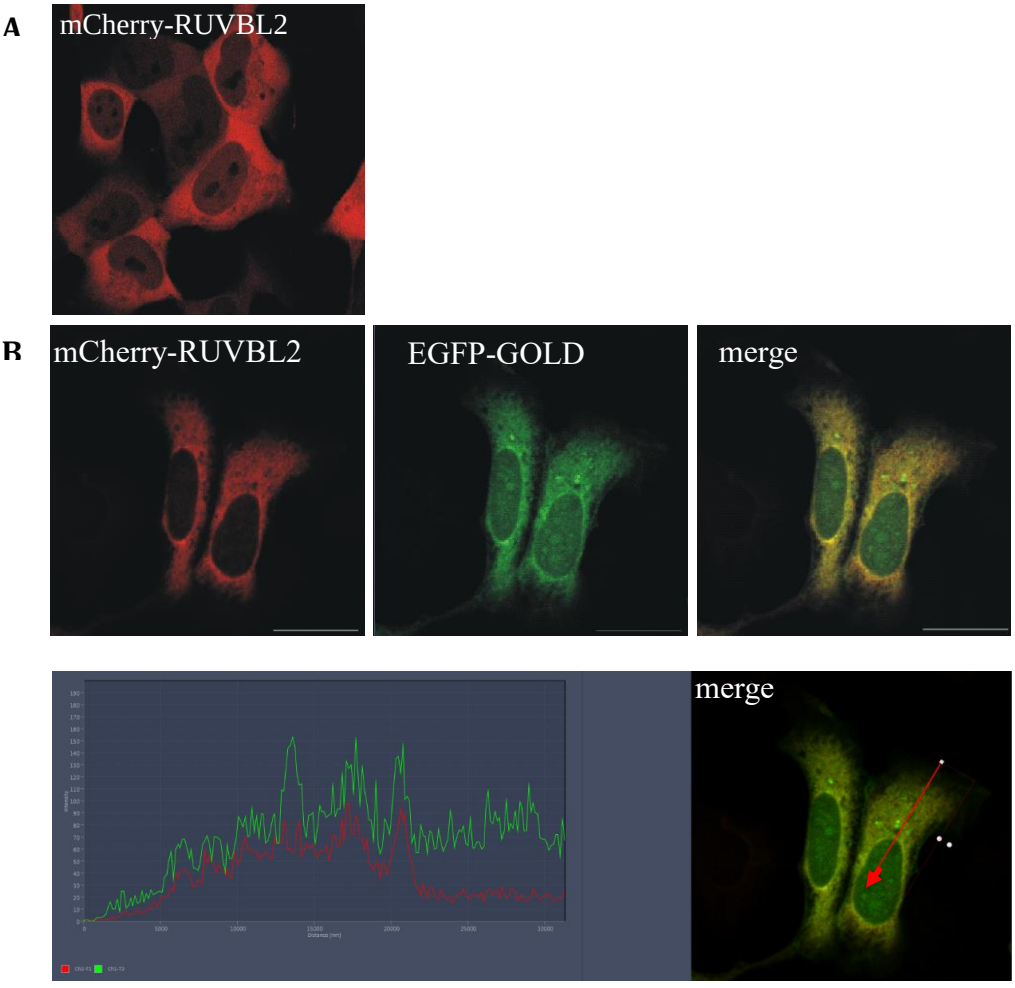

C

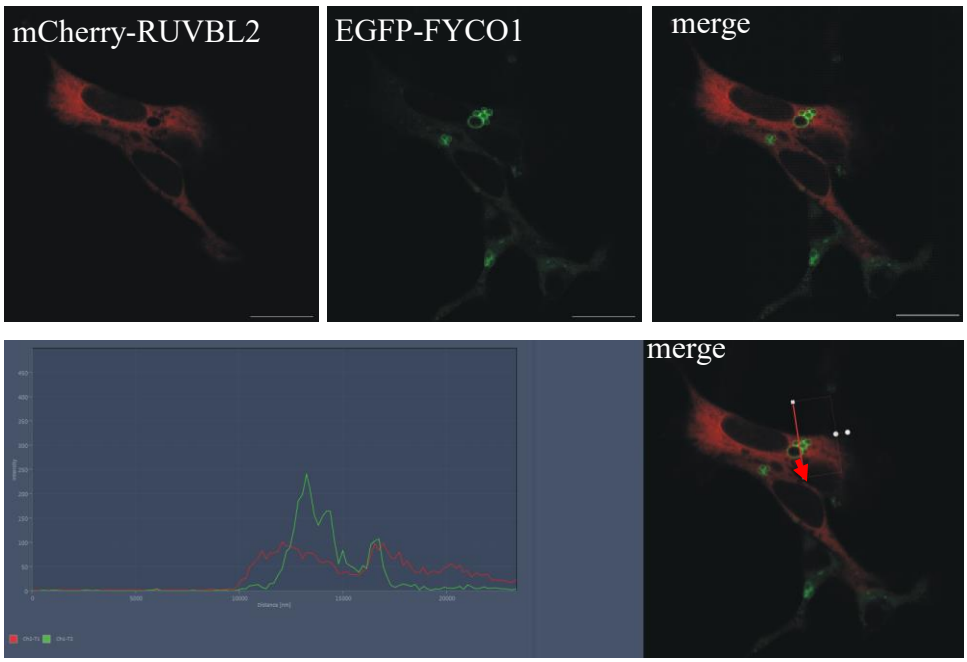

Figure 3.13: RUVBL2 shows expression similarities with the GOLD domain and locsted to ring structures made by full-length FYCO1. A: HEK293 Flp-In ZnF-FYCO1 #12 cells transfected with mCherry- RUVBL2. This image was taken of live cells. Scale bar 20µm. **B:** HEK293 Flp-In ZnF-FYCO1 #12 cells co-transfected with mCherry-RUVBL2 and the EGFP- GOLD domain. Cells were fixated with methanol (100%). Scale bar 20µm. The co-localization between RUVBL2 and the GOLD domain was measured by a line-plot (lowest image), where the intensity between the EGFP (green line) and mCherry (red line) levels were compared. **C:** HEK293 Flp-In ZnF-FYCO1 #12 stably expressing GFP-FYCO1 co-transfected with RUVBL2. Cells were fixated with methanol (100%). Scale bar 20µm.

VPS4A affect the expression and localization of the GOLD domain

Overexpressed VPS4A is known from earlier studies to make aggregated puncta's (Bishop and Woodman, 2000). In our results, shown in figure 3.14, VPS4A puncta's are localized perinuclear. These puncta's became smaller when they are co-expressed together with the GOLD domain (Figure 3.14B). The localization of the GOLD domain seemed to be affected by VPS4. The GOLD domain was observed to obtain a more VPS4A-like expression distribution in the cell when it was co-expressed with VPS4A. The co-localization between these VPS4A puncta and the dense GOLD structures was measured by a line-plot (lower image) (Figure 3.14B). Our line-plot results showed that it is observed a co-localization between VPS4A and the GOLD domain, but the intensity does not rise in the larger perinuclear puncta. More experiments are needed to clarify the issue of co-localization between VPS4A and the isolated GOLD domain as well as FYCO1.

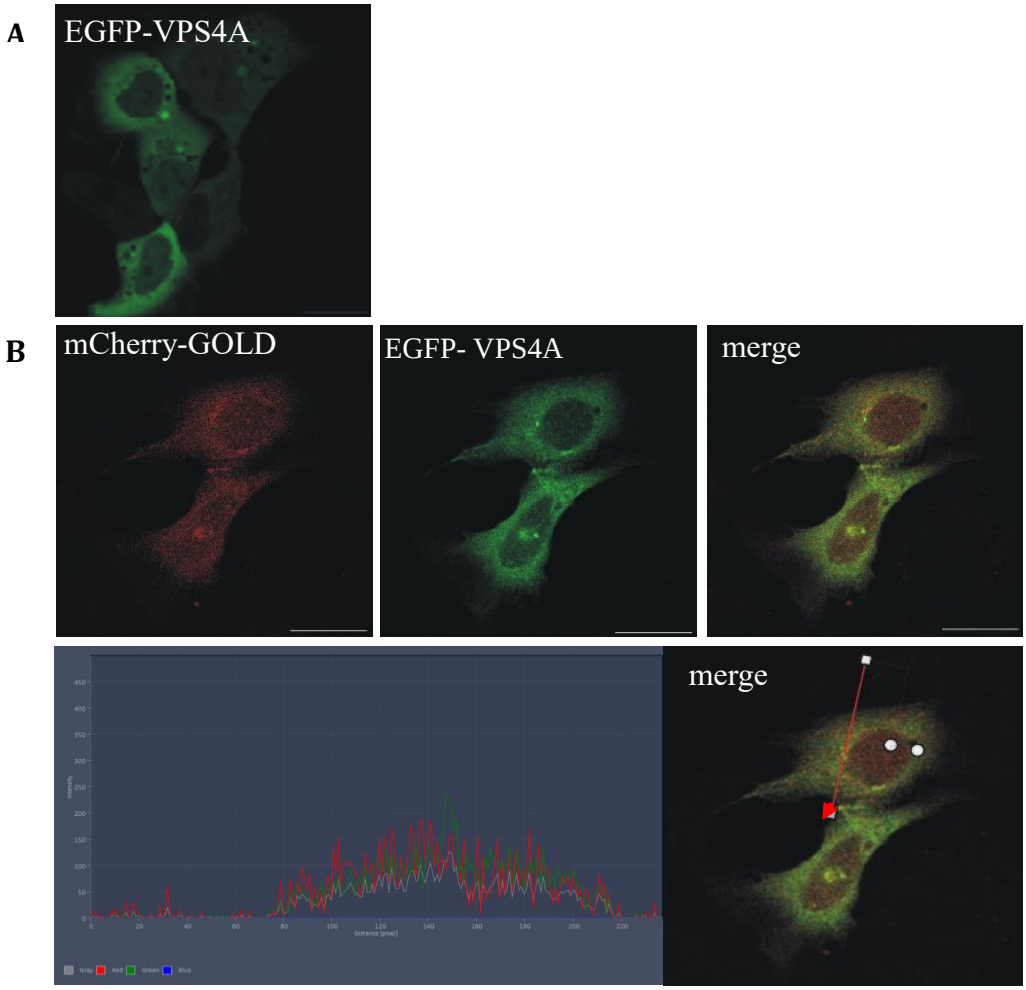

Figure 3.14: VPS4A seems to affect the expression and localization of the GOLD domain. A: HEK293 Flp-In ZnF-FYCO1 #12 cells transfected with EGFP-VPS4. Scale bare 20 µm. **B:** HEK293 Flp-In ZnF-FYCO1 #12 cells co-transfected with EGFP-VPS4A and mCherry-GOLD. Scale bare 20 µm. The co-localization level was measured by a line-plot (Lower image), where the intensity of EGFP (green line) and mCherry (red line) are compared. All cells were fixed with methanol (100%).

Diffuse expression of MON1B in cytoplasm showed a partly overlap with the GOLD domain.

MON1B was diffusely expressed in the cytoplasm, and not highly expressed inside the nucleus. The expression level and localization of the GOLD domain does not seem to be affected by MON1B. Transfection efficiency for the myc-MON1B alone was weak and not possibly to be observed. MON1B does not change the expression level or localization of the GOLD domain, but it is uncertain if MON1B expression level is influenced by the GOLD domain, since MON1B expression is examined alone. By the observation from the images and the line-plot measurements, MON1B seems to overlap with the GOLD domain were they have a higher expression level (Figure 3.15).

Next, the association of MON1B together with full-length FYCO1 was examined in HEK293 Flp-In ZnF-FYCO1 #12 cells stably expressing GFP-FYCO1. Our results shows that MON1B localized not to the FYCO1 rings, as for some of the other protein candidates (e.g. TUBA4A, TXNDC5 and RUVBL2) (Figure 3.15). However, the line-plot shows that the expression level of full-length FYCO1 is much stronger than for MON1B (Figure 3.15).More experiments are needed to clarify the issue of co-localization between MON1B and the isolated GOLD domain as well as FYCO1.

A

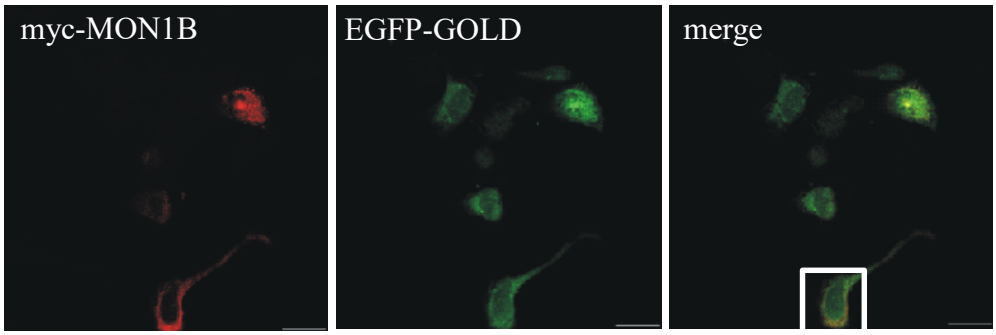

B

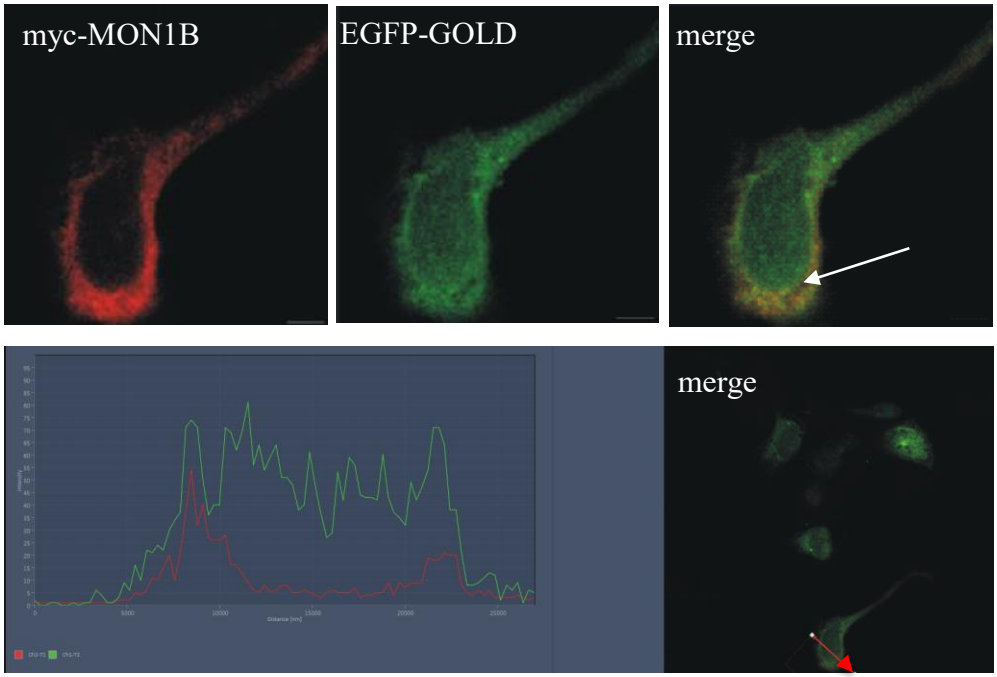

C

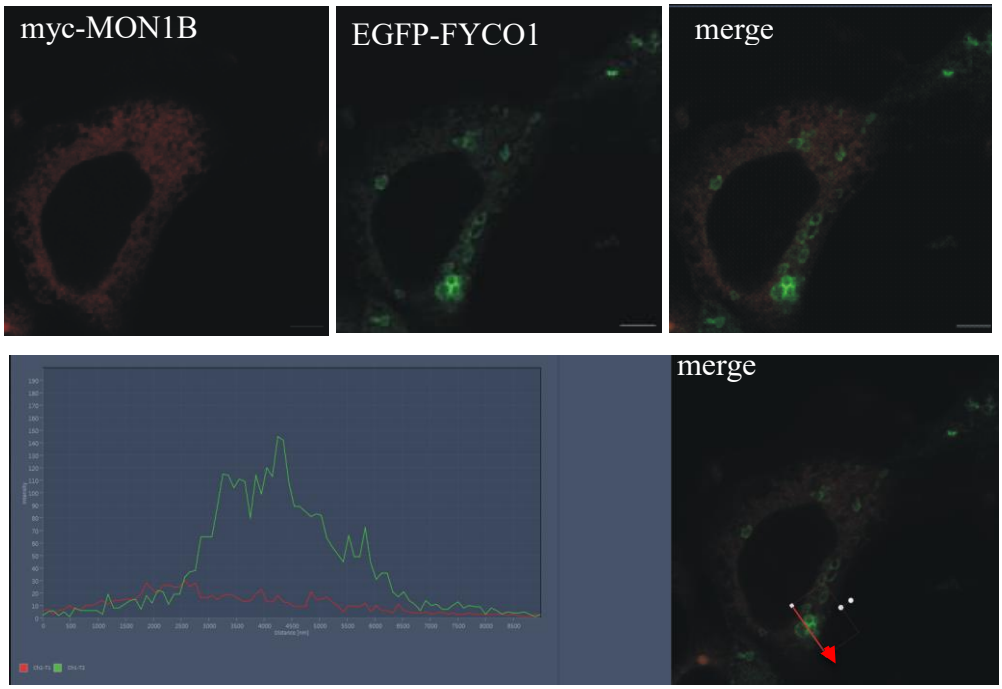

Figure 3.15: Diffuse expression of MON1B in cytoplasm showed a partly overlap with the GOLD domain in specific areas in the cell. HEK293 Flp-In ZnF-FYCO1 #12 cells and HEK293 Flp-In FYCO1 #12 cells stably expressing GFP-FYCO1 were used. All cells were fixated with methanol (100%) and stained for anti-Myc. **A:** HEK293 Flp-In ZnF-FYCO1 #12 cells were co-transfected with myc-MON1B and EGFP-GOLD domain. Scale bar 20 µm. **B:** MON1B seems to partly overlap with the GOLD domain, shown by an arrow. Scale bare 5 µm. Any co-localization was measured by a line plot (lower image) at specific localization, where the intensity of EGFP (green line) and myc-tag (red line) were compared. **C:** Transfection of myc-MON1B in HEK293 Flp-In ZnF-FYCO1 #12 cells stably expressing GFP-FYCO1 were done. Any co-localization was measured by a line plot (lower image) at specific localization, where the intensity of EGFP (green line) and myc-tag (red line) were compared. Scale bare 5 µm.

Low transfection efficiency made it difficult to look at the expression level of DNAJA1 together with the GOLD domain.

The transfection of DNAJA1 alone into HEK293 Flp-In ZnF-FYCO1 #12 cells was not possible to achieve, and the co-transfection together with the GOLD domain was weak (Figure 3.16). It was difficult to examine their co-localization. The result from a line-plot measurements, showed a much higher expression level of EGFP-GOLD than for myc-DNAJA1. Therefore, co-localization between myc-DNAJA1 and EGFP-GOLD domain was difficult to examine (Figure 3.16).

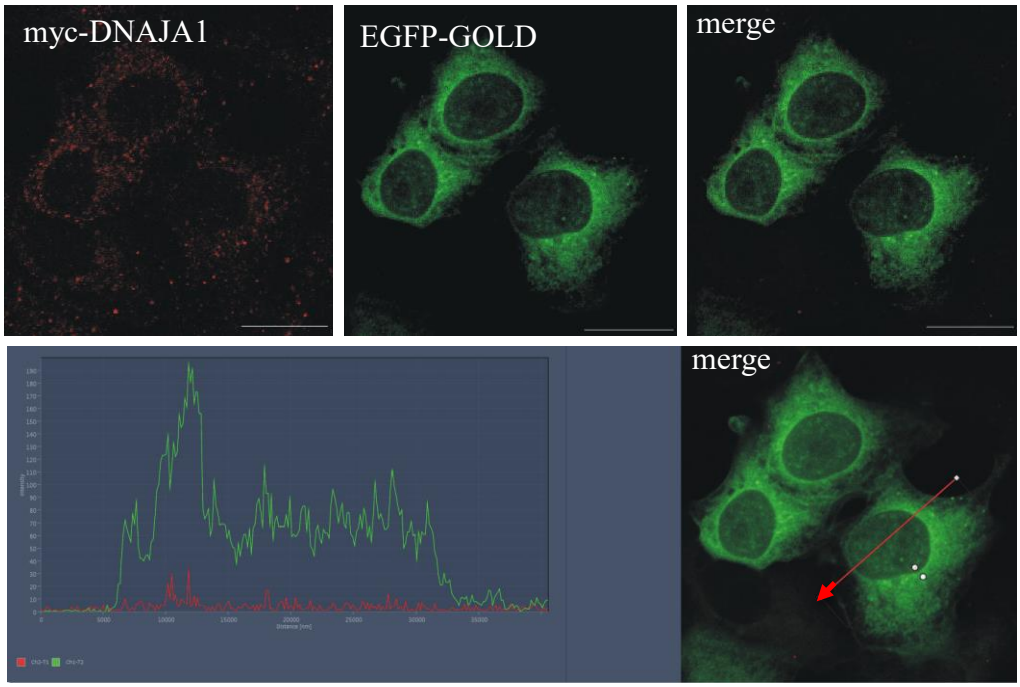

Figure 3.16: Low transfection efficiency made it difficult to look at the expression level of DNAJA1 together with the GOLD domain. HEK293 Flp-In ZnF-FYCO1 #12 cells were co-transfected with myc-DNAJA1 with EGFP- GOLD domain (upper image). Any co-localization was measured by a line plot (lower image) at specific localization, where the intensity of EGFP (green line) and myc-tag (red line) were compared. Scale bar 20µm. All cells were fixated with methanol (100%) and stained for anti-Myc-DNAJA1.

3.9 The L1376P mutation affect the expression level of the GOLD domain

Next, the cell expression differences of the wildtype GOLD- and the mutant GOLD (L1376P) domain was compared. The mutant form of the GOLD domain (L1376P) in the full-length FYCO1 did not show any differences in cellular localization (Chen et al., 2011). Therefore it was interesting to see if the mutation in the isolated GOLD domain changed the cellular localization. The wild type GOLD domain and the mutant GOLD domain (L1376P) were transiently transfected into HeLa cells, human B3 lens cells and HEK293 Flp-In ZnF-FYCO1 #12 cells (Figure 3.17). The GOLD domain is diffusely expressed throughout the cell in all of the cells types examined in this study. However, the mutant GOLD domain (L1376P) has a dramatic aggregated expression appearance distrunctly different from the wild type. This is observed in all of the cell types examined in this study (Figure 3.17).

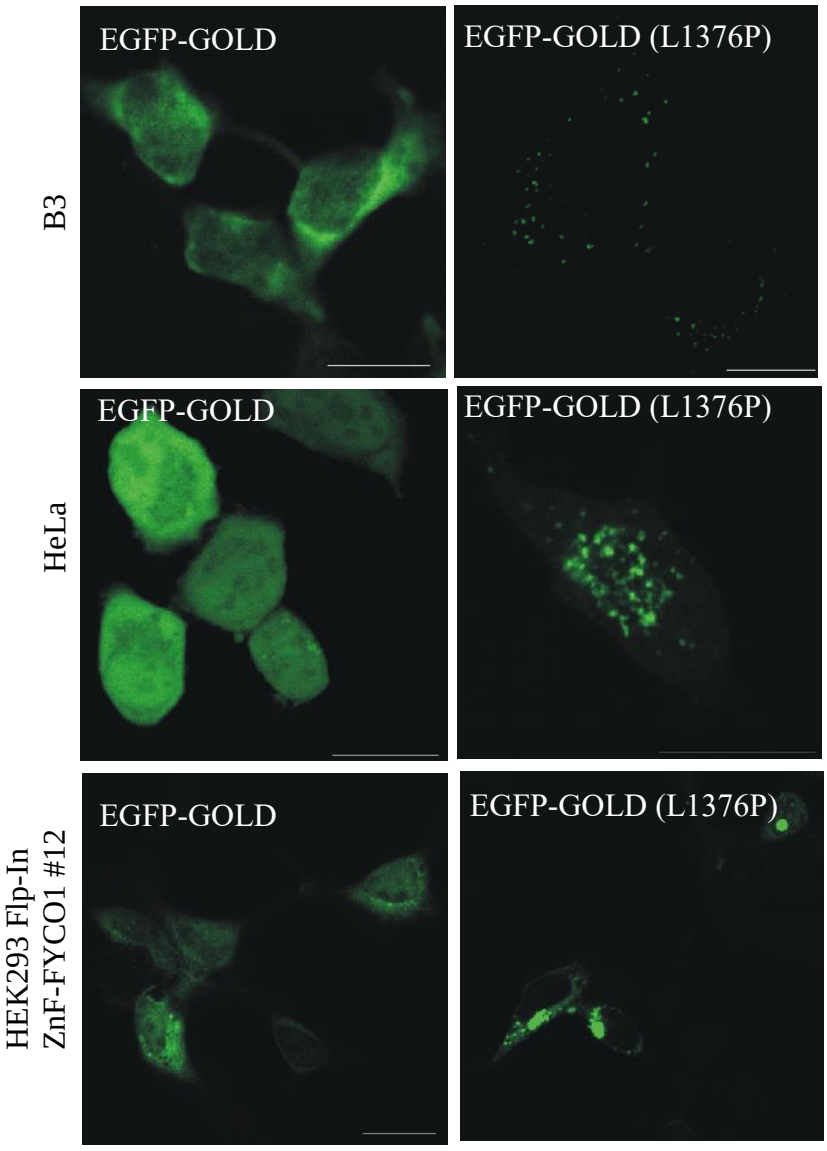

Figure 3.17: Expression of wild type EGFP-GOLD and mutant EGFP-GOLD (L1376P)-domain. B3 cells transiently transfected with wild type EGFP-GOLD and mutant EGFP-GOLD (L1376P)-domain. These cells were fixated with methanol (100%). Scale bare 20 µm. HeLa cells transfected with wild type EGFP-GOLD and EGFP-GOLD (L1376P)-domain. Live cell imagining was used for these cells. Scale bar 20µm. In the lowest line HEK Flp-In ZnF-FYCO1 #12 cells were transient transfected with GFP-GOLD and GFP –GOLD (L1376P).

2.3 FYCO1 surrounds micronuclei like structures in human B3 lens epithelial cells

Human B3 lens cells were transiently transfected with GFP-FYCO1 and the nucleus was visualized with DRAQ5. This revealed an interesting feature about FYCO1. FYCO1 appears to take up micronuclei, DNA-like structures (Figure 3.18). These w observed in approximately one time in each cell. Interestingly, this phenomenon did not appear in other cell lines, such as HeLa and HEK293 Flp-In ZnF-FYCO1 #12 (not shown). Obviously, more work is needed to validate and study this phenomenon further.

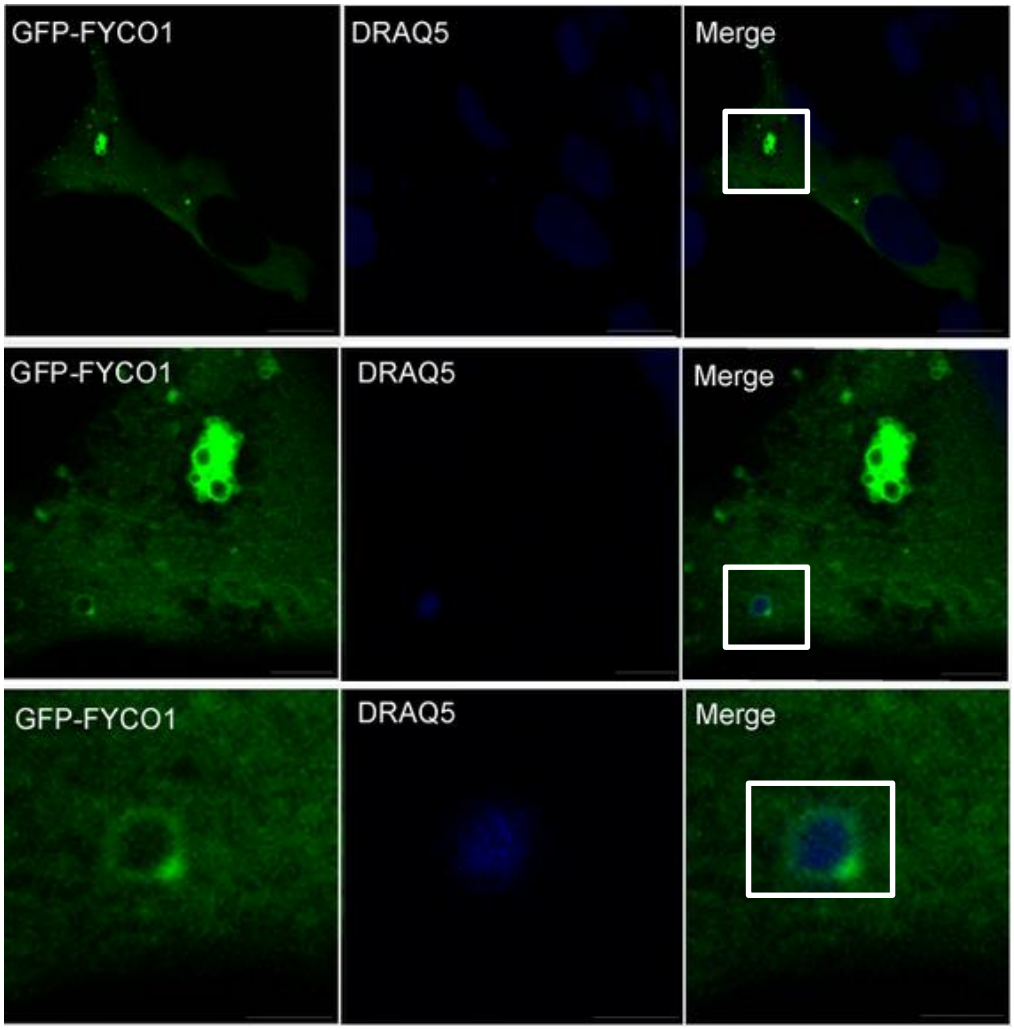

Figure 3.18: Part of the cellular DNA appears to be integrated into FYCO1 structures. Confocal images of B3 cells transfected with EGFP-FYCO1. The nucleus was visualized with DRAQ5. All cells were fixated with methanol (100%).Scale bares 20 µm, 5 µm and 2 µm.

4 Discussion

The initial aim for this study was to identify putative interaction partners for the GOLD domain and the RUN domain of FYCO1. Unfortunately, as a result of technical problems and time limitations, we early ended up to exclude the study of the RUN domain. Instead, the focus was on the identification of protein interaction partners for the GOLD domain. In general, GOLD domains are located in several other proteins with diverse function, as ER to Golgi transport and Golgi dynamics (Anantharaman and Aravind, 2002). For p24 family proteins, the GOLD domain is located at the luminal side of ER, and it was thought that the GOLD domain interacted with luminal cargoes. A recent study reveal that one specific cargo (glycosylphosphatidylinositol-anchored proteins (GPA-AP) interact with p24 proteins through their α-helical region instead of its GOLD domain, which was the first prediction (Theiler et al., 2014). However, the GOLD domain of FYCO1 is located at the C-terminus and it has been supposed that it may be involved in protein interactions. Still, it has not been examined whether the GOLD domain can interact with other proteins. However, Pankiv et at earlier suggested that the GOLD domain of FYCO1 could have intramolecular interaction possibilities, which could have an inhibitory effect on its interaction with lipids (Pankiv et al., 2010). In addition, in a recent study the GOLD domain of SEC14-like domain of supernatant protein factor (SPF) was thought to acts as a regulator, through its intramolecular interaction abilities, which would change its conformation. This occurs to favor ligand binding and release during different synthetic steps (Christen et al., 2015). This led our thought towards the GOLD domain as an intramolecular regulator of FYCO1, which may regulate the binding capabilities of FYCO1 to other proteins. However, the GOLD domain can still be involved in protein-protein interactions, and we have examined the presence of possible interaction candidates.

The results obtained from the mass spectrometry identified putative interaction proteins that were co-precipitated together with the GOLD domain. Our study revealed 182 proteins as direct or indirect protein interaction candidates for the GOLD domain. The results are highly representative, due to our eleven mass spectrometry experiments, wherein unspecific interactions of GST have been excluded. A stringent identification cut-off was set to identification in six or more experminets. Here, 30 putative proteins precipitated together with the GOLD domain in six or more experiments. Nine protein interaction candidates, TUBA4A, DNAJA1, TXNDC5, NIPSNAP1, RUVBL2, GBAS, ARF4, VPS4A and MON1B were selected for further study. From these nine six were identified to interact with membranes (DNAJA1, NIPSNAP1, RUVBL2, GBAS, ARF4 and VPS4A) (Table 3.3). These results were interesting, since FYCO1 is known to be a membrane-associated transport protein through different effector proteins (Pankiv et al., 2010). TUBA4A, RUVBL2 and MON1B were proteins which came down both in an of the interaction study of full-length FYCO1 (Behrends et al., 2010) and in our study of the GOLD domain. These proteins we considered to have the highest change of having a positive interaction capability to FYCO1 through the GOLD domain. MON1B was ranked as one of the best candidates. However, this was not observed in our results, MON1B came down in only one of the eleven experiments and its PSM value of nine, was the lowest one compared to the other nine selected candidates. However, in the Behrends interaction study, TUBA4A and RUVBL2 were ranked lower than MON1B (Behrends et al., 2010). From our study, TUBA4A was the candidate with the highest PSM value (338) and ranked as the best interaction candidate for GOLD.

In this current study, some of the candidates were tested for direct- and indirect interactions through *in vitro* (NIPSNAP1, GBAS, ARF4, DNAJA1, TUBA4A, RUVBL2 and MON1B) and *in vivo* (RUVBL2, TUBA4A, TXNDC5, DNAJA1 and MON1B) interaction assay for their interaction towards the GOLD domain and full-length FYCO1. From our *in vitro* and *in* vivo pulldown results, all of the tested protein interaction candidates were shown to have a very weak interaction affinity towards the GOLD domain.

Our MS results does not separate direct- and indirect protein interactions, proteins that co-precipitated with the GOLD domain can interact with the GOLD domain both directly and indirectly. This may be the explanation for the weak interaction through the *in vitro* and *in vivo* protein interaction assays. In addition, indirect interactions may sometimes be excluded through the transient co-overexpression of two proteins (exogenous). The protein interactions are often through protein complexes. In these types of binding assays, we examine the binding efficiency of the transiently co-overexpressed proteins (exogenous). This high amount of exogenous

protein would have a higher chance to interact and bind to each other than the endogenous proteins. The level of endogenous proteins would be much lower than the co-transfected proteins. Therefore, indirect interactions of the exogenous proteins, which are dependent on a third endogenous protein, may be excluded because of the low protein level of the third protein compared to the transiently co-transfected proteins. However, this is not a completely safe assumption and direct interactions can only be rigorously tested by using purified proteins. Further, some protein-protein interactions can be dependent on the proteins post-translational modifications (PTMs). The PTMs would affect the protein interacting network (Duan and Walther, 2015). PTMs would not be found in *in vitro* assays, and PTMs may not always be present on transient transfection proteins, due to available enzymes, which prossess the PTMs. Hence, it is possible that selected protein interaction candidates can interact with the GFP-GOLD domain in cells even if our interactions assays does not convincingly indicate a direct interaction.

Next, we were interested in examining the expression and localization of the selected protein candidates in human cells together with the GOLD domain and the full-length FYCO1. To examine this, an *in vivo* assay was used to identify their possible co-localization by confocal microcopy. The transient co-transfection of the GOLD domain together with the candidates makes it possible to examine their co-localization. The transient co-transfection increases the expression level of the protein of interest, and it would be easier to identify co-localization for these compared to the endogenous cellular proteins. To examine the co-localization of specific structures or localization, a line-plot was used. In this line- plot, it could be easier to verify if it was any association or co-localization. This measurement was done by comparing the intensity of the different fluorescent channels (GFP, mCherry, Alexa Fluor® 647, Alexa Fluor® 488 (green) and Alexa Fluor® 555 (red)). Unfortunately, the GOLD domain was highly diffusely localized in cells. However, its expression was stronger in a line around the cellular nucleus, which can indicate early ER structures (was not verified in this study). These ER structures can be identified by an ER marker or by treating the cells with Brefeldin A (BFA). BFA inhibits the secretion of proteins from ER to the Golgi apparatus through the prevention of the formation of COPI-mediated transport vesicles (Orcl et al., 1991). This drug can be used to identify any localization arrangement of the GOLD domain. A Golgi marker would also help to look at the localization pattern of the GOLD domain. However, none of these treatments were done to the GOLD domain in this study, but must be done for further study. In this study, the two protein interaction candidates, TUBA4A and VPS4A, changed the localization of the GOLD domain (Figure 11C and 14B).

TUBA4A came down in all of the eleven experiments, including full-length FYCO1. It was therefore supposed that TUBA4A may be a specific interactor of the GOLD domain of full-length FYCO1. In the further studies, TUBA4A was observed to be located at the centrosomes. TUBA4A seems to affect the localization of the GOLD domain and it was observed a redistribution of the GOLD domain to the centrosomes (Figure 3.11C) in association with TUBA4A. TUBA4A may directly or indirectly associate with the GOLD domain through a protein complex.

VPS4A localized diffusely and into some perinuclear puncta/aggregates (Figure 3.14A). These puncta could be part of endosomes. This can be confirmed by staining for endosome markers (not done in this study). Rab5 can be used as an early endosome marker. Rab5 is known to be involved in regulating the motility of early endosomes on microtubules (Nielsen et al., 1999). Rab7 can be used as a late endosome marker, since Rab7 is known to regulate late endosome trafficking (Vanlandingham and Ceresa, 2009) (not used in this study). However, VPS4A was observed to affect the localization of the GOLD domain. The diffuse expression of the GOLD domain was changed somewhat into diffuse pattern that also contained some VPS4A-positive puncta. This observation could be seen in the line-plot (Figure 3.14B).

The expression or localization level of full-length FYCO1 is not affected by either of the protein candidates

Due to time limitation, only TUBA4A, TXNDC5, RUVBL2 and MON1B were transiently transfected into HEK293 Flp-In ZnF-FYCO1 #12 cells (knockout for *FYCO1*) stably expressing GFP-FYCO1. However, through our study MON1B did not seem to make as clear FYCO1 rings (Figure 3.15C) as the other protein candidates. The other protein candidates, TUBA4A, TXNDC5 and RUVBL2 showed similar features as FYCO1 (Figure 3.11D, 3.12D and 3.13C). However, TXNDC5 is reported to mainly be located in ER structures (ProteinAtlas). The rings of full-length FYCO1 is known to be from the ER membrane (Raiborg et al., 2015). Our results did not show any ER localization for TXNDC5 by an ER marker, KDEL (Figure 11B). However, ER is distributed throughout the cell, seen as different structures and in our study. TXNDC5 seemed to be one associated best with FYCO1 structures through the line-plot (Figure 3.12D). For further experiments, another ER marker or inhibitors as BFA can be used to examine if TXNDC5 is localized on other part of the ER.

The L1376P mutation caused aggregation of the GOLD domain.

Mutations in FYCO1, including the GOLD domain mutation L1376P, have earlier been identified to cause autosomal-recessive congenital cataract (Chen et al., 2011). Here, we found that the mutant variant of the GOLD domain (L1376P) changed the expression pattern of the GOLD domain. The mutant variant was more aggregated than the wild type (Figure 3.17). This can suggest a misfolding of the GOLD domain, which can influence the export ability of FYCO1 in the lens. Mutations in FYCO1 have earlier been identified to cause autosomal-recessive congenital cataract (Chen et al., 2011). Our observed expression differences between wild type GOLD domain and mutant GOLD domain (L1376P) may be speculated to be associated with vision loss in patients with autosomal recessive congenital cataracts. By these obtained results and already known information about this mutation, the GOLD domain may be involved in the transparency of the lens. Maybe through a regulation of protein interactions. In further work, staining against structures, such as p62, ubiquitin and stress granules would be interesting to understand the localization of the wild type GOLD versus the mutant GOLD domain.

FYCO1 surrounds micronuclei-like structures in human B3 lens epithelial cells

Another interesting feature of FYCO1 was the observed micronucleus-like, DNA- containing structures inside FYCO1 rings (Figure 3.18). This phenomenon was observed in human B3 lens cells. However, this phenomena have been shown for the endosomal sorting complex required for transport -III (ESCRT-III) subunit CHMP4B (Sagona et al., 2014). CHMP4B seems to share some similar features with FYCO1, such as mutations found in patients with a form for cataract. The mutation of CHMP4B has been shown to inhibit the localization of CHMP4A to micronuclei (Sagona et al., 2014). For further study, it would be interesting to investigate if micronuclei can be found inside the rings of the FYCO1 L1376P mutant. This result may reveal new insight in what degradation cargoes FYCO1 is transporting. Since VPS4A is involved with ESCRT-III filament turnover (Raiborg and Stenmark, 2009) it must be studied if VPS4A, CHMP4B and FYCO1 act together somehow in these micronuclei-like structures.

4.1 Conclusion and further perspective

Our results suggest that the GOLD domain can interact with other proteins, such as TUBA4A VPS4A and TXNDC5. TUBA4A and VPS4Awere observed in our study to affect the localization and expression level of the transiently transfected GOLD domain. It is still unclear if these interactions are direct or indirect. TUBA4A redistribute the GOLD domain to centrosomes, where they all are associated together. In addition, VPS4A redistribute the GOLD domain into VPS4A-containing structures. However, TXNDC5 immune-precipitated together with the GOLD domain *in vivo,* and MON1B immune-precipitated together with the full-length FYCO1, which Behrends et al. have shown earlier (Behrends et al., 2010). This suggest an interaction possibility towards the GOLD domain and full-length FYCO1 respectively. However, further studies with additional bindings assay have to be performed to firmly conclude about the GOLD domain interactions focused on here

Next, we found the GOLD domain to be diffusely expressed throughout the cells. However, in our current study, the mutated GOLD domain (L1376P) formed multiple small aggregates. As previously shown by Chen and colleagues, mutations in FYCO1 have been shown to form truncated proteins and cause termination of the peptide chain before the GOLD domain. The mutation L1376P was identified to affect the transparency of the lens. It would be interesting to further examine the role of the GOLD domain mutation in full-length FYCO1 *in* vivo. Will we observe micronuclei inside FYCO1 rings in human B3 cells with the L1376P mutant? Is there any role for FYCO1 in DNA degradation during lens transparency?

5 References

ADAMS, J. 2003. The proteasome: structure, function, and role in the cell. *Cancer Treat Rev,* 29 Suppl 1**,** 3-9.

AEBERSOLD, R. & MANN, M. 2003. Mass spectrometry-based proteomics. *Nature,* 422**,** 198-207.

ALLAN, V. J. 2011. Cytoplasmic dynein. *Biochem Soc Trans,* 39**,** 1169-78.

ANANTHARAMAN, V. & ARAVIND, L. 2002. The GOLD domain, a novel protein module involved in Golgi function and secretion. *Genome Biol,* 3**,** research0023.

ANTONNY, B., BERAUD-DUFOUR, S., CHARDIN, P. & CHABRE, M. 1997. N-terminal hydrophobic residues of the G-protein ADP-ribosylation factor-1 insert into membrane phospholipids upon GDP to GTP exchange. *Biochemistry,* 36**,** 4675-84.

AO, X., ZOU, L. & WU, Y. 2014. Regulation of autophagy by the Rab GTPase network. *Cell Death Differ,* 21**,** 348-358.

BEHRENDS, C., SOWA, M. E., GYGI, S. P. & HARPER, J. W. 2010. Network organization of the human autophagy system. *Nature,* 466**,** 68-76.

BERSHADSKY, A. D. & VASILIEV, J. M. 2012. *Cytoskeleton,* Springer Science & Business Media.

BIRNBOIM, H. C. & DOLY, J. 1979. A rapid alkaline extraction procedure for screening recombinant plasmid DNA. *Nucleic Acids Res,* 7**,** 1513-23.

BISHOP, N. & WOODMAN, P. 2000. ATPase-defective mammalian VPS4 localizes to aberrant endosomes and impairs cholesterol trafficking. *Mol Biol Cell,* 11**,** 227-39.

BLANCHOIN, L., BOUJEMAA-PATERSKI, R., SYKES, C. & PLASTINO, J. 2014. Actin Dynamics, Architecture, and Mechanics in Cell Motility. *Physiological Reviews,* 94**,** 235-263.

CABRERA, M., NORDMANN, M., PERZ, A., SCHMEDT, D., GERONDOPOULOS, A., BARR, F., PIEHLER, J., ENGELBRECHT-VANDRE, S. & UNGERMANN, C. 2014. The Mon1-Ccz1 GEF activates the Rab7 GTPase Ypt7 via a longin-fold-Rab interface and association with PI3P-positive membranes. *J Cell Sci,* 127**,** 1043-51.

CALLEBAUT, I., DE GUNZBURG, J., GOUD, B. & MORNON, J. P. 2001. RUN domains: a new family of domains involved in Ras-like GTPase signaling. *Trends Biochem Sci,* 26**,** 79-83.

CANTALUPO, G., ALIFANO, P., ROBERTI, V., BRUNI, C. B. & BUCCI, C. 2001. Rab-interacting lysosomal protein (RILP): the Rab7 effector required for transport to lysosomes. *Embo j,* 20**,** 683-93.

CARDOSO, C., GROTH-PEDERSEN, L., HØYER-HANSEN, M., KIRKEGAARD, T., CORCELLE, E., ANDERSEN, J. S., JÄÄTTELÄ, M. & NYLANDSTED, J. 2009. Depletion of kinesin 5B affects lysosomal distribution and stability and induces peri-nuclear accumulation of autophagosomes in cancer cells. *PLoS One,* 4**,** e4424.

CHARLTON, H. K., WEBSTER, J., KRUGER, S., SIMPSON, F., RICHARDS, A. A. & WHITEHEAD, J. P. 2010. ERp46 binds to AdipoR1, but not AdipoR2, and modulates adiponectin signalling. *Biochem Biophys Res Commun,* 392**,** 234-9.

CHEN, J., MA, Z., JIAO, X., FARISS, R., KANTOROW, WANDA L., KANTOROW, M., PRAS, E., FRYDMAN, M., PRAS, E., RIAZUDDIN, S., RIAZUDDIN, S. A. & HEJTMANCIK, J. F. 2011. Mutations in FYCO1 Cause Autosomal-Recessive Congenital Cataracts. *The American Journal of Human Genetics,* 88**,** 827-838.

CHRISTEN, M., MARCAIDA, M. J., LAMPRAKIS, C., AESCHIMANN, W., VAITHILINGAM, J., SCHNEIDER, P., HILBERT, M., SCHNEIDER, G., CASCELLA, M. & STOCKER, A. 2015. Structural insights on cholesterol endosynthesis: Binding of squalene and 2,3-oxidosqualene to supernatant protein factor. *J Struct Biol,* 190**,** 261-70.

CONDE, C. & CACERES, A. 2009. Microtubule assembly, organization and dynamics in axons and dendrites. *Nat Rev Neurosci,* 10**,** 319-332.
CONSORTIUM, T. U. 2015. UniProt: a hub for protein information. *Nucleic Acids Research,* 43**,** D204-D212.
D'SOUZA-SCHOREY, C. & CHAVRIER, P. 2006. ARF proteins: roles in membrane traffic and beyond. *Nat Rev Mol Cell Biol,* 7**,** 347-58.
DONALDSON, J. G. & JACKSON, C. L. 2011. ARF family G proteins and their regulators: roles in membrane transport, development and disease. *Nat Rev Mol Cell Biol,* 12**,** 362-375.
DOOLEY, H. C., RAZI, M., POLSON, H. E., GIRARDIN, S. E., WILSON, M. I. & TOOZE, S. A. 2014. WIPI2 links LC3 conjugation with PI3P, autophagosome formation, and pathogen clearance by recruiting Atg12-5-16L1. *Mol Cell,* 55**,** 238-52.
DUAN, G. & WALTHER, D. 2015. The Roles of Post-translational Modifications in the Context of Protein Interaction Networks. *PLoS Computational Biology,* 11**,** e1004049.
EUROPEAN BIOINFORMATICS INSTITUTE (EMBL-EBI), C. O. 2016. *Help - Clustal Omega FAQ* [Online]. Available: http://www.ebi.ac.uk/Tools/msa/clustalo/help/faq.html#23 [Accessed 2016].
FENN, J. B., MANN, M., MENG, C. K., WONG, S. F. & WHITEHOUSE, C. M. 1989. Electrospray ionization for mass spectrometry of large biomolecules. *Science,* 246**,** 64-71.
FLETCHER, D. A. & MULLINS, R. D. 2010. Cell mechanics and the cytoskeleton. *Nature,* 463**,** 485-492.
GASKELL, A., CRENNELL, S. & TAYLOR, G. 1995. The three domains of a bacterial sialidase: a beta-propeller, an immunoglobulin module and a galactose-binding jelly-roll. *Structure,* 3**,** 1197-205.
GAULLIER, J. M., SIMONSEN, A., D'ARRIGO, A., BREMNES, B., STENMARK, H. & AASLAND, R. 1998. FYVE fingers bind PtdIns(3)P. *Nature,* 394**,** 432-3.
GOUJON, M., MCWILLIAM, H., LI, W., VALENTIN, F., SQUIZZATO, S., PAERN, J. & LOPEZ, R. 2010. A new bioinformatics analysis tools framework at EMBL–EBI. *Nucleic Acids Research,* 38**,** W695-W699.
HAILEY, D. W., RAMBOLD, A. S., SATPUTE-KRISHNAN, P., MITRA, K., SOUGRAT, R., KIM, P. K. & LIPPINCOTT-SCHWARTZ, J. 2010. Mitochondria supply membranes for autophagosome biogenesis during starvation. *Cell,* 141**,** 656-67.
HAMMER III, J. A. & WU, X. S. 2002. Rabs grab motors: defining the connections between Rab GTPases and motor proteins. *Current Opinion in Cell Biology,* 14**,** 69-75.
HARTLEY, J. L., TEMPLE, G. F. & BRASCH, M. A. 2000. DNA cloning using in vitro site-specific recombination. *Genome Res,* 10**,** 1788-95.
HARVARD. 2016. *Harvard PlasmID collection* [Online]. Available: https://plasmid.med.harvard.edu/PLASMID/Home.xhtml [Accessed 2016].
HERRMANN, H. & AEBI, U. 2004. Intermediate filaments: molecular structure, assembly mechanism, and integration into functionally distinct intracellular Scaffolds. *Annu Rev Biochem,* 73**,** 749-89.
HIROKAWA, N. 1998. Kinesin and Dynein Superfamily Proteins and the Mechanism of Organelle Transport. *Science,* 279**,** 519-526.
HYTTINEN, J. M. T., NIITTYKOSKI, M., SALMINEN, A. & KAARNIRANTA, K. 2013. Maturation of autophagosomes and endosomes: A key role for Rab7. *Biochimica et Biophysica Acta (BBA) - Molecular Cell Research,* 1833**,** 503-510.
INVITROGEN 2010. Flp-In™ System,For Generating Stable Mammalian Expression,Cell Lines by Flp Recombinase-Mediated Integration, User Manual, Version E, Cat.no: K6010–01, K6010–02

JOHANSEN, T. & LAMARK, T. 2011. Selective autophagy mediated by autophagic adapter proteins. *Autophagy,* 7**,** 279-296.
JOHNSON, D. E., OSTROWSKI, P., JAUMOUILLE, V. & GRINSTEIN, S. 2016. The position of lysosomes within the cell determines their luminal pH. *J Cell Biol,* 212**,** 677-92.
KELLEY, L. A., MEZULIS, S., YATES, C. M., WASS, M. N. & STERNBERG, M. J. E. 2015. The Phyre2 web portal for protein modeling, prediction and analysis. *Nat. Protocols,* 10**,** 845-858.
KIM, J., KUNDU, M., VIOLLET, B. & GUAN, K.-L. 2011. AMPK and mTOR regulate autophagy through direct phosphorylation of Ulk1. *Nat Cell Biol,* 13**,** 132-141.
KISS, H., YANG, Y., KISS, C., ANDERSSON, K., KLEIN, G., IMREH, S. & DUMANSKI, J. P. 2002. The transcriptional map of the common eliminated region 1 (C3CER1) in 3p21.3. *Eur J Hum Genet,* 10**,** 52-61.
KITAGISHI, Y. & MATSUDA, S. 2013. RUFY, Rab and Rap Family Proteins Involved in a Regulation of Cell Polarity and Membrane Trafficking. *Int J Mol Sci,* 14**,** 6487-98.
LAMARK, T., PERANDER, M., OUTZEN, H., KRISTIANSEN, K., OVERVATN, A., MICHAELSEN, E., BJORKOY, G. & JOHANSEN, T. 2003. Interaction codes within the family of mammalian Phox and Bem1p domain-containing proteins. *J Biol Chem,* 278**,** 34568-81.
LEMMON, M. A. 2008. Membrane recognition by phospholipid-binding domains. *Nat Rev Mol Cell Biol,* 9**,** 99-111.
LI, W.-W., LI, J. & BAO, J.-K. 2011. Microautophagy: lesser-known self-eating. *Cellular and Molecular Life Sciences,* 69**,** 1125-1136.
LICHTMAN, J. W. & CONCHELLO, J. A. 2005. Fluorescence microscopy. *Nat Methods,* 2**,** 910-9.
LIN, W. J., YANG, C. Y., LI, L. L., YI, Y. H., CHEN, K. W., LIN, Y. C., LIU, C. C. & LIN, C. H. 2012. Lysosomal targeting of phafin1 mediated by Rab7 induces autophagosome formation. *Biochem Biophys Res Commun,* 417**,** 35-42.
MA, J., BECKER, C., REYES, C. & UNDERHILL, D. M. 2014. Cutting edge: FYCO1 recruitment to dectin-1 phagosomes is accelerated by light chain 3 protein and regulates phagosome maturation and reactive oxygen production. *J Immunol,* 192**,** 1356-60.
MARZA, E., TAOUJI, S., BARROSO, K., RAYMOND, A. A., GUIGNARD, L., BONNEU, M., PALLARES-LUPON, N., DUPUY, J. W., FERNANDEZ-ZAPICO, M. E., ROSENBAUM, J., PALLADINO, F., DUPUY, D. & CHEVET, E. 2015. Genome-wide screen identifies a novel p97/CDC-48-dependent pathway regulating ER-stress-induced gene transcription. *EMBO Rep,* 16**,** 332-40.
MICHALSKI, A., DAMOC, E., HAUSCHILD, J.-P., LANGE, O., WIEGHAUS, A., MAKAROV, A., NAGARAJ, N., COX, J., MANN, M. & HORNING, S. 2011. Mass Spectrometry-based Proteomics Using Q Exactive, a High-performance Benchtop Quadrupole Orbitrap Mass Spectrometer. *Molecular & Cellular Proteomics,* 10.
MIZUSHIMA, N. & KOMATSU, M. 2011. Autophagy: Renovation of Cells and Tissues. *Cell,* 147**,** 728-741.
MIZUSHIMA, N., YAMAMOTO, A., HATANO, M., KOBAYASHI, Y., KABEYA, Y., SUZUKI, K., TOKUHISA, T., OHSUMI, Y. & YOSHIMORI, T. 2001. Dissection of autophagosome formation using Apg5-deficient mouse embryonic stem cells. *J Cell Biol,* 152**,** 657-68.
MIZUSHIMA, N., YOSHIMORI, T. & OHSUMI, Y. 2011. The role of Atg proteins in autophagosome formation. *Annu Rev Cell Dev Biol,* 27**,** 107-32.
MOURINO-PEREZ, R. R., RIQUELME, M., CALLEJAS-NEGRETE, O. A. & GALVAN-MENDOZA, J. I. 2016. Microtubules and associated molecular motors in Neurospora crassa. *Mycologia*.

MUNRO, S. & PELHAM, H. R. B. 1987. A C-terminal signal prevents secretion of luminal ER proteins. *Cell,* 48**,** 899-907.
NAKATOGAWA, H., SUZUKI, K., KAMADA, Y. & OHSUMI, Y. 2009. Dynamics and diversity in autophagy mechanisms: lessons from yeast. *Nat Rev Mol Cell Biol,* 10**,** 458-467.
NIELSEN, E., SEVERIN, F., BACKER, J. M., HYMAN, A. A. & ZERIAL, M. 1999. Rab5 regulates motility of early endosomes on microtubules. *Nat Cell Biol,* 1**,** 376-82.
NODA, N. N., OHSUMI, Y. & INAGAKI, F. 2010. Atg8-family interacting motif crucial for selective autophagy. *FEBS Lett,* 584**,** 1379-85.
OLSEN, J. V., ONG, S. E. & MANN, M. 2004. Trypsin cleaves exclusively C-terminal to arginine and lysine residues. *Mol Cell Proteomics,* 3**,** 608-14.
OLSVIK, H. L., LAMARK, T., TAKAGI, K., BOWITZ LARSEN, K., EVJEN, G., OVERVATN, A., MIZUSHIMA, T. & JOHANSEN, T. 2015. FYCO1 Contains a C-terminally Extended, LC3A/B-preferring LC3-Interacting Region (LIR) Motif Required for Efficient Maturation of Autophagosomes During Basal Autophagy. *J Biol Chem.*
ORCL, L., TAGAYA, M., AMHERDT, M., PERRELET, A., DONALDSON, J. G., LIPPINCOTT-SCHWARTZ, J., KLAUSNER, R. D. & ROTHMAN, J. E. 1991. Brefeldin A, a drug that blocks secretion, prevents the assembly of non-clathrin-coated buds on Golgi cisternae. *Cell,* 64**,** 1183-1195.
ORENSTEIN, S. J. & CUERVO, A. M. 2010. Chaperone-mediated autophagy: Molecular mechanisms and physiological relevance. *Seminars in cell & developmental biology,* 21**,** 719-726.
PANKIV, S., ALEMU, E. A., BRECH, A., BRUUN, J. A., LAMARK, T., OVERVATN, A., BJORKOY, G. & JOHANSEN, T. 2010. FYCO1 is a Rab7 effector that binds to LC3 and PI3P to mediate microtubule plus end-directed vesicle transport. *J Cell Biol,* 188**,** 253-69.
PANKIV, S., CLAUSEN, T. H., LAMARK, T., BRECH, A., BRUUN, J. A., OUTZEN, H., OVERVATN, A., BJORKOY, G. & JOHANSEN, T. 2007. p62/SQSTM1 binds directly to Atg8/LC3 to facilitate degradation of ubiquitinated protein aggregates by autophagy. *J Biol Chem,* 282**,** 24131-45.
PERKINS, D. N., PAPPIN, D. J., CREASY, D. M. & COTTRELL, J. S. 1999. Probability-based protein identification by searching sequence databases using mass spectrometry data. *Electrophoresis,* 20**,** 3551-67.
PICKART, C. M. & COHEN, R. E. 2004. Proteasomes and their kin: proteases in the machine age. *Nat Rev Mol Cell Biol,* 5**,** 177-87.
PROTEINATLAS. *Human Protein Atlas, TXNDC5* [Online]. Available: http://www.proteinatlas.org/ENSG00000239264-TXNDC5/subcellular [Accessed 2016].
QIU, X. B., SHAO, Y. M., MIAO, S. & WANG, L. 2006. The diversity of the DnaJ/Hsp40 family, the crucial partners for Hsp70 chaperones. *Cell Mol Life Sci,* 63**,** 2560-70.
RAIBORG, C. & STENMARK, H. 2009. The ESCRT machinery in endosomal sorting of ubiquitylated membrane proteins. *Nature,* 458**,** 445-52.
RAIBORG, C., WENZEL, E. M., PEDERSEN, N. M., OLSVIK, H., SCHINK, K. O., SCHULTZ, S. W., VIETRI, M., NISI, V., BUCCI, C., BRECH, A., JOHANSEN, T. & STENMARK, H. 2015. Repeated ER–endosome contacts promote endosome translocation and neurite outgrowth. *Nature,* 520**,** 234-238.
RAVIKUMAR, B., MOREAU, K., JAHREISS, L., PURI, C. & RUBINSZTEIN, D. C. 2010. Plasma membrane contributes to the formation of pre-autophagosomal structures. *Nat Cell Biol,* 12**,** 747-57.

RECACHA, R., BOULET, A., JOLLIVET, F., MONIER, S., HOUDUSSE, A., GOUD, B. & KHAN, A. R. 2009. Structural basis for recruitment of Rab6-interacting protein 1 to Golgi via a RUN domain. *Structure,* 17**,** 21-30.

ROBINSON, G. C., JAN, J. E. & KINNIS, C. 1987. Congenital ocular blindness in children, 1945 to 1984. *Am J Dis Child,* 141**,** 1321-4.

ROSE, A., SCHRAEGLE, S. J., STAHLBERG, E. A. & MEIER, I. 2005. Coiled-coil protein composition of 22 proteomes – differences and common themes in subcellular infrastructure and traffic control. *BMC Evolutionary Biology,* 5**,** 1-21.

SAFTIG, P. & KLUMPERMAN, J. 2009. Lysosome biogenesis and lysosomal membrane proteins: trafficking meets function. *Nat Rev Mol Cell Biol,* 10**,** 623-35.

SAGONA, A. P., NEZIS, I. P. & STENMARK, H. 2014. Association of CHMP4B and autophagy with micronuclei: implications for cataract formation. *BioMed research international,* 2014.

SCHEURING, S., ROHRICHT, R. A., SCHONING-BURKHARDT, B., BEYER, A., MULLER, S., ABTS, H. F. & KOHRER, K. 2001. Mammalian cells express two VPS4 proteins both of which are involved in intracellular protein trafficking. *J Mol Biol,* 312**,** 469-80.

SCHUIKI, I. & VOLCHUK, A. 2012. Diverse roles for the p24 family of proteins in eukaryotic cells. *Biomol Concepts,* 3**,** 561-70.

SHEVCHENKO, A., TOMAS, H., HAVLIS, J., OLSEN, J. V. & MANN, M. 2007. In-gel digestion for mass spectrometric characterization of proteins and proteomes. *Nat. Protocols,* 1**,** 2856-2860.

SIEVERS, F., WILM, A., DINEEN, D., GIBSON, T. J., KARPLUS, K., LI, W., LOPEZ, R., MCWILLIAM, H., REMMERT, M., SÖDING, J., THOMPSON, J. D. & HIGGINS, D. G. 2011. Fast, scalable generation of high-quality protein multiple sequence alignments using Clustal Omega. *Molecular Systems Biology,* 7.

SOHDA, M., MISUMI, Y., YAMAMOTO, A., YANO, A., NAKAMURA, N. & IKEHARA, Y. 2001. Identification and characterization of a novel Golgi protein, GCP60, that interacts with the integral membrane protein giantin. *J Biol Chem,* 276**,** 45298-306.

STENMARK, H. 2009. Rab GTPases as coordinators of vesicle traffic. *Nat Rev Mol Cell Biol,* 10**,** 513-525.

STRATING, J. R. P. M., VAN BAKEL, N. H. M., LEUNISSEN, J. A. M. & MARTENS, G. J. M. 2009. A Comprehensive Overview of the Vertebrate p24 Family: Identification of a Novel Tissue-Specifically Expressed Member. *Molecular Biology and Evolution,* 26**,** 1707-1714.

THEILER, R., FUJITA, M., NAGAE, M., YAMAGUCHI, Y., MAEDA, Y. & KINOSHITA, T. 2014. The alpha-helical region in p24gamma2 subunit of p24 protein cargo receptor is pivotal for the recognition and transport of glycosylphosphatidylinositol-anchored proteins. *J Biol Chem,* 289**,** 16835-43.

TOOZE, S. A. & YOSHIMORI, T. 2010. The origin of the autophagosomal membrane. *Nat Cell Biol,* 12**,** 831-5.

UHLEN, M., FAGERBERG, L., HALLSTROM, B. M., LINDSKOG, C., OKSVOLD, P., MARDINOGLU, A., SIVERTSSON, A., KAMPF, C., SJOSTEDT, E., ASPLUND, A., OLSSON, I., EDLUND, K., LUNDBERG, E., NAVANI, S., SZIGYARTO, C. A., ODEBERG, J., DJUREINOVIC, D., TAKANEN, J. O., HOBER, S., ALM, T., EDQVIST, P. H., BERLING, H., TEGEL, H., MULDER, J., ROCKBERG, J., NILSSON, P., SCHWENK, J. M., HAMSTEN, M., VON FEILITZEN, K., FORSBERG, M., PERSSON, L., JOHANSSON, F., ZWAHLEN, M., VON HEIJNE, G., NIELSEN, J. & PONTEN, F. 2015. Proteomics. Tissue-based map of the human proteome. *Science,* 347**,** 1260419.

UNIPROT. 2016. *The Universal Protein Resource* [Online]. Available: http://www.uniprot.org/ [Accessed 2016].

VALE, R. D., SCHNAPP, B. J., REESE, T. S. & SHEETZ, M. P. 1985. Movement of organelles along filaments dissociated from the axoplasm of the squid giant axon. *Cell,* 40**,** 449-454.

VAN DER KANT, R., FISH, A., JANSSEN, L., JANSSEN, H., KROM, S., HO, N., BRUMMELKAMP, T., CARETTE, J., ROCHA, N. & NEEFJES, J. 2013. Late endosomal transport and tethering are coupled processes controlled by RILP and the cholesterol sensor ORP1L. *Journal of Cell Science,* 126**,** 3462-3474.

VANLANDINGHAM, P. A. & CERESA, B. P. 2009. Rab7 Regulates Late Endocytic Trafficking Downstream of Multivesicular Body Biogenesis and Cargo Sequestration. *The Journal of Biological Chemistry,* 284**,** 12110-12124.

VIKIS, H. G. & GUAN, K. L. 2004. Glutathione-S-transferase-fusion based assays for studying protein-protein interactions. *Methods Mol Biol,* 261**,** 175-86.

VOGESER, M. & PARHOFER, K. G. 2007. Liquid chromatography tandem-mass spectrometry (LC-MS/MS)--technique and applications in endocrinology. *Exp Clin Endocrinol Diabetes,* 115**,** 559-70.

WANG, T., MING, Z., XIAOCHUN, W. & HONG, W. 2011. Rab7: role of its protein interaction cascades in endo-lysosomal traffic. *Cell Signal,* 23**,** 516-21.

WRIGHT, S. J. & WRIGHT, D. J. 2002. Introduction to confocal microscopy. *Methods Cell Biol,* 70**,** 1-85.

ZHENG, Z. Y., CHENG, C. M., FU, X. R., CHEN, L. Y., XU, L., TERRILLON, S., WONG, S. T., BAR-SAGI, D., SONGYANG, Z. & CHANG, E. C. 2012. CHMP6 and VPS4A mediate the recycling of Ras to the plasma membrane to promote growth factor signaling. *Oncogene,* 31**,** 4630-4638.

6 Appendix:

Table 6.1 LC-MS/MS data over the 182 Proteins co-precipitated with the GOLD domain from HEK293 T-Rex Flp-In (HEK293) and HeLa cells. GST is used as negative control

Accession	Description	Gene ID	# Peptides	# PSMs	# Unique Peptides	MW [kDa]	HEK293	HEK293	HEK293	HEK293	HEK293	HeLa	HeLa	HeLa	HeLa	HeLa	HeLa	GST	GST	GST	GST	GST	GST
Q9BVA1	Tubulin beta-2B chain OS=Homo sapiens GN=TUBB2B PE=1 SV=1	TUBB2B	19	411	3	49,921	High	High	Not Found	High	Not Found	Not Found	Not Found	Not Found	Not Found	Not Found	Not Found	Not Found	Not Found	Not Found	Not Found	Not Found	Not Found
Q71U36	Tubulin alpha-1A chain OS=Homo sapiens GN=TUBA1A PE=1 SV=1	TUBA1A	22	417	1	50,104	Not Found	Not Found	Not Found	Medium	Not Found	Not Found	High	Not Found	Not Found	Not Found	Not Found	Not Found	Not Found	Not Found	Not Found	Not Found	Not Found
P68366	Tubulin alpha-4A chain OS=Homo sapiens GN=TUBA4A PE=1 SV=1	TUBA4A	20	338	4	49,892	High	High	High	High	High	High	High	High	High	High	High	Not Found	Not Found	Not Found	Not Found	Not Found	Not Found
P31689	DnaJ homolog subfamily A member 1 OS=Homo sapiens GN=DNAJA1 PE=1 SV=2	DNAJA1	17	212	17	44,839	High	High	High	High	High	High	High	High	High	High	Not Found	Not Found	Not Found	Not Found	Not Found	Not Found	Not Found
Q96C36	Pyrroline-5-carboxylate reductase 2 OS=Homo sapiens GN=PYCR2 PE=1 SV=1	PYCR2	11	97	10	33,616	High	High	High	High	High	High	High	High	High	Not Found	Not Found	Not Found	Not Found	Not Found	Not Found	Not Found	Not Found
F5H5D3	Tubulin alpha-1C chain OS=Homo sapiens GN=TUBA1C PE=3 SV=1	TUBA1C	22	435	2	57,693	High	High	High	Medium	High	High	High	Medium	High	Not Found	Not Found	Not Found	Not Found	Not Found	Not Found	Not Found	Not Found
P05141	ADP/ATP translocase 2 OS=Homo sapiens GN=SLC25A5 PE=1 SV=7	SLC25A5	16	199	6	32,831	High	High	High	High	High	High	High	High	High	High	Not Found	Not Found	Not Found	Not Found	Not Found	Not Found	Not Found
P42677	40S ribosomal protein S27 OS=Homo sapiens GN=RPS27 PE=1 SV=3	RPS27	3	26	1	9,455	Not Found	High	Not Found	Not Found	High	High	Not Found	High	High	Not Found	Not Found	Not Found	Not Found	Not Found	Not Found	Not Found	Not Found
Q9BUF5	Tubulin beta-6 chain OS=Homo sapiens GN=TUBB6 PE=1 SV=1	TUBB6	16	163	9	49,825	High	Not Found	High	Not Found	Not Found	Not Found	High	Not Found	High	Not Found	Not Found	Not Found	Not Found	Not Found	Not Found	Not Found	Not Found
F8VVM2	Phosphate carrier protein, mitochondrial OS=Homo sapiens GN=SLC25A3 PE=3 SV=1		12	90	12	36,138	Medium	High	High	High	Medium	High	High	High	High	Not Found	Not Found	Not Found	Not Found	Not Found	Not Found	Not Found	Not Found

Accession	Description	Gene ID	# Peptides	# PSMs	# Unique Peptides	MW [kDa]	HEK293	HEK293	HEK293	HEK293	HEK293	HeLa	HeLa	HeLa	HeLa	HeLa	HeLa	GST	GST	GST	GST	GST	GST
P12236	ADP/ATP translocase 3 OS=Homo sapiens GN=SLC25A6 PE=1 SV=4	SLC25A6	15	169	1	32,845	Not Found	Not Found	High	Medium	High	High	High	High	High	Not Found	Not Found	Not Found	Not Found	Not Found	Not Found	Not Found	Not Found
P12235	ADP/ATP translocase 1 OS=Homo sapiens GN=SLC25A4 PE=1 SV=4	SLC25A4	13	131	1	33,043	Not Found	Not Found	High	Not Found	Not Found	Not Found	Not Found	Not Found	Not Found	Not Found	Not Found	Not Found	Not Found	Not Found	Not Found	Not Found	Not Found
Q9BPW8	Protein NipSnap homolog 1 OS=Homo sapiens GN=NIPSNAP1 PE=1 SV=1	NIPSNAP1	11	73	11	33,289	Not Found	High	High	High	High	High	High	High	High	Not Found	Not Found	Not Found	Not Found	Not Found	Not Found	Not Found	Not Found
P62829	60S ribosomal protein L23 OS=Homo sapiens GN=RPL23 PE=1 SV=1	RPL23	5	29	5	14,856	Not Found	Not Found	Not Found	High	High	High	High	High	High	Not Found	Not Found	Not Found	Not Found	Not Found	Not Found	Not Found	Not Found
P18085	ADP-ribosylation factor 4 OS=Homo sapiens GN=ARF4 PE=1 SV=3	ARF4	7	31	5	20,498	Not Found	High	Not Found	High	Not Found	High	High	High	High	Not Found	Not Found	Not Found	Not Found	Not Found	Not Found	Not Found	Not Found
P63173	60S ribosomal protein L38 OS=Homo sapiens GN=RPL38 PE=1 SV=2	RPL38	2	2	2	8,213	Not Found	Not Found	Not Found	Not Found	High	Not Found	Not Found	Not Found	Not Found	Not Found	Not Found	Not Found	Not Found	Not Found	Not Found	Not Found	Not Found
O60884	DnaJ homolog subfamily A member 2 OS=Homo sapiens GN=DNAJA2 PE=1 SV=1	DNAJA2	13	116	13	45,717	High	High	High	High	High	High	High	High	High	Medium	Not Found	Not Found	Not Found	Not Found	Not Found	Not Found	Not Found
H0YMV8	40S ribosomal protein S27 OS=Homo sapiens GN=RPS27L PE=3 SV=1		3	22	1	11,338	Not Found	Not Found	Not Found	Not Found	High	Not Found	Not Found	Not Found	High	Not Found	Not Found	Not Found	Not Found	Not Found	Not Found	Not Found	Not Found
Q8NBS9	Thioredoxin domain-containing protein 5 OS=Homo sapiens GN=TXNDC5 PE=1 SV=2	TXNDC5	14	123	14	47,599	High	High	High	High	High	High	High	High	High	Not Found	Not Found	Not Found	Not Found	Not Found	Not Found	Not Found	Not Found
P25705	ATP synthase subunit alpha, mitochondrial OS=Homo sapiens GN=ATP5A1 PE=1 SV=1	ATP5A1	18	109	18	59,714	High	High	High	High	High	High	High	High	High	Not Found	Not Found	Not Found	Not Found	Not Found	Not Found	Not Found	Not Found
B4DMU0	Pyrroline-5-carboxylate reductase OS=Homo sapiens GN=PYCR1 PE=2 SV=1	PYCR1	8	44	7	35,958	Not Found	Medium	Medium	High	Not Found	High	High	High	High	Not Found	Not Found	Not Found	Not Found	Not Found	Not Found	Not Found	Not Found

Accession	Description	Gene ID	# Peptides	# PSMs	# Unique Peptides	MW [kDa]	HEK293	HEK293	HEK293	HEK293	HEK293	HeLa	HeLa	HeLa	HeLa	HeLa	HeLa	GST	GST	GST	GST	GST	GST
P63244	Guanine nucleotide-binding protein subunit beta-2-like 1 OS=Homo sapiens	GNB2L1	13	58	13	35,055	Not Found	High	High	High	High	High	High	High	High	High	Not Found	Not Found	Not Found	Not Found	Not Found	Not Found	Not Found
Q53H12	Acylglycerol kinase, mitochondrial OS=Homo sapiens GN=AGK PE=1 SV=2	AGK	12	44	12	47,107	High	High	High	High	Not Found	Not Found	High	Not Found	Not Found	Not Found	Not Found	Not Found	Not Found	Not Found	Not Found	Not Found	Not Found
P68431	Histone H3.1 OS=Homo sapiens GN=HIST1H3A PE=1 SV=2	HIST1H3F; HIST1H3C; HIST1H3D;	3	31	1	15,394	Not Found	Not Found	Not Found	Not Found	Not Found	High	Not Found	Medium	Not Found	Not Found	Not Found	Not Found	Not Found	Not Found	Not Found	Not Found	Not Found
P84243	Histone H3.3 OS=Homo sapiens GN=H3F3A PE=1 SV=2	H3F3A; H3F3AP4; H3F3B	3	30	1	15,319	Not Found	Not Found	Not Found	Not Found	Not Found	High	Not Found	Not Found	Not Found	Not Found	Not Found	Not Found	Not Found	Not Found	Not Found	Not Found	Not Found
Q9BSD7	Cancer-related nucleoside-triphosphatase OS=Homo sapiens GN=NTPCR PE=1 SV=1	NTPCR	6	29	6	20,7	Not Found	High	Medium	High	High	High	High	High	High	Not Found	Not Found	Not Found	Not Found	Not Found	Not Found	Not Found	Not Found
P06899	Histone H2B type 1-J OS=Homo sapiens GN=HIST1H2BJ PE=1 SV=3	HIST1H2BJ	4	48	1	13,896	Not Found	Not Found	Not Found	Not Found	Not Found	Medium	Not Found	High	Medium	Not Found	Not Found	Not Found	Not Found	Not Found	Not Found	Not Found	Not Found
P61204	ADP-ribosylation factor 3 OS=Homo sapiens GN=ARF3 PE=1 SV=2	ARF3	5	18	3	20,588	Not Found	Not Found	Not Found	High	Not Found	Not Found	Not Found	High	High	Not Found	Not Found	Not Found	Not Found	Not Found	Not Found	Not Found	Not Found
P06493	Cyclin-dependent kinase 1 OS=Homo sapiens GN=CDK1 PE=1 SV=3	CDK1	9	13	9	34,074	Not Found	Not Found	Not Found	Medium	High	Not Found	Not Found	Not Found	Not Found	High	Not Found	Not Found	Not Found	Not Found	Not Found	Not Found	Not Found
Q3ZCQ8	Mitochondrial import inner membrane translocase subunit TIM50 OS=Homo sapiens	TIMM50	7	27	7	39,622	Not Found	Not Found	High	High	High	High	High	High	High	Not Found	Not Found	Not Found	Not Found	Not Found	Not Found	Not Found	Not Found
Q9UBS4	DnaJ homolog subfamily B member 11 OS=Homo sapiens GN=DNAJB11 PE=1	DNAJB11	8	31	8	40,489	High	High	High	High	Not Found	High	High	High	High	Not Found	Not Found	Not Found	Not Found	Not Found	Not Found	Not Found	Not Found
K7ELC2	40S ribosomal protein S15 OS=Homo sapiens GN=RPS15 PE=3 SV=1	RPS15	2	8	2	17,712	Not Found	Not Found	Not Found	High	Not Found	High	High	High	High	Not Found	Not Found	Not Found	Not Found	Not Found	Not Found	Not Found	Not Found

Accession	Description	Gene ID	# Peptides	# PSMs	# Unique Peptides	MW [kDa]	HEK293	HEK293	HEK293	HEK293	HEK293	HeLa	HeLa	HeLa	HeLa	HeLa	HeLa	GST	GST	GST	GST	GST	GST
O75396	Vesicle-trafficking protein SEC22b OS=Homo sapiens GN=SEC22B PE=1 SV=4	SEC22B	5	7	5	24,578	Not Found	Not Found	Not Found	Not Found	High	Not Found	Not Found	Not Found	Medium	Not Found	Not Found	Not Found	Not Found	Not Found	Not Found	Not Found	Not Found
Q01813	6-phosphofructokinase type C OS=Homo sapiens GN=PFKP PE=1 SV=2	PFKP	13	59	10	85,542	High	High	High	Not Found	High	High	High	High	High	Not Found	Not Found	Not Found	Not Found	Not Found	Not Found	Not Found	Not Found
P08574	Cytochrome c1, heme protein, mitochondrial OS=Homo sapiens GN=CYC1 PE=1 SV=3	CYC1	7	34	7	35,399	Not Found	Not Found	High	High	Not Found	High	High	High	High	Not Found	Not Found	Not Found	Not Found	Not Found	Not Found	Not Found	Not Found
Q92743	Serine protease HTRA1 OS=Homo sapiens GN=HTRA1 PE=1 SV=1	HTRA1	9	22	9	51,255	Not Found	Not Found	Not Found	Not Found	Not Found	High	High	High	High	Not Found	Not Found	Not Found	Not Found	Not Found	Not Found	Not Found	Not Found
P10809	60 kDa heat shock protein, mitochondrial OS=Homo sapiens GN=HSPD1 PE=1 SV=2	HSPD1	13	34	13	61,016	High	Not Found	High	High	Not Found	High	High	High	High	Not Found	Not Found	Not Found	Not Found	Not Found	Not Found	Not Found	Not Found
Q96EY1	DnaJ homolog subfamily A member 3, mitochondrial OS=Homo sapiens GN=DNAJA	DNAJA3	8	36	8	52,456	High	Not Found	High	High	High	High	High	High	High	Medium	Not Found	Not Found	Not Found	Not Found	Not Found	Not Found	Not Found
P06702	Protein S100-A9 OS=Homo sapiens GN=S100A9 PE=1 SV=1	S100A9	3	4	3	13,234	Not Found	Not Found	Not Found	Not Found	Not Found	Not Found	Not Found	Not Found	High	Not Found	Not Found	Not Found	Not Found	Not Found	Not Found	Not Found	Not Found
H0Y368	Dolichol-phosphate mannosyltransferase (Fragment) OS=Homo sapiens GN=DPM1		6	34	6	33,307	Not Found	Not Found	High	High	Not Found	High	High	High	High	Not Found	Not Found	Not Found	Not Found	Not Found	Not Found	Not Found	Not Found
J3KPF3	4F2 cell-surface antigen heavy chain OS=Homo sapiens GN=SLC3A2 PE=4 SV=1	SLC3A2	12	35	12	68,059	Not Found	Not Found	Not Found	Not Found	Not Found	High	High	High	High	Not Found	Not Found	Not Found	Not Found	Not Found	Not Found	Not Found	Not Found
Q53GQ0	Estradiol 17-beta-dehydrogenase 12 OS=Homo sapiens GN=HSD17B12 PE=1	HSD17B12	5	9	5	34,302	Not Found	Not Found	High	Not Found	High	Not Found	Not Found	Not Found	Not Found	Not Found	Not Found	Not Found	Not Found	Not Found	Not Found	Not Found	Not Found
O43175	D-3-phosphoglycerate dehydrogenase OS=Homo sapiens GN=PHGDH PE=1 SV=4	PHGDH	9	35	9	56,614	High	High	High	High	Not Found	High	High	High	High	Not Found	Not Found	Not Found	Not Found	Not Found	Not Found	Not Found	Not Found

Accession	Description	Gene ID	# Peptides	# PSMs	# Unique Peptides	MW [kDa]	HEK293	HEK293	HEK293	HEK293	HEK293	HeLa	HeLa	HeLa	HeLa	HeLa	HeLa	GST	GST	GST	GST	GST	GST
P36542	ATP synthase subunit gamma, mitochondrial OS=Homo sapiens GN=ATP5C1 PE=1 SV=1	ATP5C1	6	26	6	32,975	Not Found	High	High	High	High	High	High	High	High	Not Found	Not Found	Not Found	Not Found	Not Found	Not Found	Not Found	Not Found
P60468	Protein transport protein Sec61 subunit beta OS=Homo sapiens GN=SEC61B PE=1 SV=2	SEC61B	2	12	2	9,968	Not Found	Not Found	High	Not Found	Not Found	High	High	High	High	Not Found	Not Found	Not Found	Not Found	Not Found	Not Found	Not Found	Not Found
P46777	60S ribosomal protein L5 OS=Homo sapiens GN=RPL5 PE=1 SV=3	RPL5	6	13	6	34,341	Not Found	High	High	Not Found	Not Found	Not Found	High	High	High	Not Found	Not Found	Not Found	Not Found	Not Found	Not Found	Not Found	Not Found
P49207	60S ribosomal protein L34 OS=Homo sapiens GN=RPL34 PE=1 SV=3	RPL34	2	4	2	13,284	Not Found	High	Not Found	Not Found	Not Found	Not Found	High	High	Not Found	Not Found	Not Found	Not Found	Not Found	Not Found	Not Found	Not Found	Not Found
P62424	60S ribosomal protein L7a OS=Homo sapiens GN=RPL7A PE=1 SV=2	RPL7A	5	13	5	29,977	High	Medium	High	High	Not Found	Medium	High	Medium	High	Not Found	Not Found	Not Found	Not Found	Not Found	Not Found	Not Found	Not Found
P61254	60S ribosomal protein L26 OS=Homo sapiens GN=RPL26 PE=1 SV=1	RPL26	3	11	3	17,248	Not Found	High	High	Not Found	Not Found	Medium	High	High	High	Not Found	Not Found	Not Found	Not Found	Not Found	Not Found	Not Found	Not Found
O14949	Cytochrome b-c1 complex subunit 8 OS=Homo sapiens GN=UQCRQ PE=1 SV=4	UQCRQ	2	2	2	9,9	Not Found	Not Found	Not Found	Not Found	Not Found	Not Found	High	Not Found	Not Found	Not Found	Not Found	Not Found	Not Found	Not Found	Not Found	Not Found	Not Found
P46783	40S ribosomal protein S10 OS=Homo sapiens GN=RPS10 PE=1 SV=1	RPS10	4	14	4	18,886	Not Found	High	Not Found	High	Not Found	Medium	High	High	High	Not Found	Not Found	Not Found	Not Found	Not Found	Not Found	Not Found	Not Found
P68032	Actin, alpha cardiac muscle 1 OS=Homo sapiens GN=ACTC1 PE=1 SV=1	ACTC1	7	71	1	41,992	High	Not Found	Not Found	Not Found	Not Found	Not Found	High	High	High	Not Found	Not Found	Not Found	Not Found	Not Found	Not Found	Not Found	Not Found
Q5VT66	MOSC domain-containing protein 1, mitochondrial OS=Homo sapiens GN=MARC1	MARC1	4	9	4	37,476	Not Found	Not Found	Not Found	Not Found	High	Not Found	Medium	Medium	Not Found	High	Not Found	Not Found	Not Found	Not Found	Not Found	Not Found	Not Found
F8VYN9	ADP-ribosylation factor-like protein 1 OS=Homo sapiens GN=ARL1 PE=3 SV=1		3	4	3	21,764	Not Found	Not Found	Not Found	High	High	Not Found	Not Found	Not Found	Not Found	Not Found	Not Found	Not Found	Not Found	Not Found	Not Found	Not Found	Not Found

Accession	Description	Gene ID	# Peptides	# PSMs	# Unique Peptides	MW [kDa]	HEK293	HEK293	HEK293	HEK293	HEK293	HeLa	HeLa	HeLa	HeLa	HeLa	HeLa	GST	GST	GST	GST	GST	GST
P00387	NADH-cytochrome b5 reductase 3 OS=Homo sapiens GN=CYB5R3 PE=1 SV=3	CYB5R3	4	5	4	34,213	Not Found	Not Found	Not Found	Not Found	High	Not Found	Not Found	Not Found	Not Found	Not Found	Not Found	Not Found	Not Found	Not Found	Not Found	Not Found	Not Found
P48594	Serpin B4 OS=Homo sapiens GN=SERPINB4 PE=1 SV=2	SERPINB4	7	8	7	44,825	Not Found	Not Found	Not Found	Not Found	Not Found	Not Found	Not Found	Not Found	High	Not Found	Not Found	Not Found	Not Found	Not Found	Not Found	Not Found	Not Found
P62847	40S ribosomal protein S24 OS=Homo sapiens GN=RPS24 PE=1 SV=1	RPS24	2	5	2	15,413	Not Found	Not Found	Not Found	Not Found	Not Found	High	High	High	High	Not Found	Not Found	Not Found	Not Found	Not Found	Not Found	Not Found	Not Found
Q9NP72	Ras-related protein Rab-18 OS=Homo sapiens GN=RAB18 PE=1 SV=1	RAB18	4	4	4	22,963	Not Found	Not Found	Not Found	Not Found	High	Not Found	Not Found	Not Found	Not Found	Not Found	Not Found	Not Found	Not Found	Not Found	Not Found	Not Found	Not Found
P31327	Carbamoyl-phosphate synthase [ammonia], mitochondrial OS=Homo sapiens GN=CPS1	CPS1	22	71	22	164,835	High	High	Not Found	High	High	High	High	High	High	High	Not Found	Not Found	Not Found	Not Found	Not Found	Not Found	Not Found
P22695	Cytochrome b-c1 complex subunit 2, mitochondrial OS=Homo sapiens GN=UQCRC2 PE=1 SV=3	UQCRC2	8	23	8	48,413	High	High	High	High	Not Found	High	High	High	High	Not Found	Not Found	Not Found	Not Found	Not Found	Not Found	Not Found	Not Found
P22626	Heterogeneous nuclear ribonucleoproteins A2/B1 OS=Homo sapiens GN=HNRNPA2B1 PE=1	HNRNPA2B1	5	14	5	37,407	Not Found	Not Found	High	High	Not Found	High	High	High	High	Not Found	Not Found	Not Found	Not Found	Not Found	Not Found	Not Found	Not Found
O75323	Protein NipSnap homolog 2 OS=Homo sapiens GN=GBAS PE=1 SV=1	GBAS	5	18	5	33,721	Not Found	High	High	High	Not Found	Not Found	High	High	High	Not Found	Not Found	Not Found	Not Found	Not Found	Not Found	Not Found	Not Found
P62304	Small nuclear ribonucleoprotein E OS=Homo sapiens GN=SNRPE PE=1 SV=1	SNRPE	1	2	1	10,797	Not Found	Not Found	Not Found	Not Found	High	Not Found	Not Found	Not Found	Not Found	Not Found	Not Found	Not Found	Not Found	Not Found	Not Found	Not Found	Not Found
P61224	Ras-related protein Rap-1b OS=Homo sapiens GN=RAP1B PE=1 SV=1	RAP1B	3	8	3	20,812	Not Found	Not Found	Not Found	High	High	High	High	High	High	Not Found	Not Found	Not Found	Not Found	Not Found	Not Found	Not Found	Not Found
P05109	Protein S100-A8 OS=Homo sapiens GN=S100A8 PE=1 SV=1	S100A8	2	6	2	10,828	Not Found	Not Found	Not Found	Not Found	Not Found	Not Found	Not Found	Not Found	High	Not Found	Not Found	Not Found	Not Found	Not Found	Not Found	Not Found	Not Found

Accession	Description	Gene ID	# Peptides	# PSMs	# Unique Peptides	MW [kDa]	HEK293	HEK293	HEK293	HEK293	HEK293	HeLa	HeLa	HeLa	HeLa	HeLa	HeLa	GST	GST	GST	GST	GST	GST
Q16795	NADH dehydrogenase [ubiquinone] 1 alpha subcomplex subunit 9, mitochondrial	NDUFA9	7	16	7	42,483	Not Found	Not Found	High	High	Medium	High	High	High	High	Not Found	Not Found	Not Found	Not Found	Not Found	Not Found	Not Found	Not Found
P61006	Ras-related protein Rab-8A OS=Homo sapiens GN=RAB8A PE=1 SV=1	RAB8A	4	11	2	23,653	Not Found	Not Found	Not Found	High	High	Not Found	High	High	High	Not Found	Not Found	Not Found	Not Found	Not Found	Not Found	Not Found	Not Found
P86790	Vacuolar fusion protein CCZ1 homolog B OS=Homo sapiens GN=CCZ1B PE=1 SV=1	CCZ1; CCZ1B	8	13	8	55,83	High	Not Found	Not Found	High	Not Found	Not Found	Medium	Not Found	High	Not Found	Not Found	Not Found	Not Found	Not Found	Not Found	Not Found	Not Found
K7ER00	Phenylalanine--tRNA ligase alpha subunit OS=Homo sapiens GN=FARSA PE=4 SV=1		5	11	5	62,356	High	High	High	High	Not Found	Not Found	Not Found	Not Found	Not Found	Not Found	Not Found	Not Found	Not Found	Not Found	Not Found	Not Found	Not Found
P09543	2',3'-cyclic-nucleotide 3'-phosphodiesterase OS=Homo sapiens GN=CNP PE=1 SV=2	CNP	7	28	7	47,549	High	Not Found	High	High	High	High	High	High	High	Not Found	Not Found	Not Found	Not Found	Not Found	Not Found	Not Found	Not Found
P50416	Carnitine O-palmitoyltransferase 1, liver isoform OS=Homo sapiens GN=CPT1A PE=1 SV=2	CPT1A	10	19	10	88,311	Not Found	Not Found	Not Found	Not Found	Not Found	High	High	High	High	Not Found	Not Found	Not Found	Not Found	Not Found	Not Found	Not Found	Not Found
P48047	ATP synthase subunit O, mitochondrial OS=Homo sapiens GN=ATP5O PE=1 SV=1	ATP5O	3	3	3	23,263	Not Found	Not Found	Not Found	Not Found	Not Found	Not Found	High	High	High	Not Found	Not Found	Not Found	Not Found	Not Found	Not Found	Not Found	Not Found
P05089	Arginase-1 OS=Homo sapiens GN=ARG1 PE=1 SV=2	ARG1	4	4	4	34,713	Not Found	Not Found	Not Found	Not Found	Not Found	Not Found	High	Not Found	Not Found	Not Found	Not Found	Not Found	Not Found	Not Found	Not Found	Not Found	Not Found
Q08188	Protein-glutamine gamma-glutamyltransferase E OS=Homo sapiens GN=TGM3	TGM3	8	14	8	76,584	Not Found	Not Found	Medium	Not Found	Not Found	Medium	High	Not Found	Not Found	Not Found	Not Found	Not Found	Not Found	Not Found	Not Found	Not Found	Not Found
Q9UN37	Vacuolar protein sorting-associated protein 4A OS=Homo sapiens GN=VPS4A	VPS4A	6	18	6	48,867	High	High	High	Medium	Not Found	Not Found	High	Not Found	High	Not Found	Not Found	Not Found	Not Found	Not Found	Not Found	Not Found	Not Found
Q00839	Heterogeneous nuclear ribonucleoprotein U OS=Homo sapiens GN=HNRNPU PE=1	HNRNPU	7	32	7	90,528	High	High	Not Found	High	Not Found	High	High	High	Not Found	Not Found	Not Found	Not Found	Not Found	Not Found	Not Found	Not Found	Not Found

Accession	Description	Gene ID	# Peptides	# PSMs	# Unique Peptides	MW [kDa]	HEK293	HEK293	HEK293	HEK293	HEK293	HeLa	HeLa	HeLa	HeLa	HeLa	HeLa	GST	GST	GST	GST	GST	GST
Q15366	Poly(rC)-binding protein 2 OS=Homo sapiens GN=PCBP2 PE=1 SV=1	PCBP2	4	28	3	38,556	Medium	Medium	High	High	Not Found	High	High	High	High	Not Found	Not Found	Not Found	Not Found	Not Found	Not Found	Not Found	Not Found
P51153	Ras-related protein Rab-13 OS=Homo sapiens GN=RAB13 PE=1 SV=1	RAB13	3	7	1	22,76	Not Found	Not Found	Not Found	Not Found	High	Not Found	Not Found	High	High	Not Found	Not Found	Not Found	Not Found	Not Found	Not Found	Not Found	Not Found
Q92499	ATP-dependent RNA helicase DDX1 OS=Homo sapiens GN=DDX1 PE=1 SV=2	DDX1	6	9	6	82,38	High	Not Found	Not Found	Not Found	Not Found	Not Found	Not Found	Not Found	High	Not Found	Not Found	Not Found	Not Found	Not Found	Not Found	Not Found	Not Found
Q15365	Poly(rC)-binding protein 1 OS=Homo sapiens GN=PCBP1 PE=1 SV=2	PCBP1	4	26	3	37,474	Medium	Not Found	High	High	Not Found	High	High	Medium	High	Not Found	Not Found	Not Found	Not Found	Not Found	Not Found	Not Found	Not Found
Q9UJS0	Calcium-binding mitochondrial carrier protein Aralar2 OS=Homo sapiens	SLC25A13	6	18	6	74,129	High	High	High	High	Not Found	Not Found	High	Medium	High	Not Found	Not Found	Not Found	Not Found	Not Found	Not Found	Not Found	Not Found
P18621	60S ribosomal protein L17 OS=Homo sapiens GN=RPL17 PE=1 SV=3	RPL17	2	6	2	21,383	Not Found	Not Found	High	Not Found	Not Found	Not Found	High	Medium	Medium	Not Found	Not Found	Not Found	Not Found	Not Found	Not Found	Not Found	Not Found
Q3SYB4	SERPINB12 protein OS=Homo sapiens GN=SERPINB12 PE=2 SV=1	SERPINB12	4	5	4	48,415	Not Found	Not Found	Not Found	Not Found	Not Found	Not Found	High	Not Found	Not Found	Not Found	Not Found	Not Found	Not Found	Not Found	Not Found	Not Found	Not Found
P37268	Squalene synthase OS=Homo sapiens GN=FDFT1 PE=1 SV=1	FDFT1	4	4	4	48,084	Not Found	Not Found	Not Found	Not Found	High	Not Found	Not Found	Not Found	Not Found	Not Found	Not Found	Not Found	Not Found	Not Found	Not Found	Not Found	Not Found
P57088	Transmembrane protein 33 OS=Homo sapiens GN=TMEM33 PE=1 SV=2	TMEM33	2	4	2	27,96	Not Found	Not Found	Not Found	Not Found	Not Found	Not Found	High	High	High	Not Found	Not Found	Not Found	Not Found	Not Found	Not Found	Not Found	Not Found
O15427	Monocarboxylate transporter 4 OS=Homo sapiens GN=SLC16A3 PE=1 SV=1	SLC16A3	3	9	3	49,437	Not Found	Not Found	Not Found	Not Found	Not Found	High	High	Medium	High	Not Found	Not Found	Not Found	Not Found	Not Found	Not Found	Not Found	Not Found
Q9Y3I0	tRNA-splicing ligase RtcB homolog OS=Homo sapiens GN=RTCB PE=1 SV=1	C22orf28; RTCB	5	6	5	55,175	High	Not Found	Not Found	Not Found	Not Found	Not Found	Not Found	Not Found	Medium	Not Found	Not Found	Not Found	Not Found	Not Found	Not Found	Not Found	Not Found

Accession	Description	Gene ID	# Peptides	# PSMs	# Unique Peptides	MW [kDa]	HEK293	HEK293	HEK293	HEK293	HEK293	HeLa	HeLa	HeLa	HeLa	HeLa	HeLa	GST	GST	GST	GST	GST	GST
Q14739	Lamin-B receptor OS=Homo sapiens GN=LBR PE=1 SV=2	LBR	4	11	4	70,658	High	High	High	High	Not Found	Not Found	Not Found	Not Found	Not Found	Not Found	Not Found	Not Found	Not Found	Not Found	Not Found	Not Found	Not Found
E9PK25	Cofilin-1 OS=Homo sapiens GN=CFL1 PE=4 SV=1		2	3	2	22,714	Not Found	Not Found	Not Found	High	Not Found	High	Not Found	Not Found	Not Found	Not Found	Not Found	Not Found	Not Found	Not Found	Not Found	Not Found	Not Found
O75251	NADH dehydrogenase [ubiquinone] iron-sulfur protein 7, mitochondrial OS=Homo	NDUFS7	2	5	2	23,548	Not Found	Not Found	Not Found	High	High	High	Not Found	High	High	Not Found	Not Found	Not Found	Not Found	Not Found	Not Found	Not Found	Not Found
Q969X5	Endoplasmic reticulum-Golgi intermediate compartment protein 1 OS=Homo sapiens	ERGIC1	2	3	2	32,571	Not Found	Not Found	Not Found	Not Found	Not Found	Not Found	High	High	Not Found	Not Found	Not Found	Not Found	Not Found	Not Found	Not Found	Not Found	Not Found
P31151	Protein S100-A7 OS=Homo sapiens GN=S100A7 PE=1 SV=4	S100A7	1	1	1	11,464	Not Found	Not Found	Not Found	Not Found	Not Found	Not Found	Not Found	Not Found	High	Not Found	Not Found	Not Found	Not Found	Not Found	Not Found	Not Found	Not Found
Q8NF37	Lysophosphatidylcholine acyltransferase 1 OS=Homo sapiens GN=LPCAT1 PE=1 SV=2	LPCAT1	4	12	4	59,113	Not Found	High	High	Medium	High	Not Found	High	High	Not Found	High	High	Not Found	Not Found	Not Found	Not Found	Not Found	Not Found
H3BLZ8	Probable ATP-dependent RNA helicase DDX17 OS=Homo sapiens GN=DDX17		6	26	1	80,389	Not Found	Not Found	Not Found	Not Found	Not Found	Not Found	Not Found	High	Not Found	Not Found	Not Found	Not Found	Not Found	Not Found	Not Found	Not Found	Not Found
O95573	Long-chain-fatty-acid--CoA ligase 3 OS=Homo sapiens GN=ACSL3 PE=1 SV=3	ACSL3	6	17	6	80,368	High	Not Found	Not Found	Not Found	High	Medium	High	Not Found	Medium	High	Not Found	Not Found	Not Found	Not Found	Not Found	Not Found	Not Found
D6RBZ0	Heterogeneous nuclear ribonucleoprotein A/B OS=Homo sapiens GN=HNRNPAB PE=4		2	5	1	35,66	Not Found	Not Found	Not Found	Not Found	Not Found	Not Found	Not Found	High	Not Found	Not Found	Not Found	Not Found	Not Found	Not Found	Not Found	Not Found	Not Found
Q6ZVX7	F-box only protein 50 OS=Homo sapiens GN=NCCRP1 PE=1 SV=1	NCCRP1	2	2	2	30,828	Not Found	Not Found	Not Found	Not Found	Not Found	Not Found	High	Not Found	Not Found	Not Found	Not Found	Not Found	Not Found	Not Found	Not Found	Not Found	Not Found
O75663	TIP41-like protein OS=Homo sapiens GN=TIPRL PE=1 SV=2	TIPRL	3	3	3	31,424	Not Found	Not Found	Not Found	High	Not Found	Not Found	Not Found	Not Found	Not Found	Not Found	Not Found	Not Found	Not Found	Not Found	Not Found	Not Found	Not Found

Accession	Description	Gene ID	# Peptides	# PSMs	# Unique Peptides	MW [kDa]	HEK293	HEK293	HEK293	HEK293	HEK293	HeLa	HeLa	HeLa	HeLa	HeLa	HeLa	GST	GST	GST	GST	GST	GST
Q9Y305	Acyl-coenzyme A thioesterase 9, mitochondrial OS=Homo sapiens GN=ACOT9	ACOT9	4	9	4	49,87	High	High	Not Found	Not Found	Not Found	Not Found	High	High	Medium	Not Found	Not Found	Not Found	Not Found	Not Found	Not Found	Not Found	Not Found
P17858	6-phosphofructokinase, liver type OS=Homo sapiens GN=PFKL PE=1 SV=6	PFKL	5	24	2	84,964	High	High	High	Not Found	High	Not Found	Not Found	Not Found	Not Found	Not Found	Not Found	Not Found	Not Found	Not Found	Not Found	Not Found	Not Found
P62873	Guanine nucleotide-binding protein G(I)/G(S)/G(T) subunit beta-1 OS=Homo	GNB1	2	9	2	37,353	Not Found	Not Found	High	High	High	High	High	High	Not Found	Not Found	Not Found	Not Found	Not Found	Not Found	Not Found	Not Found	Not Found
P01857	Ig gamma-1 chain C region OS=Homo sapiens GN=IGHG1 PE=1 SV=1	IGHG1	2	3	2	36,083	Not Found	Not Found	Not Found	Not Found	Not Found	Not Found	Not Found	Not Found	High	Not Found	Not Found	Not Found	Not Found	Not Found	Not Found	Not Found	Not Found
P55209	Nucleosome assembly protein 1-like 1 OS=Homo sapiens GN=NAP1L1 PE=1 SV=1	NAP1L1	2	2	2	45,346	Not Found	Not Found	Not Found	Not Found	Not Found	Not Found	High	Not Found	Not Found	Not Found	Not Found	Not Found	Not Found	Not Found	Not Found	Not Found	Not Found
Q14103	Heterogeneous nuclear ribonucleoprotein D0 OS=Homo sapiens GN=HNRNPD PE=1	HNRNPD	2	11	1	38,41	Not Found	High	High	High	Not Found	High	High	High	Medium	Not Found	Not Found	Not Found	Not Found	Not Found	Not Found	Not Found	Not Found
P41091	Eukaryotic translation initiation factor 2 subunit 3 OS=Homo sapiens GN=EIF2S3	EIF2S3	3	5	3	51,077	High	Not Found	High	Not Found	Not Found	Not Found	High	High	Not Found	Not Found	Not Found	Not Found	Not Found	Not Found	Not Found	Not Found	Not Found
Q5VV89	Microsomal glutathione S-transferase 3 OS=Homo sapiens GN=MGST3 PE=4 SV=1	MGST3	1	1	1	18,405	Not Found	Not Found	Not Found	Not Found	Not Found	High	Not Found	Not Found	Not Found	Not Found	Not Found	Not Found	Not Found	Not Found	Not Found	Not Found	Not Found
O60506	Heterogeneous nuclear ribonucleoprotein Q OS=Homo sapiens GN=SYNCRIP PE=1	SYNCRIP	5	12	5	69,56	High	Not Found	High	Not Found	Not Found	High	High	High	High	Not Found	Not Found	Not Found	Not Found	Not Found	Not Found	Not Found	Not Found
Q7L1V2	Vacuolar fusion protein MON1 homolog B OS=Homo sapiens GN=MON1B PE=1 SV=1	MON1B	3	4	3	59,18	High	Not Found	Not Found	Not Found	Not Found	Not Found	Not Found	Not Found	Not Found	Not Found	Not Found	Not Found	Not Found	Not Found	Not Found	Not Found	Not Found
Q15645	Pachytene checkpoint protein 2 homolog OS=Homo sapiens GN=TRIP13 PE=1 SV=2	TRIP13	3	3	3	48,52	Not Found	Not Found	Not Found	Not Found	Not Found	Not Found	High	Not Found	Not Found	Not Found	Not Found	Not Found	Not Found	Not Found	Not Found	Not Found	Not Found

Accession	Description	Gene ID	# Peptides	# PSMs	# Unique Peptides	MW [kDa]	HEK293	HEK293	HEK293	HEK293	HEK293	HeLa	HeLa	HeLa	HeLa	HeLa	HeLa	GST	GST	GST	GST	GST	GST
P11166	Solute carrier family 2, facilitated glucose transporter member 1 OS=Homo sapiens	SLC2A1	2	3	2	54,049	Not Found	Not Found	Not Found	Not Found	Not Found	High	Not Found	Not Found	High	Not Found	Not Found	Not Found	Not Found	Not Found	Not Found	Not Found	Not Found
P53985	Monocarboxylate transporter 1 OS=Homo sapiens GN=SLC16A1 PE=1 SV=3	SLC16A1	2	4	2	53,909	Medium	Not Found	Not Found	Not Found	Not Found	High	High	Not Found	Not Found	Not Found	Not Found	Not Found	Not Found	Not Found	Not Found	Not Found	Not Found
K7ERQ8	Uncharacterized protein (Fragment) OS=Homo sapiens PE=3 SV=1		2	2	2	31,372	Not Found	Not Found	Not Found	Not Found	High	Not Found	Not Found	Not Found	Not Found	Not Found	Not Found	Not Found	Not Found	Not Found	Not Found	Not Found	Not Found
P31944	Caspase-14 OS=Homo sapiens GN=CASP14 PE=1 SV=2	CASP14	2	2	2	27,662	Not Found	Not Found	Not Found	Not Found	Not Found	Not Found	High	Not Found	Not Found	Not Found	Not Found	Not Found	Not Found	Not Found	Not Found	Not Found	Not Found
P62318	Small nuclear ribonucleoprotein Sm D3 OS=Homo sapiens GN=SNRPD3 PE=1 SV=1	SNRPD3	1	1	1	13,907	Not Found	Not Found	Not Found	Not Found	High	Not Found	Not Found	Not Found	Not Found	Not Found	Not Found	Not Found	Not Found	Not Found	Not Found	Not Found	Not Found
Q15233	Non-POU domain-containing octamer-binding protein OS=Homo sapiens	NONO	3	14	2	54,197	High	Not Found	Not Found	Not Found	Not Found	High	Not Found	Not Found	High	Not Found	Not Found	Not Found	Not Found	Not Found	Not Found	Not Found	Not Found
Q15884	Protein FAM189A2 OS=Homo sapiens GN=FAM189A2 PE=1 SV=3	FAM189A2	1	4	1	49,671	Not Found	Not Found	Not Found	High	Not Found	Not Found	Medium	Not Found	High	Not Found	Not Found	Not Found	Not Found	Not Found	Not Found	Not Found	Not Found
Q9Y230	RuvB-like 2 OS=Homo sapiens GN=RUVBL2 PE=1 SV=3	RUVBL2	3	9	3	51,125	High	High	High	High	High	Not Found	High	High	Not Found	Not Found	Not Found	Not Found	Not Found	Not Found	Not Found	Not Found	Not Found
P33993	DNA replication licensing factor MCM7 OS=Homo sapiens GN=MCM7 PE=1 SV=4	MCM7	5	11	5	81,257	High	High	High	High	Not Found	High	High	Not Found	Not Found	Not Found	Not Found	Not Found	Not Found	Not Found	Not Found	Not Found	Not Found
Q01650	Large neutral amino acids transporter small subunit 1 OS=Homo sapiens GN=SLC7A5 PE=1 SV=2	SLC7A5	2	5	2	54,974	Not Found	Not Found	Not Found	Not Found	Not Found	Medium	High	High	High	Not Found	Not Found	Not Found	Not Found	Not Found	Not Found	Not Found	Not Found
P35613	Basigin OS=Homo sapiens GN=BSG PE=1 SV=2	BSG	2	3	2	42,174	Not Found	Not Found	Not Found	Not Found	Not Found	Not Found	High	Not Found	High	Not Found	Not Found	Not Found	Not Found	Not Found	Not Found	Not Found	Not Found

Accession	Description	Gene ID	# Peptides	# PSMs	# Unique Peptides	MW [kDa]	HEK293	HEK293	HEK293	HEK293	HEK293	HeLa	HeLa	HeLa	HeLa	HeLa	HeLa	GST	GST	GST	GST	GST	GST
Q6IAN0	Dehydrogenase/reductase SDR family member 7B OS=Homo sapiens GN=DHRS7B PE=1	DHRS7B	2	3	2	35,097	Not Found	Not Found	High	Not Found	High	Not Found	Not Found	Not Found	Not Found	Not Found	Not Found	Not Found	Not Found	Not Found	Not Found	Not Found	Not Found
B4DR61	Protein transport protein Sec61 subunit alpha isoform 1 OS=Homo sapiens GN=SEC61A	SEC61A1	2	5	2	52,915	Not Found	Not Found	High	Not Found	Not Found	Not Found	High	High	High	Not Found	Not Found	Not Found	Not Found	Not Found	Not Found	Not Found	Not Found
Q02978	Mitochondrial 2-oxoglutarate/malate carrier protein OS=Homo sapiens GN=SLC25A	SLC25A11	2	3	2	34,04	Not Found	Not Found	High	Not Found	Not Found	Not Found	Not Found	High	Not Found	Not Found	Not Found	Not Found	Not Found	Not Found	Not Found	Not Found	Not Found
P10909	Clusterin OS=Homo sapiens GN=CLU PE=1 SV=1	CLU	2	2	2	52,461	Not Found	Not Found	Not Found	Not Found	Not Found	Not Found	High	Not Found	Not Found	Not Found	Not Found	Not Found	Not Found	Not Found	Not Found	Not Found	Not Found
Q8WWC4	Uncharacterized protein C2orf47, mitochondrial OS=Homo sapiens GN=C2orf47 PE=1 SV=1	C2orf47	2	2	2	32,524	Not Found	Not Found	Not Found	Not Found	Not Found	Not Found	High	High	Not Found	Not Found	Not Found	Not Found	Not Found	Not Found	Not Found	Not Found	Not Found
C9IZQ1	Translocon-associated protein subunit alpha OS=Homo sapiens GN=SSR1 PE=4 SV=1		1	1	1	33,866	Not Found	Not Found	Not Found	Not Found	Not Found	Not Found	High	Not Found	Not Found	Not Found	Not Found	Not Found	Not Found	Not Found	Not Found	Not Found	Not Found
A6NIM6	Solute carrier family 15 member 5 OS=Homo sapiens GN=SLC15A5 PE=3 SV=2	SLC15A5	1	4	1	65,22	Not Found	Not Found	Medium	Not Found	Not Found	Not Found	Medium	High	Not Found	Not Found	Not Found	Not Found	Not Found	Not Found	Not Found	Not Found	Not Found
P00338	L-lactate dehydrogenase A chain OS=Homo sapiens GN=LDHA PE=1 SV=2	LDHA	2	7	2	36,665	Not Found	Not Found	Medium	Not Found	Not Found	Not Found	High	High	High	Not Found	Not Found	Not Found	Not Found	Not Found	Not Found	Not Found	Not Found
P26599	Polypyrimidine tract-binding protein 1 OS=Homo sapiens GN=PTBP1 PE=1 SV=1	PTBP1	2	2	2	57,186	Not Found	Not Found	Not Found	High	Not Found	High	Not Found	Not Found	Not Found	Not Found	Not Found	Not Found	Not Found	Not Found	Not Found	Not Found	Not Found
Q15392	Delta(24)-sterol reductase OS=Homo sapiens GN=DHCR24 PE=1 SV=2	DHCR24	2	8	2	60,062	High	High	High	Not Found	High	Not Found	High	High	High	Not Found	Not Found	Not Found	Not Found	Not Found	Not Found	Not Found	Not Found
O75306	NADH dehydrogenase [ubiquinone] iron-sulfur protein 2, mitochondrial OS=Homo	NDUFS2	2	4	2	52,512	Not Found	Not Found	High	Not Found	High	Not Found	High	Not Found	Not Found	Not Found	Not Found	Not Found	Not Found	Not Found	Not Found	Not Found	Not Found

Accession	Description	Gene ID	# Peptides	# PSMs	# Unique Peptides	MW [kDa]	HEK293	HEK293	HEK293	HEK293	HEK293	HeLa	HeLa	HeLa	HeLa	HeLa	HeLa	GST	GST	GST	GST	GST	GST
Q9HCN8	Stromal cell-derived factor 2-like protein 1 OS=Homo sapiens GN=SDF2L1 PE=1 SV=2	SDF2L1	1	1	1	23,584	Not Found	Not Found	Not Found	High	Not Found	Not Found	Not Found	Not Found	Not Found	Not Found	Not Found	Not Found	Not Found	Not Found	Not Found	Not Found	Not Found
Q8WXC9	NADH dehydrogenase [ubiquinone] 1 alpha subcomplex subunit 10, mitochondrial	NDUFA10	2	2	2	48,532	Not Found	Not Found	High	High	Not Found	Not Found	Not Found	Not Found	Not Found	Not Found	Not Found	Not Found	Not Found	Not Found	Not Found	Not Found	Not Found
Q13867	Bleomycin hydrolase OS=Homo sapiens GN=BLMH PE=1 SV=1	BLMH	2	3	2	52,528	Not Found	Not Found	Not Found	Not Found	Not Found	Not Found	High	Not Found	Not Found	Not Found	Not Found	Not Found	Not Found	Not Found	Not Found	Not Found	Not Found
F8VQ10	Spliceosome RNA helicase DDX39B OS=Homo sapiens GN=DDX39B PE=4 SV=1		2	2	2	50,713	Not Found	Not Found	Not Found	High	Not Found	Not Found	Not Found	Not Found	Not Found	Not Found	Not Found	Not Found	Not Found	Not Found	Not Found	Not Found	Not Found
P24534	Elongation factor 1-beta OS=Homo sapiens GN=EEF1B2 PE=1 SV=3	EEF1B2	1	1	1	24,748	Not Found	Not Found	Not Found	High	Not Found	Not Found	Not Found	Not Found	Not Found	Not Found	Not Found	Not Found	Not Found	Not Found	Not Found	Not Found	Not Found
P23284	Peptidyl-prolyl cis-trans isomerase B OS=Homo sapiens GN=PPIB PE=1 SV=2	PPIB	1	2	1	23,728	Not Found	Not Found	Not Found	Not Found	Not Found	Not Found	High	Not Found	High	Not Found	Not Found	Not Found	Not Found	Not Found	Not Found	Not Found	Not Found
B3KVR1	Small nuclear ribonucleoprotein-associated protein OS=Homo sapiens GN=SNRPN	SNRPN	1	1	1	25,059	Not Found	Not Found	Not Found	High	Not Found	Not Found	Not Found	Not Found	Not Found	Not Found	Not Found	Not Found	Not Found	Not Found	Not Found	Not Found	Not Found
P04040	Catalase OS=Homo sapiens GN=CAT PE=1 SV=3	CAT	2	2	2	59,719	Not Found	Not Found	Not Found	Not Found	Not Found	Not Found	High	Not Found	Not Found	Not Found	Not Found	Not Found	Not Found	Not Found	Not Found	Not Found	Not Found
O14732	Inositol monophosphatase 2 OS=Homo sapiens GN=IMPA2 PE=1 SV=1	IMPA2	1	1	1	31,301	Not Found	Not Found	Not Found	Not Found	Not Found	High	Not Found	Not Found	Not Found	Not Found	Not Found	Not Found	Not Found	Not Found	Not Found	Not Found	Not Found
P23246	Splicing factor, proline- and glutamine-rich OS=Homo sapiens GN=SFPQ	SFPQ	2	12	1	76,102	Not Found	Not Found	High	Not Found	Not Found	Not Found	Not Found	Not Found	Not Found	Not Found	Not Found	Not Found	Not Found	Not Found	Not Found	Not Found	Not Found
P62258	14-3-3 protein epsilon OS=Homo sapiens GN=YWHAE PE=1 SV=1	YWHAE	1	1	1	29,155	Not Found	Not Found	Not Found	High	Not Found	Not Found	Not Found	Not Found	Not Found	Not Found	Not Found	Not Found	Not Found	Not Found	Not Found	Not Found	Not Found

Accession	Description	Gene ID	# Peptides	# PSMs	# Unique Peptides	MW [kDa]	HEK293	HEK293	HEK293	HEK293	HEK293	HeLa	HeLa	HeLa	HeLa	HeLa	HeLa	GST	GST	GST	GST	GST	GST
Q6NZI2	Polymerase I and transcript release factor OS=Homo sapiens GN=PTRF PE=1 SV=1	PTRF	1	1	1	43,45	Not Found	Not Found	Not Found	Not Found	Not Found	Not Found	High	Not Found	Not Found	Not Found	Not Found	Not Found	Not Found	Not Found	Not Found	Not Found	Not Found
Q96DM3	Uncharacterized protein C18orf8 OS=Homo sapiens GN=C18orf8 PE=2 SV=2	C18orf8	2	2	2	74,927	High	Not Found	Not Found	High	Not Found	Not Found	Not Found	Not Found	Not Found	Not Found	Not Found	Not Found	Not Found	Not Found	Not Found	Not Found	Not Found
Q5D862	Filaggrin-2 OS=Homo sapiens GN=FLG2 PE=1 SV=1	FLG2	5	7	5	247,928	Not Found	High	Not Found	Not Found	Not Found	Not Found	High	Not Found	Not Found	Not Found	Not Found	Not Found	Not Found	Not Found	Not Found	Not Found	Not Found
P31040	Succinate dehydrogenase [ubiquinone] flavoprotein subunit, mitochondrial OS=Homo	SDHA	2	2	2	72,645	High	Not Found	Not Found	Not Found	Not Found	High	Not Found	Not Found	Not Found	Not Found	Not Found	Not Found	Not Found	Not Found	Not Found	Not Found	Not Found
P25311	Zinc-alpha-2-glycoprotein OS=Homo sapiens GN=AZGP1 PE=1 SV=2	AZGP1	1	1	1	34,237	Not Found	Not Found	Not Found	Not Found	Not Found	Not Found	Not Found	High	Not Found	Not Found	Not Found	Not Found	Not Found	Not Found	Not Found	Not Found	Not Found
P42166	Lamina-associated polypeptide 2, isoform alpha OS=Homo sapiens GN=TMPO	TMPO	2	4	2	75,446	Not Found	Medium	Not Found	High	Not Found	High	Not Found	Not Found	Not Found	Not Found	Not Found	Not Found	Not Found	Not Found	Not Found	Not Found	Not Found
B3KSQ1	Very-long-chain enoyl-CoA reductase OS=Homo sapiens GN=TECR PE=2 SV=1	TECR	1	3	1	37,443	Not Found	Not Found	Not Found	Not Found	Not Found	Not Found	High	High	High	Not Found	Not Found	Not Found	Not Found	Not Found	Not Found	Not Found	Not Found
P09110	3-ketoacyl-CoA thiolase, peroxisomal OS=Homo sapiens GN=ACAA1 PE=1 SV=2	ACAA1	1	1	1	44,264	Not Found	Not Found	Not Found	High	Not Found	Not Found	Not Found	Not Found	Not Found	Not Found	Not Found	Not Found	Not Found	Not Found	Not Found	Not Found	Not Found
Q9H9B4	Sideroflexin-1 OS=Homo sapiens GN=SFXN1 PE=1 SV=4	SFXN1	1	1	1	35,596	Not Found	Not Found	High	Not Found	Not Found	Not Found	Not Found	Not Found	Not Found	Not Found	Not Found	Not Found	Not Found	Not Found	Not Found	Not Found	Not Found
Q9BRQ8	Apoptosis-inducing factor 2 OS=Homo sapiens GN=AIFM2 PE=1 SV=1	AIFM2	1	4	1	40,501	Not Found	Not Found	Not Found	Not Found	Not Found	Not Found	Not Found	High	High	High	Not Found	Not Found	Not Found	Not Found	Not Found	Not Found	Not Found
Q9Y673	Dolichyl-phosphate beta-glucosyltransferase OS=Homo sapiens GN=ALG5	ALG5	1	1	1	36,922	Not Found	Not Found	Not Found	Not Found	High	Not Found	Not Found	Not Found	Not Found	Not Found	Not Found	Not Found	Not Found	Not Found	Not Found	Not Found	Not Found

Accession	Description	Gene ID	# Peptides	# PSMs	# Unique Peptides	MW [kDa]	HEK293	HEK293	HEK293	HEK293	HEK293	HeLa	HeLa	HeLa	HeLa	HeLa	HeLa	GST	GST	GST	GST	GST	GST
Q6P4A7	Sideroflexin-4 OS=Homo sapiens GN=SFXN4 PE=1 SV=1	SFXN4	1	1	1	37,974	Not Found	Not Found	High	Not Found	Not Found	Not Found	Not Found	Not Found	Not Found	Not Found	Not Found	Not Found	Not Found	Not Found	Not Found	Not Found	Not Found
Q15758	Neutral amino acid transporter B(0) OS=Homo sapiens GN=SLC1A5 PE=1 SV=2	SLC1A5	1	5	1	56,562	High	High	High	Not Found	Not Found	Not Found	High	Not Found	High	Not Found	Not Found	Not Found	Not Found	Not Found	Not Found	Not Found	Not Found
H0Y449	Nuclease-sensitive element-binding protein 1 (Fragment) OS=Homo sapiens		1	5	1	41,99	High	Medium	Not Found	High	Not Found	Not Found	High	High	Not Found	Not Found	Not Found	Not Found	Not Found	Not Found	Not Found	Not Found	Not Found
G3V325	Pentatricopeptide repeat-containing protein 1, mitochondrial OS=Homo sapiens GN=ATP5J2-	ATP5J2-PTCD1	2	8	2	84,057	Not Found	Not Found	Not Found	High	Not Found	Not Found	High	High	High	Not Found	Not Found	Not Found	Not Found	Not Found	Not Found	Not Found	Not Found
P05198	Eukaryotic translation initiation factor 2 subunit 1 OS=Homo sapiens GN=EIF2S1	EIF2S1	1	5	1	36,089	Not Found	Not Found	High	Not Found	Not Found	High	High	High	High	Not Found	Not Found	Not Found	Not Found	Not Found	Not Found	Not Found	Not Found
Q13724	Mannosyl-oligosaccharide glucosidase OS=Homo sapiens GN=MOGS PE=1 SV=5	MOGS	2	2	2	91,861	Not Found	Not Found	Not Found	High	High	Not Found	Not Found	Not Found	Not Found	Not Found	Not Found	Not Found	Not Found	Not Found	Not Found	Not Found	Not Found
J3KQ73	Peptidyl-prolyl cis-trans isomerase FKBP8 OS=Homo sapiens GN=FKBP8	FKBP8	1	2	1	47,114	High	Not Found	Not Found	Not Found	High	Not Found	Not Found	Not Found	Not Found	Not Found	Not Found	Not Found	Not Found	Not Found	Not Found	Not Found	Not Found
Q8NBX0	Saccharopine dehydrogenase-like oxidoreductase OS=Homo sapiens GN=SCCPDH PE=1	SCCPDH	1	2	1	47,121	Not Found	Not Found	Not Found	Not Found	Not Found	Not Found	High	Medium	Not Found	Not Found	Not Found	Not Found	Not Found	Not Found	Not Found	Not Found	Not Found
Q14240	Eukaryotic initiation factor 4A-II OS=Homo sapiens GN=EIF4A2 PE=1 SV=2	EIF4A2	1	1	1	46,373	Not Found	Not Found	Not Found	High	Not Found	Not Found	Not Found	Not Found	Not Found	Not Found	Not Found	Not Found	Not Found	Not Found	Not Found	Not Found	Not Found
P51648	Fatty aldehyde dehydrogenase OS=Homo sapiens GN=ALDH3A2 PE=1 SV=1	ALDH3A2	1	1	1	54,813	Not Found	Not Found	Not Found	Not Found	Not Found	Not Found	High	Not Found	Not Found	Not Found	Not Found	Not Found	Not Found	Not Found	Not Found	Not Found	Not Found
Q8NC51	Plasminogen activator inhibitor 1 RNA-binding protein OS=Homo sapiens GN=SERBP1	SERBP1	1	5	1	44,938	Medium	Medium	Not Found	Not Found	Not Found	High	High	Not Found	High	Not Found	Not Found	Not Found	Not Found	Not Found	Not Found	Not Found	Not Found

Accession	Description	Gene ID	# Peptides	# PSMs	# Unique Peptides	MW [kDa]	HEK293	HEK293	HEK293	HEK293	HEK293	HeLa	HeLa	HeLa	HeLa	HeLa	HeLa	GST	GST	GST	GST	GST	GST
P33992	DNA replication licensing factor MCM5 OS=Homo sapiens GN=MCM5 PE=1 SV=5	MCM5	2	2	2	82,233	Not Found	Not Found	Not Found	Not Found	High	Not Found	Not Found	Not Found	Not Found	High	Not Found	Not Found	Not Found	Not Found	Not Found	Not Found	Not Found
O14556	Glyceraldehy de-3-phosphate dehydrogenas e, testis-specific OS=Homo sapiens	GAPDHS	1	14	1	44,473	Not Found	Not Found	Not Found	High	High	High	High	High	High	High	Not Found	Not Found	Not Found	Not Found	Not Found	Not Found	Not Found
P05023	Sodium/potas sium-transporting ATPase subunit alpha-1 OS=Homo sapiens	ATP1A1	2	2	2	112,824	High	Not Found	Not Found	Not Found	Not Found	Not Found	Not Found	Not Found	Not Found	Not Found	Not Found	Not Found	Not Found	Not Found	Not Found	Not Found	Not Found
J3KPX7	Prohibitin-2 OS=Homo sapiens GN=PHB2 PE=4 SV=1		1	1	1	33,382	Not Found	Not Found	Not Found	High	Not Found	Not Found	Not Found	Not Found	Not Found	Not Found	Not Found	Not Found	Not Found	Not Found	Not Found	Not Found	Not Found
Q9H7Z7	Prostaglandin E synthase 2 OS=Homo sapiens GN=PTGES2 PE=1 SV=1	PTGES2	1	1	1	41,917	Not Found	Not Found	Not Found	Not Found	Not Found	High	Not Found	Not Found	Not Found	Not Found	Not Found	Not Found	Not Found	Not Found	Not Found	Not Found	Not Found
Q96CS3	FAS-associated factor 2 OS=Homo sapiens GN=FAF2 PE=1 SV=2	FAF2	1	1	1	52,591	Not Found	Not Found	High	Not Found	Not Found	Not Found	Not Found	Not Found	Not Found	Not Found	Not Found	Not Found	Not Found	Not Found	Not Found	Not Found	Not Found
P06733	Alpha-enolase OS=Homo sapiens GN=ENO1 PE=1 SV=2	ENO1	1	1	1	47,139	Not Found	Not Found	Not Found	Not Found	Not Found	Not Found	High	Not Found	Not Found	Not Found	Not Found	Not Found	Not Found	Not Found	Not Found	Not Found	Not Found
P04844	Dolichyl-diphosphooli gosaccharide--protein glycosyltransf erase subunit 2 OS=Homo sapiens	RPN2	1	1	1	69,241	Not Found	Not Found	Not Found	Not Found	Not Found	Not Found	High	Not Found	Not Found	Not Found	Not Found	Not Found	Not Found	Not Found	Not Found	Not Found	Not Found
P29401	Transketolase OS=Homo sapiens GN=TKT PE=1 SV=3	TKT	1	1	1	67,835	Not Found	Not Found	Not Found	Not Found	Not Found	Not Found	Not Found	Not Found	High	Not Found	Not Found	Not Found	Not Found	Not Found	Not Found	Not Found	Not Found
Q10471	Polypeptide N-acetylgalactos aminyltransfe rase 2 OS=Homo sapiens GN=GALNT	GALNT2	1	1	1	64,691	Not Found	Not Found	Not Found	Not Found	Not Found	Not Found	Not Found	Not Found	Not Found	High	Not Found	Not Found	Not Found	Not Found	Not Found	Not Found	Not Found
Q12797	Aspartyl/aspara ginyl beta-hydroxylase OS=Homo sapiens GN=ASPH PE=1 SV=3	ASPH	1	1	1	85,809	Not Found	Not Found	Not Found	Not Found	Not Found	Not Found	High	Not Found	Not Found	Not Found	Not Found	Not Found	Not Found	Not Found	Not Found	Not Found	Not Found

Q9UPA5	Q8IWZ3	Q07283	O76031	P14868	Q08211	P48643	**Accession**
Protein bassoon OS=Homo sapiens GN=BSN PE=2 SV=4	Ankyrin repeat and KH domain-containing protein 1 OS=Homo sapiens GN=ANKHD1 PE=1 SV=1	Trichohyalin OS=Homo sapiens GN=TCHH PE=1 SV=2	ATP-dependent Clp protease ATP-binding subunit clpX-like, mitochondrial OS=Homo sapiens	Aspartate--tRNA ligase, cytoplasmic OS=Homo sapiens GN=DARS PE=1 SV=2	ATP-dependent RNA helicase A OS=Homo sapiens GN=DHX9 PE=1 SV=4	T-complex protein 1 subunit epsilon OS=Homo sapiens GN=CCT5 PE=1 SV=1	**Description**
BSN	ANKHD1	TCHH	CLPX	DARS	DHX9	CCT5	**Gene ID**
1	1	1	1	1	2	1	**# Peptides**
1	4	2	5	3	2	1	**# PSMs**
1	1	1	1	1	2	1	**# Unique Peptides**
416,214	269,291	253,777	69,181	57,1	140,869	59,633	**MW [kDa]**
Not Found	Not Found	Not Found	High	High	High	Not Found	**HEK293**
Not Found	Not Found	Not Found	High	High	Not Found	Not Found	**HEK293**
Not Found	Not Found	Not Found	Not Found	Not Found	Not Found	Not Found	**HEK293**
Not Found	High	Not Found	High	High	Not Found	High	**HEK293**
Not Found	High	Not Found	Not Found	Not Found	Not Found	Not Found	**HEK293**
Not Found	Not Found	Not Found	Not Found	Not Found	Not Found	Not Found	**HeLa**
Not Found	Not Found	Not Found	High	Not Found	Not Found	Not Found	**HeLa**
High	Not Found	High	Not Found	Not Found	Not Found	Not Found	**HeLa**
Not Found	Not Found	Not Found	High	Not Found	Not Found	Not Found	**HeLa**
Not Found	Not Found	Not Found	Not Found	Not Found	Not Found	Not Found	**HeLa**
Not Found	Not Found	Not Found	Not Found	Not Found	Not Found	Not Found	**HeLa**
Not Found	Not Found	Not Found	Not Found	Not Found	Not Found	Not Found	**GST**
Not Found	Not Found	Not Found	Not Found	Not Found	Not Found	Not Found	**GST**
Not Found	Not Found	Not Found	Not Found	Not Found	Not Found	Not Found	**GST**
Not Found	Not Found	Not Found	Not Found	Not Found	Not Found	Not Found	**GST**
Not Found	Not Found	Not Found	Not Found	Not Found	Not Found	Not Found	**GST**
Not Found	Not Found	Not Found	Not Found	Not Found	Not Found	Not Found	**GST**